**TESIS DOCTORAL**

# Caracterización del Flujo Hidrodinámico y Evaluación de su Impacto en la Acumulación y Producción de Hidrocarburos en el Sector Sur de la Cuenca de Llanos, Colombia.


**AUTOR:**

**RICARDO ANDRES GOMEZ MONCADA**

**DIRECTORES:**

**PhD. MARCELA JARAMILLO URIBE - EAFIT**

**PhD. ANDRES ROBERTO MORA BOHORQUEZ - ECOPETROL**

**ESCUELA DE CIENCIAS**

**DOCTORADO EN CIENCIAS DE LA TIERRA**

**UNIVERSIDAD EAFIT**


**2022**

# CONTENIDO

Resumen ..... 3

Abstract ..... 4

1. INTRODUCCIÓN ..... 5

2. APORTES A LA INVESTIGACIÓN-1 ..... 8

3. APORTES A LA INVESTIGACIÓN-2 ..... 76

4. TRABAJOS FUTUROS ..... 143

# Resumen

El sector sur de la Cuenca de los Llanos en Colombia ha sido identificado como una zona donde el flujo hidrodinámico ha influenciado el potencial de almacenamiento y producción de hidrocarburos. En esta zona el flujo hidrodinámico coincide con una provincia de crudos pesados y extrapesados, lo que se ha hipotetizado para esta zona, una condición crítica que disminuye el potencial de retención de hidrocarburos por el efecto del flujo hidrodinámico y la naturaleza geoquímica de los fluidos. Este trabajo proporciona una visión integral para describir el impacto del flujo hidrodinámico regional en la retención de las acumulaciones de petróleo pesado presentes en los reservorios que forman parte de la unidad de flujo regional más importante del sector sur de la Cuenca de Llanos. La Unidad de Flujo Basal constituye una unidad de flujo a escala de cuenca que conecta hidráulica y lateralmente rocas desde el Cretácico (oeste) hasta el Oligoceno (este) y se extiende desde el margen suroccidental hasta cientos de kilómetros hacia el *foreland* de la cuenca de los Llanos, y cuya principal zona de recarga hídrica se ha identificada hacia el flanco oriental de la Serranía de la Macarena. Para comprender el impacto de las propiedades fisicoquímicas de los fluidos en el potencial de retención de hidrocarburos, analizamos la relación entre los datos hidráulicos y las principales características de los fluidos presentes en la Unidad de Flujo Basal, y así mismo, su distribución espacial en la configuración actual de esta unidad de flujo. Este análisis integró información de cabezas hidráulicas, análisis SARA (saturados, aromáticos, resinas y asfaltenos), análisis de cromatografía de gases *whole oil*, gravedades API y densidades de aceite. Además, se realizaron análisis hidroquímicos de los iones primarios y análisis de isótopos estables ($\delta^{18}O$ and $\delta D$) en muestras de aguas subterráneas provenientes de la Unidad de Flujo Basal, los cuales fueron integrados con datos de resistividad profunda medida en pozos de petróleo del área. Los análisis isotópicos realizados en muestras de fuentes hídricas superficiales ($\delta^{18}O$ y $\delta D$), y datos de estudios previos realizados en la zona, permitieron establecer la Línea de Agua Meteórica Local para la cuenca de los Llanos. Los valores de $\delta^{18}O$ y $\delta D$ de las muestras de agua subterránea tomadas en los pozos profundos del área siguen la Línea de Agua Meteórica Local propuesta para la cuenca de Llanos, soportando así la presencia de aguas meteóricas en la Unidad de Flujo Basal, y cuya influencia se extiende desde la zona de recarga hasta más de 300 km de distancia al este de la cuenca. Los resultados permitieron identificar la esquina suroccidental del sector sur de la Cuenca de Llanos como la zona con mayor impacto de flujo hidrodinámico, y por tanto, la zona con menor potencial de retención de hidrocarburos, atribuyendo como causas principales: 1) la proximidad a las zonas de recarga, y 2) el bajo contraste de densidades entre los fluidos (aguas frescas y crudos pesados altamente biodegradados), lo que implica altos valores de *Tilt Amplification Factor* (*TAF*). Además, los cambios graduales en las resistividades y la concentración de iones en las aguas subterráneas sugieren el flanco oriental de la Serranía de la Macarena como la principal zona de recarga hídrica para la Unidad de Flujo Basal. Finalmente, se utilizaron técnicas de simulación numérica para analizar el comportamiento del drenaje de hidrocarburos bajo condiciones hidrodinámicas, obteniendo una primera aproximación a las velocidades lineales promedio del flujo de aguas subterráneas entre $10^{-3}$ y $10^{-4}$ pies/día.

# Abstract

The southern sector of the Llanos Basin in Colombia has been identified as a basin where the hydrodynamic flow has influenced the potential of hydrocarbon storage and production. In this area the hydrodynamic flow coincides with a province of heavy and extra-heavy crude oils, which has hypothesized for this area, a critical condition that decreases the potential for hydrocarbon retention by the effect of hydrodynamic flow and the geochemical nature of the fluids. This work provides a comprehensive view to describe the impact of regional hydrodynamic flow on retention of the heavy oil accumulations present in the reservoirs that are part of the most important regional flow unit identified in the Southern Llanos Basin. The *Basal Flow Unit (BFU)* constitutes a basin-scale flow unit that hydraulically and laterally connects rocks from the Cretaceous (west) to the Oligocene (east) and extends from the basin's southwestern margin up to hundreds of kilometers within the Llanos foreland basin, and whose main water recharge zone has been identified towards the eastern flank of the Serranía de la Macarena. To understand the impact of the physicochemical properties of the fluids, we analyze the relationship between hydraulic data and the main characteristics of the fluids present in the BFU, and their spatial distribution on the present-day configuration of this flow unit. This analysis integrated information from hydraulic heads, SARA analysis (Saturates, Aromatics, Resins, and Asphaltenes), Whole Oil Gas Chromatography analysis, API-gravity, and oil densities. In addition, hydrochemical analysis of the primary ions and isotopic analysis ($\delta^{18}O$ and $\delta D$) was performed in groundwater samples from the BFU, which was integrated with deep resistivity data measured in producing and exploratory oil wells in the area. The new isotopic analyzes of this study ($\delta^{18}O$ and $\delta D$), and data from previous studies, allowed establishing the Local Meteoric Water Line (LMWL) for the Llanos basin. The $\delta^{18}O$ and $\delta D$ values of the groundwater samples follow the Local Meteoric Water Line proposed for the Llanos basin, supporting the presence of meteoric waters in the Basal Flow Unit and whose influence it extends from the recharge zone to more than 300 km east of the basin. The results allowed identifying the southwestern corner of the southern Llanos Basin as the area with the highest hydrodynamic flow impact, and therefore, the area with the least potential for hydrocarbon retention, attributing as the main causes: 1) the proximity to recharge areas, and 2) the low contrast of fluids densities (freshwaters and highly biodegraded heavy crude oils), implying high Tilt Amplification Factor (TAF) values. Furthermore, gradual changes in resistivities and ions concentration in groundwaters suggest the eastern flank of the Serranía de la Macarena as the main recharge zone of meteoric waters into the BFU. Finally, numerical simulation techniques were used to analyze the behavior of hydrocarbon drainage under hydrodynamic conditions, obtaining a first approximation to the average linear groundwater flow velocities between $10^{-3}$ and $10^{-4}$ ft/day.

# 1. INTRODUCCIÓN

En el contexto de la industria petrolera en Colombia, se visualiza un riesgo a corto y mediano plazo atribuido a los bajos índices de reposición de reservas de hidrocarburos de las últimas décadas. Una de las cuencas más prolíficas y exploradas en Colombia corresponde a la cuenca de los Llanos de donde proviene aproximadamente una cuarta parte de la producción actual de petróleo del territorio nacional. Sin embargo, de acuerdo con los resultados exploratorios obtenidos en los últimos años, donde los nuevos descubrimientos han estado limitados, se identifica la necesidad de mejorar el entendimiento de los factores que han controlado la acumulación y producción de hidrocarburos en la cuenca de Llanos, en especial hacia el sector sur de la cuenca en donde el potencial energético está asociado principalmente a la presencia de aceites crudos pesados y extrapesados.

Aunque la cuenca de Llanos es una de las cuencas sedimentarias más productivas de Colombia, algunas evidencias previamente reportadas muestran que las acumulaciones y la producción de hidrocarburos en la cuenca se encuentran influenciadas por la variable hidrodinámica del sector. Si bien existen evidencias de la influencia del régimen hidrodinámico en la cuenca de los Llanos, es necesario conocer la configuración de la unidad de flujo regional por donde el agua es transportada desde superficie hasta cientos de kilómetros hacia el *forebulge* de la cuenca, y así mismo, definir el impacto de este flujo hidrodinámico en el potencial de retención de hidrocarburos en estructuras previamente cargadas, considerando las características fisicoquímicas de los crudos y las aguas subterráneas del área. Adicionalmente, conocer el grado de influencia de las aguas meteóricas en la unidad de flujo regional y su relación con las zonas de recarga hídrica del sistema, permite identificar las áreas que representen el mayor riesgo de retención de hidrocarburos del sector sur de la cuenca de Llanos.

La presente investigación planteó resolver las siguientes preguntas para entender el fenómeno del flujo hidrodinámico y sus efectos en las acumulaciones de hidrocarburos del sector sur de la cuenca de los Llanos:

- ¿Cómo se relacionan las características físicas y químicas de los fluidos presentes en el área con el potencial de acumulación de hidrocarburos considerando la condición hidrodinámica?

- ¿Cuáles son las zonas de mayor influencia del régimen hidrodinámico y cómo ha afectado en el potencial de acumulación de hidrocarburos?

- ¿Cómo está conformada la unidad de flujo por la cual tiene lugar el tránsito de aguas subterráneas en el sistema hidrodinámico?

Por su parte, la hipótesis de investigación principal plantea que las acumulaciones de hidrocarburos en el sector sur de la cuenca de Llanos han estado controladas por la fuerza hidrodinámica y las características fisicoquímicas de los fluidos presentes en el área.

Producto de la investigación fueron sometidos dos manuscritos que resumen los resultados de la caracterización del sistema hidrodinámico del sector sur de la cuenca de Llanos. El primero de ellos, el cual será desplegado en el **Capítulo 2**, es titulado "***Implications of Groundwater Flow on Preservation of Heavy and Extra-Heavy Oil Accumulations in Southern Llanos Basin, Colombia***", y se enfoca en la descripción del fenómeno hidrodinámico a nivel regional, mostrando la extensión y configuración actual de la Unidad de Flujo Basal, por donde el flujo de aguas subterráneas tiene lugar desde superficie hasta el subsuelo en el sector sur de la cuenca de Llanos. Así mismo, se presentan las características fisicoquímicas de los fluidos presentes en esta Unidad de Flujo Basal (i.e., agua y aceites crudos) y se evalúa el impacto que la interacción de estos fluidos ha tenido en el potencial de retención de hidrocarburos del área. De igual manera se describen los cambios regionales en las concentraciones de los principales iones en las aguas subterráneas reconocidas sobre la Unidad de Flujo Basal, lo cual integrado con datos de resistividades del agua de formación medidos en pozos, permite relacionarlos con las principales zonas de recarga que han sido identificadas en el sector sur de Llanos. Finalmente, se proponen velocidades lineales promedio del flujo de aguas subterráneas en un área del sector sur de Llanos, las cuales fueron estimadas a partir de técnicas de simulación numérica, utilizando como restricción principal del modelo numérico los datos de la inclinación del contacto agua-aceite observada en un campo petrolero del área, las condiciones PVT (Pressure-Volume-Temperature) de los fluidos y las características petrofísicas de la Unidad de Flujo Basal hacia dicho sector.

Los análisis incluidos en este manuscrito ayudan a explicar el bajo potencial de acumulación y producción de hidrocarburos evidenciado hacia la esquina suroccidental de la cuenca de los Llanos, cerca de la Serranía de la Macarena. Este bajo potencial de retención de hidrocarburos se atribuye principalmente a la proximidad a la zona de recarga de agua del sistema hidrodinámico (frente oriental de la Serranía de la Macarena) y al bajo contraste de densidades entre el agua y el crudo, lo

que ha favorecido el drenaje de acumulaciones de crudo previamente cargado. A pesar de que la mayor parte de la cuenca afectaría negativamente a la Unidad de Flujo Basal debido al flujo de agua subterránea, las trampas hidrodinámicas tipo *down-dip* representan una alternativa de trampas a explorar con mayor probabilidad de éxito.

El segundo artículo descrito en el **Capítulo 3**, es titulado "***Decoding of Groundwater Recharge in Deep Aquifers of Foreland Basins Using Stable Isotopes ($\delta^{18}O$ and $\delta D$), and Anion-Cation Analysis: A Case Study in the Southern Llanos Basin, Colombia***", y describe la relación existente entre las zonas de recarga hídrica del sistema acuífero profundo del sector sur de la cuenca de Llanos y la complejidad estructural del frente de deformación que limita el borde suroccidental la cuenca, en las áreas de influencia de la Cordillera Oriental y la Serranía de la Macarena. Así mismo, se evalúa regionalmente el comportamiento isotópico e hidroquímico de las aguas subterráneas reconocidas en la Unidad de Flujo Basal, a partir de análisis de isótopos estables de $\delta^{18}O$ - $\delta D$, y análisis de los principales aniones y cationes de las aguas subterráneas del sector ($HCO_3$, $CO_3$, $SO_4$, Cl, Na, K, Ca, Mg). Los análisis isotópicos a su vez incluyeron muestras de las principales fuentes hídricas superficiales del sector sur de la cuenca del Río Orinoco, los cuales fueron integrados con análisis previamente reportados del área para construir de la Línea de Agua Meteórica Local de Llanos. Estos resultados fueron contrastados con la huella isotópica de las aguas subterráneas tomadas sobre la Unidad de Flujo Basal para así evaluar el grado de influencia de las aguas meteóricas en los principales reservorios de petróleo del área de estudio. De igual forma, a partir de las concentraciones isotópicas de las aguas subterráneas, fueron definidos rangos probables de altitud relacionados con la proveniencia de las aguas que actualmente están siendo reconocidas en la Unidad de Flujo Basal. Finalmente son presentadas las facies hidroquímicas dominantes en las aguas subterráneas del sector sur de la cuenca de Llanos y los cambios relativos en la concentración de iones a lo largo de la Unidad de Flujo Basal, relacionados con el grado de influencia de las aguas meteóricas desde las zonas de recarga hasta las partes más distales donde el sistema hidrodinámico está actuando.

# 2. APORTES A LA INVESTIGACIÓN-1

## Implications of Groundwater Flow on Preservation of Heavy and Extra-Heavy Oil Accumulations in Southern Llanos Basin, Colombia.

Ricardo Andrés Gómez-Moncada[a], Andrés Mora[b], Marcela Jaramillo[c], Mauricio Parra[d], Andrés Martínez[e], Henry Mayorga[e], Jorge Sandoval-Muñoz[a], Arcadio Cuy-Cipamocha[e], Davis Suárez[a], Jose Sandoval-Ruiz[a], Rolando Ramírez[e], Robert Márquez[a], Ricardo Bueno[a].

[a]*Innovation and Technology Center of ECOPETROL S.A - ICP, Santander, Colombia.*

[b]*Ecopetrol Oleo E Gas Do Brasil Ltda, Rio de Janeiro, Brasil.*

[c]*EAFIT University, Medellín, Colombia.*

[d]*Institute of Geosciences, University of Sao Paulo, Brasil.*

[e]*TIP Colombia, Santander, Colombia.*

Corresponding author (ricardoandres.gomez@ecopetrol.com.co)

Corresponding author address: Ricardo Gómez-Moncada, Innovation and Technology Center of ECOPETROL S.A - ICP, Km. 7 via Piedecuesta, Santander, Colombia.

# Abstract

The southern sector of the Llanos Basin in Colombia is a heavy and extra-heavy crude oil province where it has been hypothesized that hydrodynamic flow has influenced the potential of hydrocarbon storage and production. In this area, the hydrodynamic flow and the geochemical nature of the fluids are thought to decrease the potential for hydrocarbon retention. This work provides a comprehensive view on the impact of the regional hydrodynamic flow on the retention of the heavy oil accumulations present in the reservoirs that are part of the most important regional flow unit identified in the Southern Llanos Basin. The *Basal Flow Unit (BFU)* constitutes a basin-scale flow unit that hydraulically and laterally connects rocks from the Cretaceous (west) to the Oligocene (east) and extends from the basin's southwestern margin up to hundreds of kilometers within the Llanos foreland basin, and whose main water recharge zone has been identified towards the eastern flank of the Serranía de la Macarena. To understand the impact of the physicochemical properties of the fluids on hydrocarbon retention, we analyze the relationship between hydraulic data and the main characteristics of the fluids present in the BFU as well as their spatial distribution. This analysis integrated information from hydraulic heads, SARA analysis (Saturates, Aromatics, Resins, and Asphaltenes), Whole Oil Gas Chromatography analysis, API-gravity, and oil densities. In addition, hydrochemical analyses of the primary ions were performed in groundwater samples from the BFU, which was integrated with deep resistivity data measured in producing and exploratory oil wells in the area. The results allowed identifying the southwestern corner of the southern Llanos Basin as the area with the highest hydrodynamic flow impact, and therefore, the area with the least potential for hydrocarbon retention. We attribute the main causes to: 1) the proximity to recharge areas, and 2) the low contrast of fluids densities (freshwaters and highly biodegraded heavy crude oils), implying high Tilt Amplification Factor (TAF) values (10 – 100). In addition, the highest values of hydraulic heads (200 – 400 m), groundwater with the lowest ion concentrations (up to < 5 ppm $Cl^-$), highly biodegraded crude oils, and the presence of poorly developed geological structures with low dip angles occur in this area, which allows us to interpret that the water washing process has decreased the hydrocarbon retention potential for this sector of the Llanos basin. Furthermore, gradual changes in resistivities (decreasing eastward) and ions concentration (increasing eastward) in groundwaters suggest the eastern flank of the Serranía de la Macarena as the main recharge zone of meteoric waters into the BFU. Finally, numerical simulation techniques were used to analyze the behavior of hydrocarbon drainage under hydrodynamic conditions, obtaining a first approximation to the average linear groundwater flow velocities between $10^{-3}$ and $10^{-4}$ ft/day.

## 1. Introduction

Basins with oil production potential are generally analyzed under hydrostatic conditions, which implies that the fluids are not affected by groundwater flow after the migration and storage of hydrocarbons in the reservoirs. However, a hydrodynamic effect occurs when groundwater recharge processes favor the influx of water from the surface to the deep oil or gas reservoirs. In these cases, under specific properties of the fluids (e.g., water and hydrocarbon densities), the entrapment of hydrocarbons could be affected, being partially or completely drained from a particular geologic structure. This type of entrapment under hydrodynamic conditions can create oil or gas accumulations in anticlinal, homoclinal, or even synclinal structures (Hubbert 1953, 1967).

According to Hubbert´s concepts (Hubbert 1940, 1953), an accumulation of hydrocarbons under hydrodynamic conditions will produce a tilt of the fluid interface (oil-water or gas-water). The tilt (θ) of the Oil-Water-Contact (OWC) or Gas-Water-Contact (GWC) will depend on the hydraulic gradient, referred to as the slope of the potentiometric surface $dh_w/dx$, and the contrast between the densities of the water and the hydrocarbon, $\rho_w/(\rho_w - \rho_o)$, present in the reservoirs. This density relationship is described by Hubbert (1953) as the *Tilt Amplification Factor (TAF)* and corresponds to an amount that amplifies n-times the slope of the potentiometric surface. The estimation of the angle of inclination of oil-water or gas-water interfaces is given by the following equation (Hubbert, 1953):

$$Tan\theta = \frac{\rho_w}{\rho_w - \rho_o} \frac{dh_w}{dx} \qquad Ec.1$$

where θ is the tilt angle of the oil-water or the gas-water interface, $\rho_w$ is the density of the water, $\rho_o$ is the density of the oil or the gas, and $dh_w/dx$ is the slope of the potentiometric surface of the water in the horizontal direction (x).

The values of the *Tilt Amplification Factor (TAF),* expressed as $\rho_w / (\rho_w - \rho_o)$, tend towards infinity as $\rho_o$ increases, being one (1) the lowest possible value. Typical TAF values range from about 1 and 2 for gas reservoirs and about 7 and 15 for oil reservoirs (Hubbert, 1953; Dahlberg, 1994). Bearing in mind that the tilt of the interface between hydrocarbon and water is a sensitive relationship of densities (*TAF*), the most critical scenario is represented by heavy and extra-heavy crude oils.

Different driving mechanisms for groundwater flow have been described for basins around the world (Hitchon, 1969; Bond, 1972; Coustau, 1977; Chiarelli, 1978; Cathles, 1990; Bredehoeft et al., 1992; Deming, 1994; Villegas et al., 1994; Wolover et al., 2015; Mora et al., 2019a). Similarly, the geochemical relationship between the type of waters and type of hydrocarbons has been broadly studied (Washburn, 1914; Mills and Wells, 1919; Palmer, 1924), as well as its importance to facilitate the development and production of oil and gas fields, and hydrocarbon exploration (Coustau, 1977).

In Colombia, the presence of hydrodynamic flow in the Llanos Basin has been documented in previous research, indicating a strong correlation between high values of hydraulic heads (Hw), low ions concentration in the formation waters, and the proximity to elevated areas as the Serranía de la Macarena (**Figure 1**) and the Eastern flank of Eastern Cordillera (e.g. Villegas et al., 1994; Bachu et al., 1995; González-Uribe et al., 2007; Person et al., 2012; González-Penagos et al., 2014; González-Penagos et al., 2017; Mora et al., 2019a). In addition, this correlation has been examined using stable isotope analysis (δ18O and δD), which has confirmed the influence of meteoric waters that have reached the hydrocarbon-producing units from the surface, especially in the southern Llanos Basin (González-Uribe et al., 2007; González-Penagos et al., 2014). Furthermore, this influence has been observed from the western boundary towards the foreland of the Llanos Basin. It appears to be controlled by the deformation front's structural characteristics that limit the basin to the west, finding the most favorable connection conditions between surface and subsurface towards the Serranía de la Macarena sector (Mora et al., 2019a; Arias et al., 2018). In addition,

different authors have reported the correlation between high hydraulic head values, low water salinities, and the presence of biodegraded heavy crude oil in both the Llanos basin (e.g., Villegas et al., 1994; Bachu et al., 1995; Person et al., 2012; Mora et al., 2019a) and the Putumayo basin (e.g., Wolaver et al., 2015). Likewise the relationship between geothermal gradients and hydrodynamic flow in the Llanos basin has also been discussed (e.g., Bachu et al., 1995; Person et al., 2012; Mora et al., 2019a), finding that anomalies associated with low geothermal gradients seem to be more related to the thermal blanketing effect of the Neogene deposition and the type of basement underlying the Mesozoic-Cenozoic rock units, than to the effect of the flow of meteoric waters (Mora et al., 2019a).

On the other hand, although some Cretaceous reservoirs are related to marine and estuarine deposition (González-Penagos et al., 2014; Caballero et al., 2015), which are environments influenced by seawater, most of the formation waters from the southern Llanos Basin have been recognized as fresh and brackish waters (González-Penagos et al., 2014), suggesting dilution of connate water by meteoric waters associated with a hydrodynamic system (Villegas et al., 1994; Person et al., 2012; González-Penagos et al., 2014).

The crude oils in the Llanos Basin have a significant variation in their chemical composition and physical characteristics. They present a lower API gravity (< 10°API) in the southern Llanos Basin (Garcia et al., 2015, Sánchez et al., 2015), which has been mainly related to biodegradation processes (Dzou et al., 1999; Springer et al., 2010; Person et al., 2012; Garcia et al., 2015, Sánchez et al., 2015; Mora et al., 2019b). In addition, mixing processes of oil with different geochemical signatures associated with variations in the thermal histories of crude oils have also been recognized. (Springer et al., 2010).

This research focuses on the southern Llanos Basin, where a province of heavy and extra-heavy oil with hydrodynamic influence has been recognized. The main objective of this study is to describe the relationship between the hydrodynamic flow and the potential for the accumulation and production of hydrocarbons in the southern Llanos Basin, and therefore, to establish the greatest impact areas limiting hydrocarbon exploration. In addition, we present new data about the characteristics of the fluids (crude oils and groundwaters) and their impact on the preservation of hydrocarbon accumulations. Moreover, extreme TAF conditions have been recognized, limiting the retention of hydrocarbons in some sectors of the study area due to the low contrast of densities.

We study the relationship between the trend of the potentiometric surface and geochemical characteristics of crude oils in the area, integrating information from SARA analysis, whole oil chromatography, API-gravity, and densities from PVT analysis (Pressure -Volume-Temperature). In addition, we use information from anion-cation analyses of groundwater samples and deep resistivity data from wells logs that reached the Basal Flow Unit to document the lateral changes throughout the basin and relate them to the recharge zones of the system and geochemical data. Finally, we use numerical simulation techniques to evaluate the behavior of oil accumulations under hydrodynamic conditions, and thus have a first approximation of the average linear groundwater flow velocities in the study area. The simulations were performed in the black oil simulator IMEX (from Computer Modeling Group Ltd.), evaluating the PVT conditions of the fluids documented in the region and the petrophysical properties of the Basal Flow Unit in the southern Llanos Basin.

The recognition of the regional Basal Flow Unit as the main flow unit of the hydrodynamic system of the southern Llanos Basin, and the understanding of the impact of the fluids present in it improve our knowledge about the effect of hydrodynamic systems in areas of heavy oil in foreland basins and provide a starting point to delimit and have a better approximation to the hydrocarbon potential of the area.

## 2. Regional Setting

### *2.1. Geology*

The study area corresponds to the southern Llanos Basin located in eastern Colombia (**Figure 1**). The Llanos basin constitutes the foredeep of the modern Colombian foreland basin and is bounded by the Eastern Cordillera fold-thrust belt to the northwest, the Serranía de la Macarena to the southwest (**Figure 1**), and the Precambrian basement of the Guyana Shield to the east (Moreno-Lopez and Escalona, 2015).

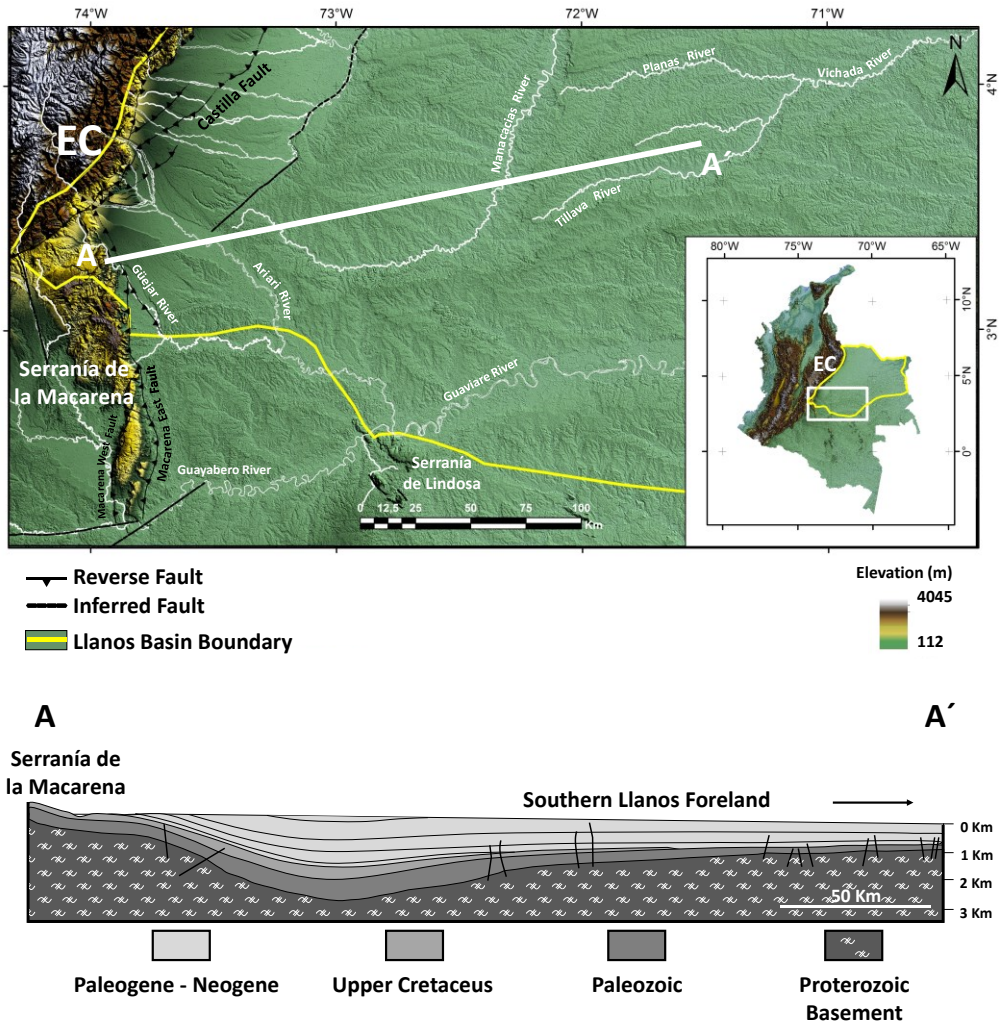


**Figure 1**. (Above) Digital elevation model (SRTM) of the study area in the southern Llanos Basin in Colombia. EC: Eastern Cordillera. (Below) An illustrative cross-section A-A´ shows Southern Llanos Basin's regional configuration from the Serranía de la Macarena to the forebulge.

In general, the sedimentary record of the Llanos Basin corresponds to siliciclastic rocks from the lower Paleozoic (Güejar Group), Upper Cretaceus (Une, Gachetá and Guadalupe Formations), Paleogene (Barco, Cuervos, Mirador Formations and the basal units of the Carbonera Formation), Neogene (Carbonera, León and Guayabo Formations) and Quaternary deposits (Reyes-Harker et al., 2015; Mora et al., 2019a) (**Figure 1**).

One of the main structural features of the southern Llanos Basin is the presence of the Serranía de la Macarena, which constitutes an important surface topographic expression towards the southwest, with altitudes that vary approximately between 800 m.a.s.l. and 1600 m.a.s.l. The Serranía de la Macarena is constituted by Proterozoic metamorphic basement (Trumpy, 1943; Harrington and Kay, 1951; Ibañez-Mejía et al., 2011) and a sedimentary cover that includes siliciclastic rocks from the Paleozoic, Mesozoic, and Cenozoic Eras (Servicio Geológico Colombiano, 2015). Structurally, the Serranía de la Macarena is bounded to the west and east by high-angle reverse faults, which have their detachment on the Proterozoic basement with some back thrust propagating westwards (Servicio Geólogico Colombiano 2015; Arias et al., 2018). The structural configuration related to the reverse faults at the eastern boundary of the Serranía de la Macarena (Guejar River Fault, Macarena East Fault) has favored the outcropping of Paleogene and Cretaceous strata that are reservoir units in the basin (Arias et al., 2018; Mora et al., 2019a). Thus, eastern flank of the Serranía de la Macarena constitutes the primary source of water recharge from southern Llanos, considering the connection observed between surface and subsurface rocks (Arias et al., 2018; Mora et al., 2019a). From those outcropping areas in the Serranía de la Macarena, a basin-scale syncline is configured, extending northeast and east towards the foreland along the southern sector of the Llanos Basin, where the Basal Flow Unit of the southern Llanos Basin is formed. (**Figure 2**).

### *2.2. Hydroclimatology and Hydrogeology*

The southern Llanos Basin is located within the Orinoco River hydrographic area, which gathers the main drainages originating from the eastern flank of the Eastern Cordillera and the Serranía de la Macarena, and which ultimately flow northward to the Caribbean Sea. The precipitations in the area increase from the eastern Orinoco River basin (2000 mm / yr to 3500 mm / yr) toward the Eastern Cordillera (up to 7000 mm / yr) (Arango et al., 2012). This increase in precipitation is favored by the orographic barrier effect of the Eastern Cordillera on the air masses transporting moisture from the Atlantic Ocean, which favors high rainfall along the Eastern Colombian Andes (Rozanski et al., 1993; Mora et al., 2008; Saylor et al., 2009).

The stratigraphic units that made up the deep aquifer system analyzed and described as the Basal Flow Unit (BFU) in this study, in turn, have shown oil potential in the area. The BFU, which onlaps Paleozoic strata to the east of the Llanos foreland basin, presents two stratigraphic configurations that differentiate the vertical hydraulic connection of the west sector of the study area (**Figures 2**, **3 and 4**). Within the southwestern sector, towards the Serranía de la Macarena, the BFU comprises rocks from the Une Formation (Upper Cretaceous) and the Mirador Formation (Eocene). These rocks are connected laterally and hydraulically to the East with rocks from the Oligocene (Carbonera Formation) subcropping at the most distal part of the foreland of the southern Llanos Basin (**Figure 2**). This configuration towards the southwestern sector at the same time favors the vertical hydraulic connection between the Une Formation and the Mirador Formation due to the partial or total absence of the aquitard of the Gachetá Formation (Upper Cretaceous) (e.g., Reyes-Harker et al., 2015) (**Figure 2**).

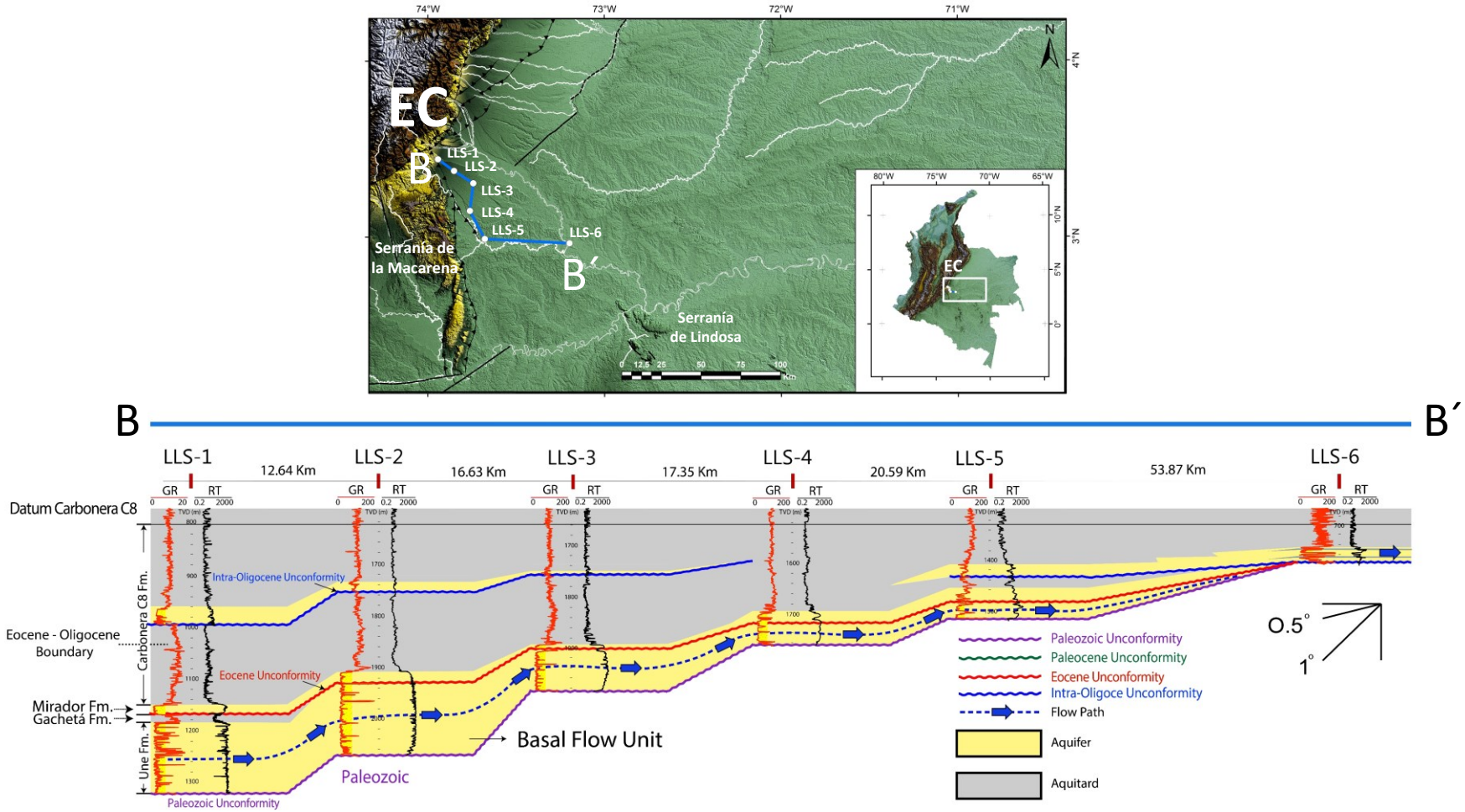


**Figure 2**. Stratigraphic correlation B-B´ of the southern Llanos Basin showing the configuration of the Basal Flow Unit toward the southwest sector showing thinner aquitard of the Gachetá Formation. Gamma Ray (GR) and Resistivity (RT) logs are presented per well. EC: Eastern Cordillera.

On the other hand, towards the northwestern sector of the study area, the BFU is composed of sandstones of the Une Formation, isolated from younger stratigraphic units of the Paleocene (Barco Formation) and Eocene (Mirador Formation) by a thick aquitard corresponding to the Gachetá Formation (**Figures 3 and 4**). As to the southernmost sector, the Basal Flow Unit in the northwestern sector extends to the East, connecting with younger rocks towards the foreland of the southern Llanos Basin (**Figure 3**).

On a regional scale, the aquitards confining the BFU in the southern Llanos Basin are related to mudstones and claystones of low permeability and low effective porosity from the Gachetá (Upper Cretaceous) and the Carbonera (Eocene and Oligocene) formations in the westernmost sector, and the Carbonera (Eocene and Oligocene) and León (Miocene) formations towards the eastern and central sectors (e.g., Reyes-Harker et al., 2015) (**Figures 2, 3 and 4**).

### *2.3. Geochemistry of Oils*

The main potential for accumulation and production of hydrocarbons in the southern Llanos heavy and extra heavy oil province is linked to the sandstones from the Upper Cretaceous (Une and Guadalupe formations), Paleocene (Barco Formation), Eocene (Mirador Formation) and Oligocene (Carbonera Formation) units. The geochemistry of crude oils from the Llanos Basin is complex, considering the processes of thermal maturity, alteration, and mixing of crude oils that have been recognized in the area (Dzou et al., 1999; Springer et al., 2010; Person et al., 2012; García et al., 2015).

For the Llanos Basin, the presence of crude oil generated mainly from source rocks of marine origin, and, to a lesser extent, terrigenous origin has been confirmed (Ramon et al., 2001; Cortes et al., 2010; García et al., 2015).

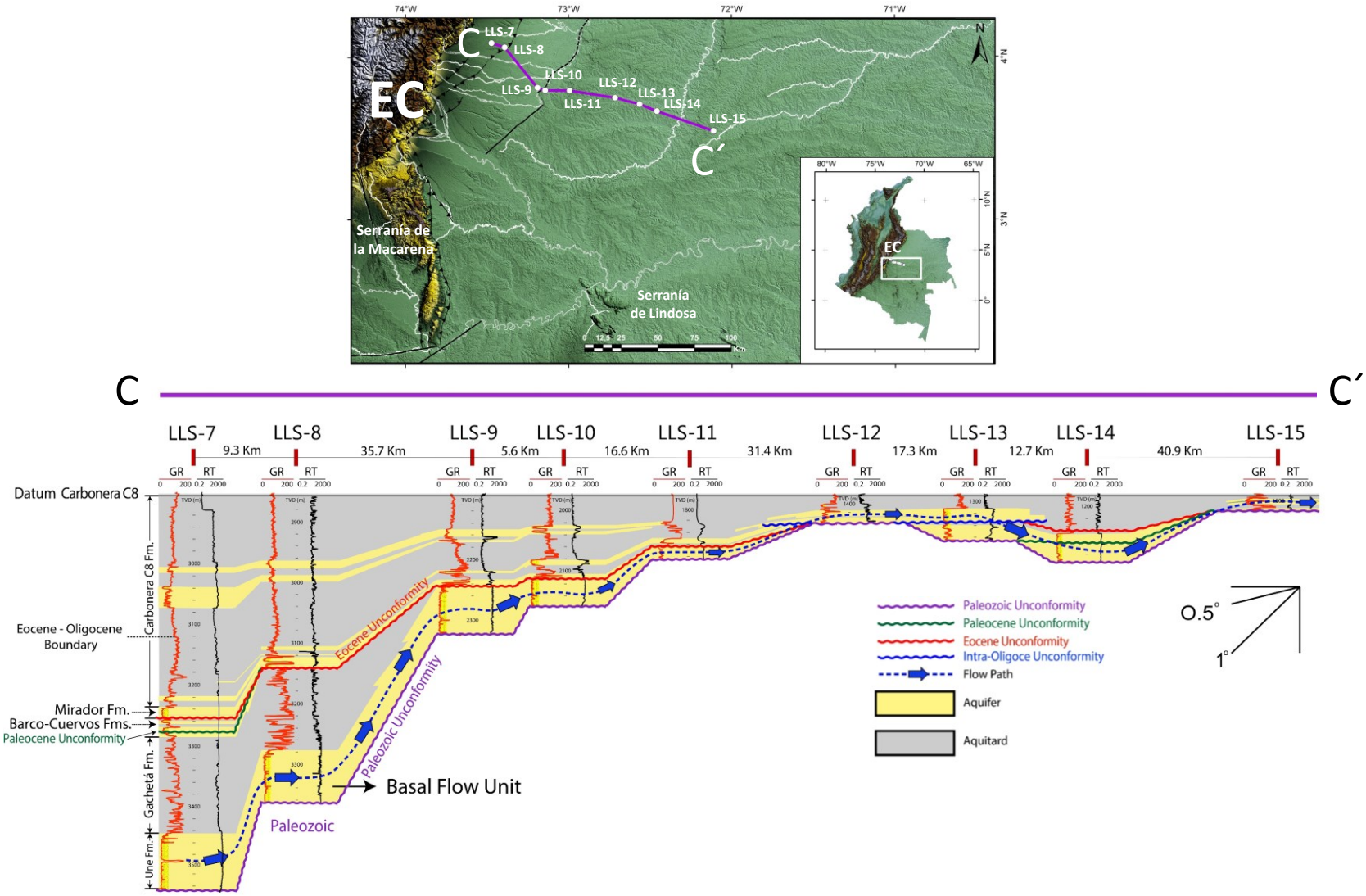


**Figure 3**. Stratigraphic correlation C-C´ of the southern Llanos Basin showing the configuration of the Basal Flow Unit toward the northwestern and thicker aquitard of the Gachetá Formation. Gamma Ray (GR) and Resistivity (RT) logs are presented for all wells. EC: Eastern Cordillera.

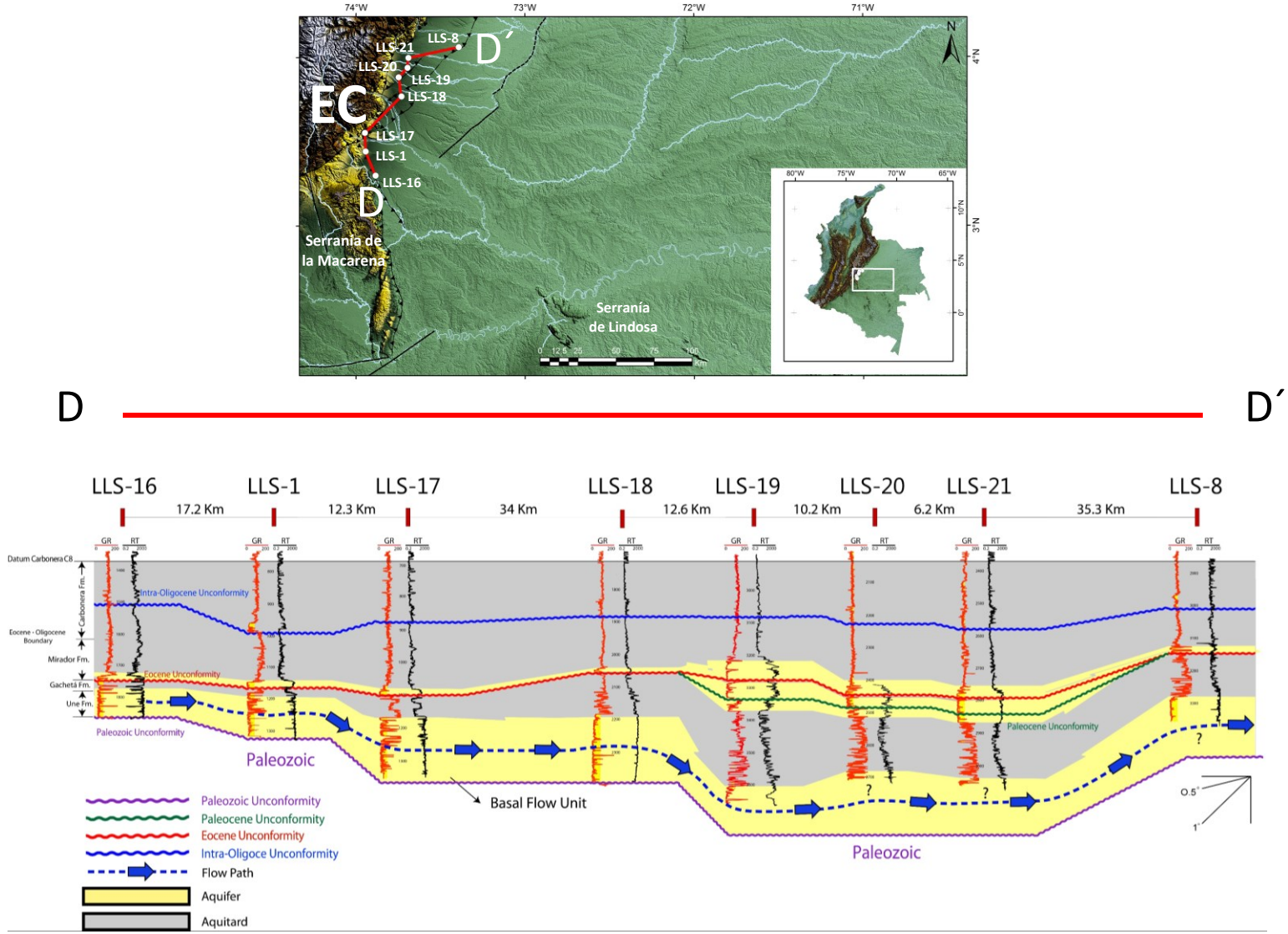


**Figure 4**. Stratigraphic correlation D-D´ of the southern Llanos Basin showing the configuration of the Basal Flow Unit toward the southwestern Llanos basin. Gamma Ray (GR) and Resistivity (RT) logs are presented for all wells. EC: Eastern Cordillera.

Toward the southern Llanos Basin, crude oils of marine origin are recognized. They have the lowest API-gravities and the highest biodegradation intensity in the Llanos Basin, with evident depletion of *n*-paraffins in the gas-chromatograms and high proportions of nitrogen, sulfur, and oxygen (NSO-compounds) (Peters et al., 2005; García et al., 2015). This biodegradation process is mainly attributed to longer residence times of the hydrocarbons in the reservoirs, at temperatures lower than 80° C (García et al., 2015) due the effect of shallower and cooler conditions in the southern Llanos Basin (Hermeston and Nemcok, 2013; García et al., 2015; Sánchez et al., 2015; Mora et al., 2019b).

## 3. Methods

In this work, we integrated information from oil-producing and exploratory wells drilled in the area to analyze the impact of the hydrodynamic system on the hydrocarbon accumulation potential of the southern Llanos. The integrated information included historical data of formation pressure, fluid analysis (crude oils and formation water samples), and electrical well logs. Likewise, new data on the geochemical characteristics of the crude oils and the hydrochemical characteristics of the groundwater were carried out in the laboratories of the Innovation and Technology Center of Ecopetrol S.A. In addition, numerical simulation models were built considering the fluids and petrophysical properties of the Basal Flow Unit. These dynamic models allowed the evaluation of the dynamic behavior of the typical fluids simulating a hydrodynamic condition.

### *3.1. Hydraulic Heads*

The total hydraulic heads (Hw) were estimated from pressure data acquired during DST´s (Drill Stem Tests) or MDT (Modular Dynamic Formation Tester) tests carried out in wells. To calculate the hydraulic heads (Hw) based on the previous information, we used the following **Equation (2)**:

$$Hw = Z + \frac{P}{\rho g} \quad Ec.2$$

where *Hw* is the hydraulic head (meters), *Z* is the elevation with respect to sea-level (0 TVDSS) of the point at which the pressure is measured (meters), *P* is the pressure at the point of measurement (Pa), $\rho$ is the density of water (1000 Kg/m$^3$), and $g$ is the gravitational acceleration (9.8 m/s$^2$). The selected data for the analysis included 43 wells where the original pressure information was acquired on the Basal Flow Unit to obtain the general view of the potentiometric surface and thus evaluate the regional flow pattern of water through the southern Llanos Basin.

### *3.2. Hydrochemistry of Formation Waters*

The hydrochemical characterization of the groundwater of the southern Llanos Basin included analysis of the main anions and cations (HCO3, CO3, Cl, SO4, Na, K, Ca, and Mg) in 93 samples of formation waters taken from oil-producing wells (63) and exploratory wells (24). The groundwater samples for analysis of the main metals were preserved with HNO3 (up to pH<2). All samples were refrigerated (<6°C) from the moment of sampling until they arrived at the laboratory. Based on these results, Stiff diagrams were made using the Python code available on the Gidahatari website (Montoya, 2016) to observe the variations across the study area and thus relate the ions concentration in the waters with the recharge zones identified in the study area.

### *3.3. Geochemistry of Crude Oils*

The geochemical analysis included whole oil Gas Chromatography with Flame Ionization Detection (GC-FID) to obtain the concentrations of the *n*-alkanes hydrocarbons, mainly in the range from *n*-C5 to *n*-C42. The analysis included crude oil samples from the westernmost sector close to the Serranía de la Macarena, and the central and eastern sectors of the foreland of the southern Llanos Basin, to observe the potential relationships between the hydrodynamic flow and the geochemical footprint

of the crude oils in the area. In turn, a total of 55 SARA analyses (Saturates, Aromatics, Resins and Asphaltenes) were included. This fractionation is based on the difference between the solubility and polarity of the four fractions: Saturates, Aromatics, Resins, and Asphaltenes (Fan et al., 2020).

To analyze this information and relate it with the geochemical data, we established the Compositional Trend Index (CTI) from the results of the fractions obtained from SARA analysis. The index was estimated by grouping the light fractions (Saturates + Aromatics) and the heavy fractions of the crude oils (Resins + Asphaltenes), and finally expressed as the sum of saturates and aromatics per the sum of resins and asphaltenes as shown in **Equation (3)**:

$$CTI = \frac{\%\ Saturates + \%\ Aromatics}{\%\ Resins + \%\ Asphaltenes} \quad Ec.3$$

The Compositional Trend Index (CTI) is a variation of the Colloidal Instability Index (CII) which is used for determining the asphaltene stability in crude oils (Asomaning & Watkinson, 2000; Asomaning, 2003). However, the CTI proposed in this study aims to identify the areas with the highest content of heavy fractions of crude oils and evaluate their relationship with biodegradation and hydrodynamic flow.

In addition, API-gravity data of crude oils (34 samples) and densities (30 samples) at reservoir conditions were integrated. This oil density information at reservoir conditions was used as the primary input for estimating the TAF values of the area. According to the low concentrations of anions and cations recognized in the Basal Flow Unit of the southern Llanos Basin, for the estimation of the TAF values, the density of the water was used as a constant value equal to 1 g/cm$^3$.

### *3.4. Resistivity Analysis*

Based on secondary information from electrical logs of exploratory and production wells drilled in the Basal Flow Unit, an analysis of deep resistivities (RT) was performed using information from 128

wells. The deep resistivity values attributed to the rock-water system were extracted from water zones, avoiding the influence of hydrocarbons. Once the water zone was defined, the deep resistivity, porosity (estimated from the density log), and temperature (T) well logs were used to estimate formation water resistivity (Rwa) values using the model proposed by Archie (1942), as described in **Equation (4)**.

$$R_w a = \Phi^m RT \qquad Ec. 4$$

where $R_w$ is the resistivity of the formation water (Ohm.m), $a$ is a dimensionless tortuosity factor, $\Phi$ is the effective porosity of the formation (fr), $m$ is the cementation exponent, and $RT$ is the true resistivity of the formation (ohm.m). In this study, the cementation exponent ($m$) is 1.8 and the tortuosity factor ($a$) is 1, according to the experimental measurements of formations resistivity factor that we have carried out in the Special Core Analysis Laboratory (SCAL) of the Innovation and Technology Center of Ecopetrol S.A., on core samples from sandstones of the Basal Flow Unit. This analysis was correlated with the concentrations of the main cations and anions of the groundwater samples and allowed us to evaluate their relationship with the recharge zones reported in the study area.

### *3.5. Numerical Simulation*

The numerical simulation allowed us to evaluate the dynamic interaction between the fluids present in the reservoirs under the hydrodynamic influence, including the features of the rocks and fluids. The properties considered in numerical models include effective porosity, permeability, relative permeabilities, water saturation, fluid densities, pressure, and temperature. The dynamic models simulated different flow velocities scenarios with different hydrocarbon densities and simulation times in geological scales up to 10 My.

2D and 3D grids were constructed for the numerical simulation. The simulations were performed using the black oil simulator IMEX of Computing Modeling Group LTD (CMG), which uses the finite difference method as a numerical solution in solving partial differential equations of flow in porous media.

A realistic 2D grid with 15,400 cells (areal cell size: 100 x 100 m) was constructed using, as the primary input, the information of an oil field that produces from the Basal Flow Unit. For this purpose, we used the inverse problem approach using numerical simulation. Thus, model parameters such as the average linear groundwater flow velocities were estimated from known data (e.g. fluid densities, petrophysical properties, structure geometry, thicknesses, and the OWC tilt of an oil field). The OWC tilt was used as the main constraint in the approximation of the groundwaters flow velocities in the Basal Flow Unit. The simulation was complemented with a sensitivity analysis considering variations in density (0.92 g/cm$^3$ - 0.95 g/cm$^3$), permeability (500 mD - 5000 mD), and the tilt of OWC (1° - 1.5°). In addition, a 3D grid was built. The model included a total of 105,000 cells (areal cell size: 100 x 100 m), with an average porosity of 20%, average permeability of 2000 mD, and oil density of 0.95 g/cm$^3$. This 3D grid considered contiguous structures, separated approximately 1.25 km between them, where the behavior of the oil-water-contact of each structure was evaluated under down-dip and up-dip flow scenarios.

In all the models (2D and 3D), an initial equilibrium with the OWC at each structure's spill point was considered as the baseline scenario (Time 0 My). According to the reservoir conditions identified in the central part of the southern Llanos Basin, the temperature and pressure conditions considered in the models were approximately 200°F and 2,992 Psi, respectively (datum: -6,451 ft True Vertical Depth Subsea).

# 4. Results

### *4.1. Hydraulic Heads*

The hydraulic head values estimated from pressure data in different wells ranged from 84.41 m to 490 m, with the highest values and hydraulic gradients of the potentiometric surface occurring towards the western sector of the study area, close to the Serranía de la Macarena and Eastern Cordillera (**Table 1, Figures 5 and 6**). The dominant trend of the potentiometric surface defines a general NNE dipping surface (**Figure 5**) with local perturbations in the southwestern sectors of the study area presumably related to the proximity of the mountains and potential recharge zones. The data available from the easternmost wells also suggest a more gently dipping trend eastwards in the easternmost sector of the study area (**Figure 5**). The described general tendency suggests the importance of the structural relief in the basin controlling the spatial patterns of the hydraulic heads (**Figure 6**).

### *4.2 Geochemistry of oils and TAF*

The densities of crude oil range between 0.90 g/cm$^3$ and 0.99 g/cm$^3$, and more than 70% of the data show density values greater than 0.95 g/cm$^3$ (**Table 2**). According to these densities, the Tilt Amplification Factor (TAF) values range from 10 to 100, where more than 70% of the data corresponds to TAF values greater than 20 (**Table 2, Figure 7**). The API-gravities recognized in the crude oils in the study area range between 4.9° API and 40.2° API. However, more than 94.2% of the integrated data corresponds to API gravities lower than 20° API, related to heavy and extra-heavy oil (**Table 3, Figure 8A**). The highest API-gravity values are associated with wells from the northwestern sector of the study area, toward the west of the Castilla Fault, where the production comes mainly from Cretaceous (Une and Gachetá formations), and the Basal Flow Unit deepens (**Figure 8A**).

The Compositional Trend Index (CTI) values estimated from SARA analysis carried out in crude oil samples range from 0.1 to 9, where more than 83.6% of the data report CTI values lower than 3, which are related to heavy crude oils of high density (**Table 4, Figure 8B**). The fraction of Saturates ranges between 3.6% and 71%, Aromatics between 4.5% and 37.1%, Resins between 6% and 41.3%, and 4% and 41.6 for Asphaltenes.

Based on the results from whole oil chromatography, crude oils from the southern Llanos Basin show a low abundance of both light and heavy *n*-paraffins, as well as pristane and phytane isoprenoids. A characteristic pattern in the biodegraded crude oils from the study area is defined by the lifting of the baseline, forming a UCM (Unresolved Complex Mixture), as observed in the great majority of chromatograms shown in **Figure 9**. However, the relatively higher abundance of light *n*-paraffins in some samples from the area suggests the occurrence of an oil recharge after the biodegradation process (i.e., refreshing), which slightly improves the quality of the crude oil.

***4.3 Anions and Cations in Groundwater***

Hydrochemical analysis in water samples from wells showed relatively low concentrations of the main cations and anions. The groundwater samples taken from different wells present a domain of mainly sodium bicarbonate and sodium chloride waters. The concentrations of bicarbonate range between 30.5 ppm to 2,120 ppm, 0 ppm to 120 ppm for carbonate, 0 ppm to 160 ppm for sulfate, and 4.1 ppm to 1,278 ppm for chloride. Cation concentrations ranged from 4.7 ppm to 1,589 ppm for sodium, 2.2 ppm 254 to 165 ppm for potassium, 0 ppm to 54 ppm for magnesium, and 0 ppm to 136 ppm for calcium (**Table 5, Figure 10**).

***4.4 Resistivity Analysis***

The Resistivity analysis show variations in average deep resistivity of the rock-fluid system (RT) between 3.41 Ohm.m and 8,600 Ohm.m for the Basal Flow Unit (**Table 6, Figures 11 and 12**). On the

other hand, the estimation of water formation resistivities (Rwa) reported values between 0.04 Ohm.m and 481.74 Ohm.m, where about 82% of the data presents values lower than 20 Ohm.m (**Table 6**). The average effective porosity estimated from density logs in sandy intervals of the Basal Flow Unit is 22%, where more than 87.5% of the data report values are greater than 15%. Finally, temperatures in intervals where the resistivities of the formation water were estimated vary between 30°C and 104.7°C.

### *4.5 Numerical Simulation*

The numerical simulation models allowed the sensitivity analysis of critical variables and the approximation of the groundwater flow velocities along the Basal Flow Unit. This evaluation was carried out under controlled scenarios of the fluid flow dynamics considering typical structures of the southern Llanos Basin.

From the 2D model that simulated a geological structure of an oil field located in the western sector of the Castilla Fault, whose main production comes from the Basal Flow Unit, the average linear groundwater flow velocities range between 0.00018 ft/day and 0.0086 ft/day, with an average value of 0.0023 ft/day (**Table 7, Figure 13**). The stabilization times to reach the final OWC inclination from equilibrium (0 My) ranged between 0.3 and 0.5 My, approximately. The stabilization times decrease at higher permeabilities, reaching hydrodynamic equilibrium sooner than when considering low permeabilities.

For the up-dip and down-dip hydrodynamic flow scenarios evaluated on the 3D grid, we observed a similar tilt of oil-water contacts in each structure but in the opposite direction if the same groundwater flow velocity and fluid-rock properties are considered (**Figure 14**). On the other hand, retention potential will favor down-dip scenarios, as reported by different authors (e.g. Hubbert, 1953; Dahlberg, 1994).

# 5. Discussion

The convergence between the regional hydrodynamic flow and the geochemical nature of the fluids present in the BFU has configured for the southern Llanos Basin a condition of particular interest to understand the hydrocarbon retention potential for the area. In this way, understanding the relationship between the physicochemical characteristics of the fluids present in the BFU, the flow of groundwater, and the zones that influence water recharge allows redefining and delimiting the area's oil potential.

### *5.1 Regional View of Southern Llanos Potentiometric Surface*

The highest values of hydraulic heads are identified in the wells near the Serranía de la Macarena, which has previously been proposed as the main recharge area of the deep aquifer systems in the southern Llanos Basin (Villegas et al., 1994; Bachu et al., 1995; Mora et al., 2019a). Although with lower magnitudes of hydraulic heads, similar behavior is observed towards the southernmost sector in proximity to the Serranía de Lindosa (**Figure 5**).

The flow direction shows regional west-east and southwest-northeast trends. Towards the eastern sector, a change in flow direction is interpreted northwesterly, whose trend has been reported in the eastern oil fields (Gomez et al., 2009; Mora et al., 2019a; Macellari, 2021). However, the absence of hydraulic heads data towards the easternmost part of the southern Llanos Basin limits understanding of the phenomenon in that sector.

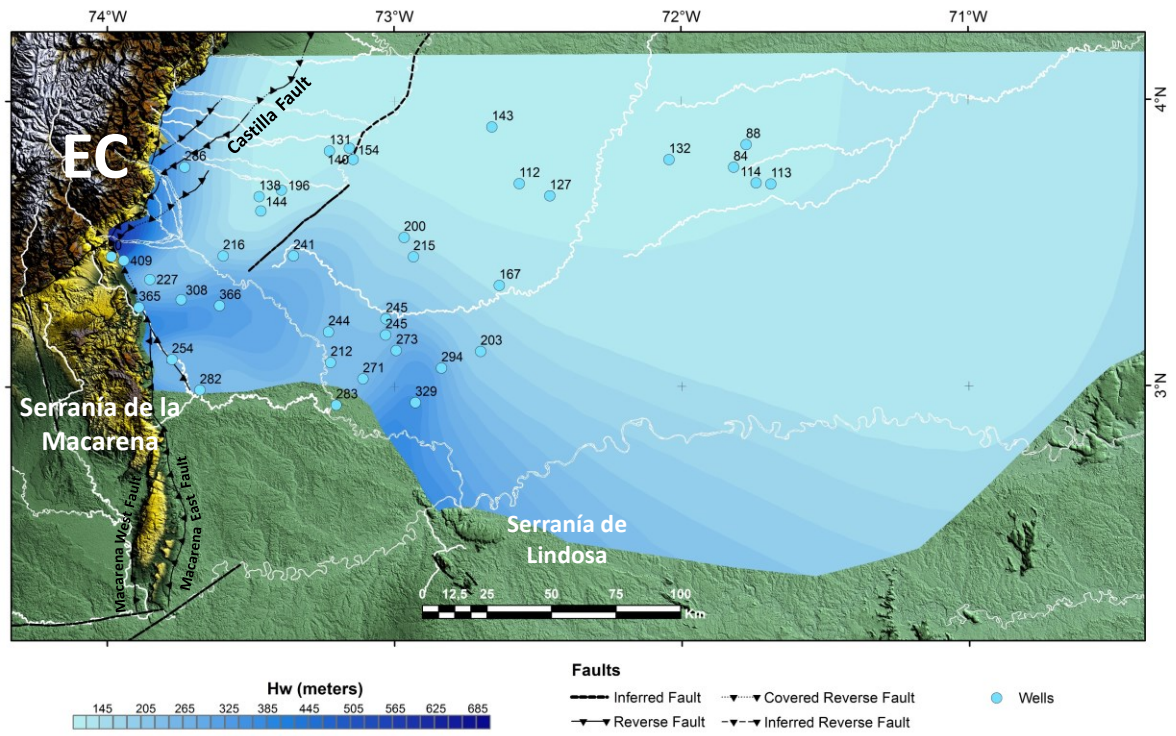


**Figure 5**. Potentiometric surface of the Basal Flow Unit generated from hydraulic heads estimated from wellbore reservoir pressure tests in exploratory and oil-producing wells of the southern Llanos Basin. EC: Easter Cordillera.

The southwestern sector hosts the areas with the most negative impact of hydrodynamic flow on the potential for accumulation and production of hydrocarbons in the area, which has been confirmed with multiple exploratory wells drilled in the area, corresponding to dry or low potential wells. Thus, we interpret that in the southwestern sector, the effect of the hydrodynamic flow in the Basal Flow Unit is amplified mainly due to three factors: 1) the proximity to the main recharge zone related to the Serranía de la Macarena, with high hydraulic gradient and hydraulic heads (**Figure 5**); 2) a greater hydraulic connection due to the better development of sands in the Basal Flow Unit and the partial or total absence of the aquitard that constitutes the Gachetá Formation (See Section BB´ in **Figure 2**), resulting in better hydraulic connectivity of the system, and therefore, favoring the drainage of previously charged accumulations; and 3) the low contrast of densities between fluids (water-oil) due to the presence of heavy crude oil and freshwaters recognized in the sector as discussed below.

Northwestwards, close to the Castilla Fault, production from adjacent oil fields comes mainly from the Cretaceous (Une and Gachetá formations) and Paleogene units (Barco and Mirador formations). This area coincides with a thicker development of the aquitard that makes up the Gachetá Formation (See Section C-C´ in **Figure 3**), acting as a vertical barrier that limits the influence of hydrodynamic flow from the BFU to the Paleogene reservoirs. This stratigraphic configuration identified in the northwestern sector has been corroborated with the historical behavior of pressure data. In that sector, the presence of pressure maintenance over time has been documented in the Upper Cretaceous formations (BFU), while the Paleogene strata (Barco and Mirador formations) have undergone a typical depletion related with a hydrostatic condition. In this way, the hydrodynamic flow has been recognized in the most basal formations that make up the Basal Flow Unit (Upper Cretaceous Formations, Fm. Une mainly).

Although the changes observed in the direction of hydrodynamic flow towards the eastern sector (**Figure 5**) will still be a matter of research and discussion in the future, it is important to observe the relationship of the structural highs with the regional hydrodynamic flow patterns. Three prominent structural highs are recognized: La Macarena, El Viento, and Guyana (**Figure 6**). The latter can be traced in an SW-NE direction from Colombia towards Venezuela, where it is called the El Baul High (e.g., Moreno-Lopez and Escalona, 2015).

Based on the potentiometric surfaces shown in **Figures 5 and 6,** La Macarena and El Viento highs would constitute areas favoring water recharge in the sector. In contrast, the Guyana high could be acting as a boundary towards the easternmost sector, which would explain the changes in the flow direction (SE - NW) reported towards the eastern sector of the area (**Figure 6**). However, to date, there are no data to the easternmost sector to support this hypothesis about the effect of the Guyana High as a limit to the east of hydrodynamic system.

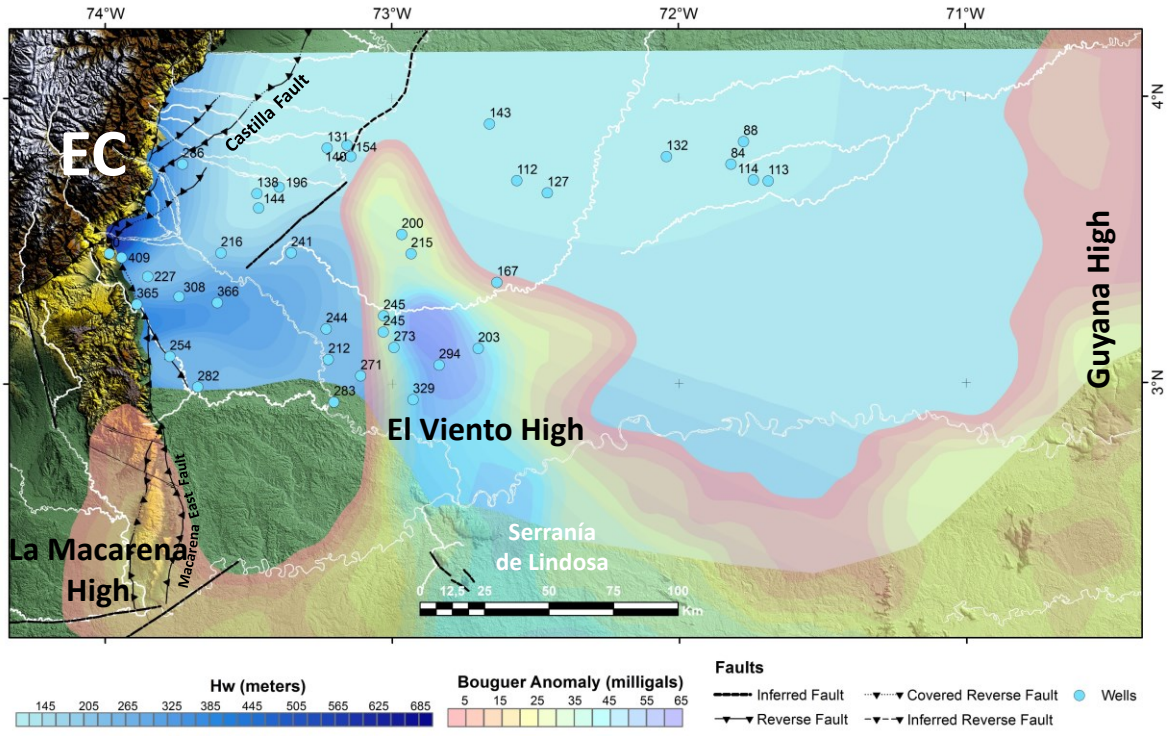


**Figure 6**. Hydraulic heads map and basement structural highs in the southern Llanos Basin built from Bouguer anomaly map. The basement structural highs are oriented south-north in the southern Llanos Basin. However, the Guyana high changes its orientation towards the southwest-northeast extending to Venezuela. EC: Eastern Cordillera.

### *5.2 Fluids and Their Implications in the Tilt Amplification Factor*

The densities of the recognized fluids in the area (heavy and extra-heavy crude oils and freshwaters) set a critical condition in terms of TAF. This condition is due to two factors: 1) the low densities of formation waters (≈ 1 g/cm$^3$), associated with low ions concentration associated with meteoric waters, and 2) the high densities of heavy and extra-heavy crude oils recognized in the sector. These characteristics of the fluids present in BFU lead to high TAF values (10 – 100) due to the low-density contrast between oil and water. These TAF values, added to high hydraulic gradients (southwestern sector) and the poorly developed structures (high interlimb angles), constitute a favorable scenario

for the partial or total drainage of hydrocarbon accumulations because of the hydrodynamic flow effect (**Figure 7, Tables 2 and 8**).

The range of crude oil densities in the area (0.90 g/cm$^3$ to 0.99 g/cm$^3$ at reservoir conditions, **Table 2**) coincides with the range of values where the low contrast of densities between the fluids (heavy oil and freshwater) will present the most significant effect in terms of TAF. Therefore, it will imply that the hydrodynamic condition will have the most drastic drainage effect on previously loaded oil accumulations (**Figure 7**). The TAF values in the southern Llanos Basin are almost ten times the highest reported by Dahlberg (1994), based in different combinations of hydrocarbon densities and formation water salinities (**Table 8**). These high TAF values could explain the limited potential for accumulation and production of hydrocarbons observed in exploration in recent years, especially in the southwestern sector of the study area.

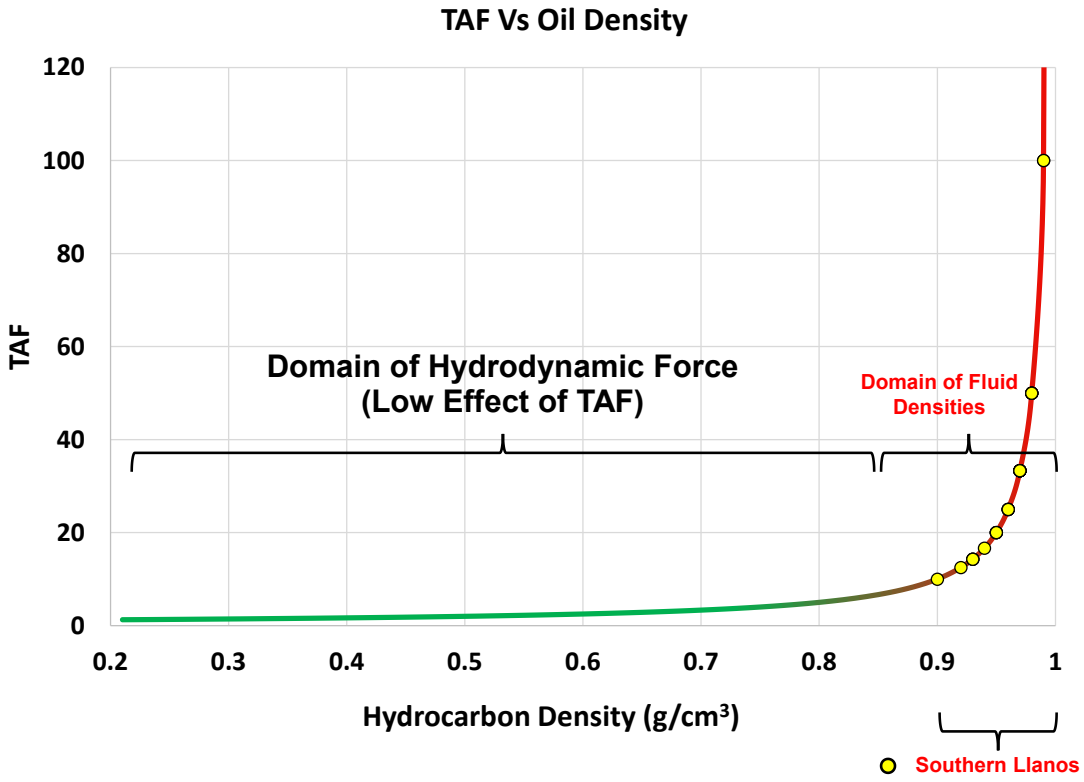


**Figure 7**. Relationship between TAF values and oil densities from the southern Llanos Basin. The water density value for estimating the TAF values in the plot is 1 g/cm$^3$. The yellow dots correspond to the TAF values according to the crude oil densities at reservoir conditions from the southern Llanos Basin.

**Table 8**. Tilt Amplification Factor (TAF) values as a function of crude oil and water densities. The first row shows the range of typical densities and TAF values considering the fluids present in the southern Llanos Basin. Modified from Dahlberg (1994).

| | Average API-Gravity (API degrees) | Density ($g/cm^3$) | Salinity (NaCl) and Density of Formation Waters | | | |
|---|---|---|---|---|---|---|
| | | | 200,000 ppm (1.14 $g/cm^3$) | 100,000 ppm (1.07 $g/cm^3$) | 15,000 ppm (1.01 $g/cm^3$) | 100 - 1000 ppm (1 $g/cm^3$) |
| **Southern Llanos (Present study)** | 13 | 0.90 - 0.99 | | | | TAF = 10 - 100 |
| **Dahlberg (1994)** | 20 | 0.93 | TAF = 5.5 | TAF = 7.9 | TAF = 13.3 | |
| | 30 | 0.87 | TAF = 4.3 | TAF = 5.5 | TAF = 7.5 | |
| | 40 | 0.82 | TAF = 3.6 | TAF = 4.4 | TAF = 5.5 | |
| | 50 | 0.78 | TAF = 3.2 | TAF = 3.7 | TAF = 4.4 | |

The TAF values reported in the present study toward the eastern sector (TAF: 12 and 20 related with oil densities: 0.92 $g/cm^3$ - 0.95 $g/cm^3$) also contrast with those published by Macellari (2021) for the same sector (close to 1, which is not an expected value bearing in mind the low contrast of densities in the area). In addition, and contrary to the interpretation of Macellari (2021), the tilt of OWC identified in some oil fields could be controlled mainly by TAF due to the low hydraulic gradients recognized towards the eastern sector.

***5.3 Geochemistry of Crude Oils and Hydrodynamics***

The distribution of API-gravities and Compositional Trend Index (CTI) towards the southwestern and southern sectors shows that the lowest values (heavier crude oils) coincide with the highest values of hydraulic heads near the Serranía de la Macarena and the Serranía de Lindosa (**Figure 8**). The API map (**Figure 8A**) shows, the dominance of heavy and extra-heavy crudes oils in the study area, with the most unfavorable zone in the southwestern sector where densities range between 0.97 $g/cm^3$ and 0.99 $g/cm^3$, and therefore result in high TAF values (**Figure 8A**). However, there is a gradual

relative improvement in the quality of the crude oils towards the eastern and central-northern sectors, where the crude oil densities range between 0.90 g/cm$^3$ and 0.97 g/cm$^3$ (**Figure 8A**).

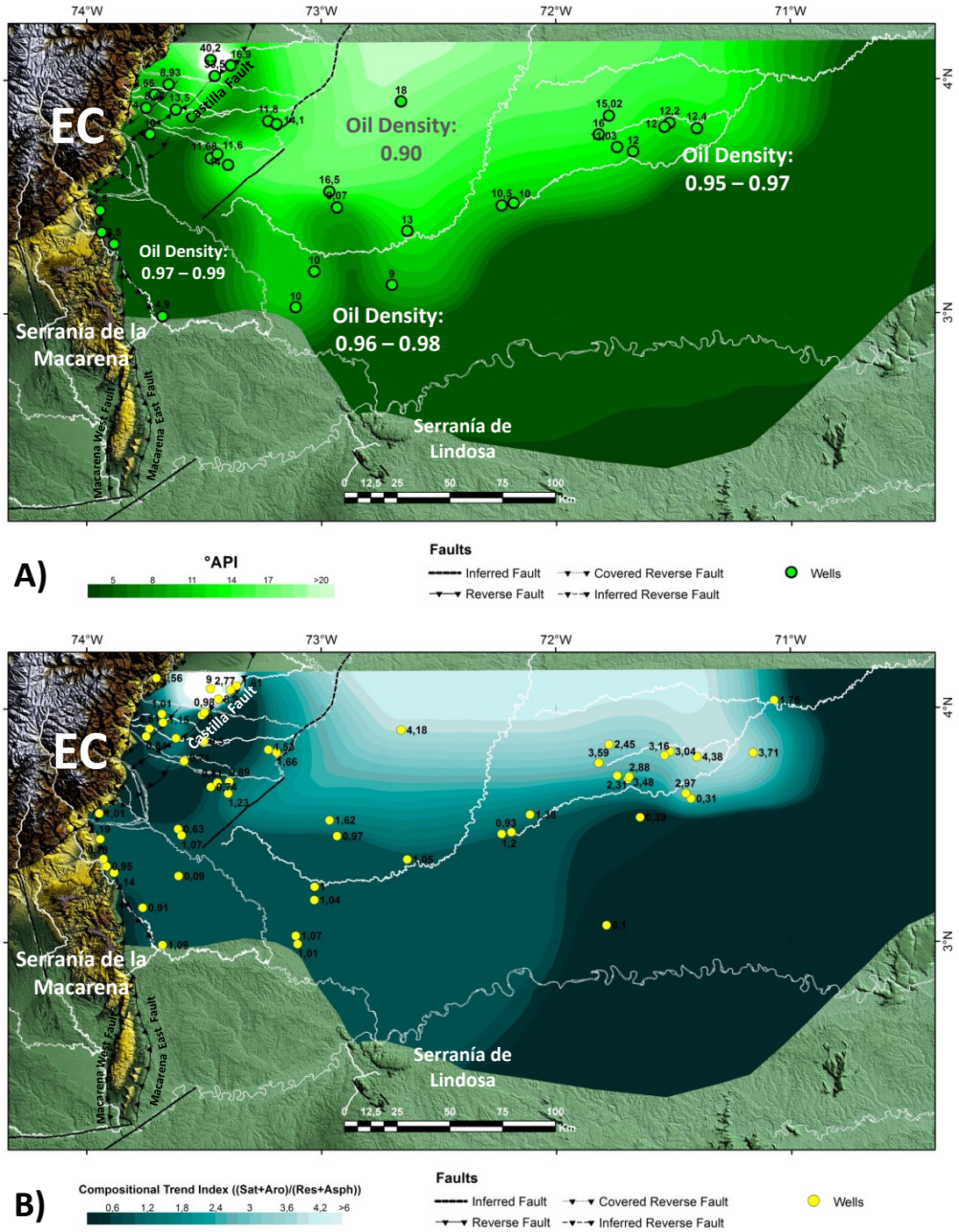


**Figure 8**. (A) API-gravity map of crude oils in the southern Llanos Basin. Representative density ranges shown in some sectors of the map are in units of g/cm$^3$. (B) Compositional Trend Index (CTI) map generated from SARA analysis in crude oil samples from the southern Llanos Basin. EC: Eastern Cordillera.

The geochemical characteristics of crude oils observed towards the western sector of the Castilla Fault are bimodal when considering the Cretaceous and Paleogene reservoirs, isolated from each other by the Gachetá Formation aquitard. Even in the deepest stratigraphic units, heavy and extra-heavy crude oils predominate in oil field production. However, some light crude oils from Cretaceous formations have been recognized in the northwestern corner of the study area.

Westward of the Castilla Fault, crude oils from the Cretaceous units (operationally named K1 and K2) with relatively high API-gravities and the highest CTI values are recognized, related to higher depths (> 2.75 Km below sea level), high temperatures (> 113°C) and the recent charge of hydrocarbons (refreshing). Thus, the Cretaceous formations in the BFU will have the largest drainage impact of previously loaded crude oil accumulations due to hydrodynamic flow, which will increase as the oil density increase (e.g., heavy oils from Cretaceous formations in the Castilla and Chichimene Oil fields). However, this impact under hydrodynamic down-dip flow conditions may represent opportunities for hydrocarbon accumulations such as those reported in the Cretaceous units (Basal Flow Unit) by Person et al. (2012), who recognize a tilted OWC with angles between 1° to 1.5° approximately.

Similarly, the CTI map indicates that the southwestern and southern sectors have the crude oils with the relatively highest fractions of resins and asphaltenes (relatively low CTI values), consistent with the API distribution and coinciding with the high values of hydraulic heads in the sector. As evidenced in the API distribution (**Figure 8A**), towards the northern sector, an improvement in crude oil quality is evidenced in response to the relative increase in the percentage of saturated and aromatic compounds (relatively high CTI values) in these crude oils (**Figure 8B**).

Heavy and extra-heavy crude oils of the southern Llanos Basin have been associated with high biodegradation intensity, controlling the physical characteristics of the crude oils in the area (Peters

et al., 2005; García et al., 2015). The biodegradation process has been understood as a sum of factors that favored high residence times of crude oils in the reservoirs at low temperatures (< 80°C). This is due to the tilt of the basin, which contributed to the shallower and cooler conditions of crude oils in the southern Llanos Basin (Hermeston and Nemcok, 2013; García et al., 2015; Sánchez et al., 2015). Whole oil chromatograms show evidence of such biodegradation throughout the southern Llanos Basin (**Figure 9**).

Different results suggest that the biodegradation of crude oil in the southern Llanos Basin can be mainly attributed to the past configuration of the basin (paleo-biodegradation) (Hermeston and Nemcok, 2013; García et al., 2015; Sánchez et al., 2015; Mora et al., 2019a). In agreement with the above-mentioned points, Mora et al. (2019a and b) suggest that the current hydrodynamic flow is interpreted as a less relevant factor in the biodegradation of crude oil. However, due to the current configuration of the southern Llanos Basin, favorable conditions for the current biodegradation of crude oils have been identified (temperatures < 80 °C and groundwater flow), especially near to the structural basement highs: La Macarena, El Viento, and eastward of foreland in the southern Llanos Basin (e.g., Rubiales oil field) where shallow, and low-temperature conditions are found (55 – 60 °C in Rubiales Field) (**Figure 9**).

The process of groundwater washing commonly accompanies the biodegradation of crude oils (Palmer, 1993). Moreover, drastic biodegradations in reservoirs worldwide are generally related to the movement of low salinity meteoric waters in shallow areas (Evans et al., 1971; Milner et al., 1977; Connan, 1984; Palmer 1993). Likewise, higher degrees of biodegradation have been identified towards oil-water interfaces (e.g., Conan, 1984; Bata et al., 2018); hence, the tilt of such interfaces can be used as an indicator of where the biodegradation process is occurring (e.g., Lafargue and Baker, 1988).

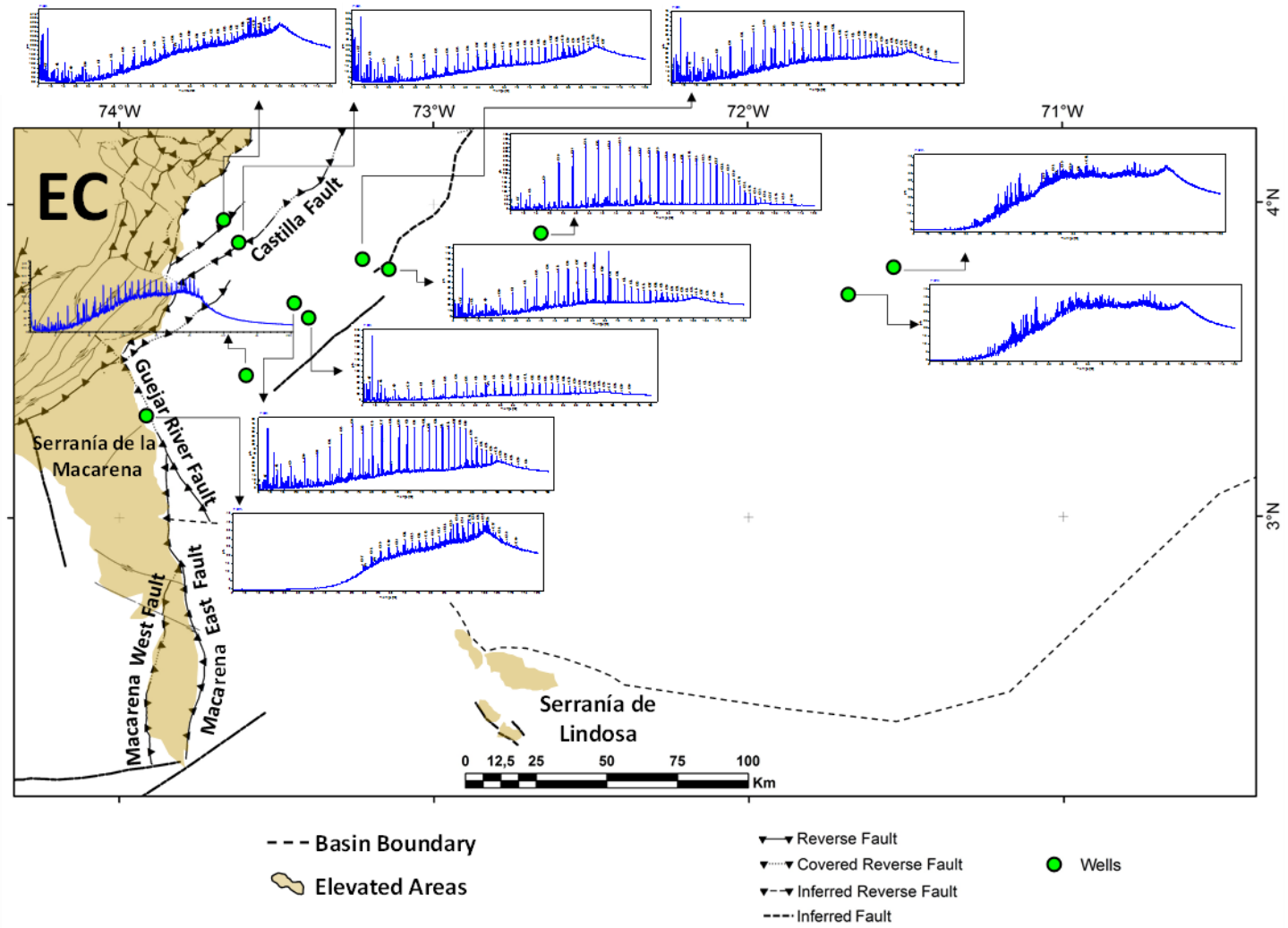


**Figure 9**. Map with of whole oil chromatograms distribution of crude oil samples from the southern Llanos Basin. A generally high degree of biodegradation is observed from Whole oils chromatograms of the area. The highest preservation of n-paraffins is observed in the north-central and western sectors. The distribution of chromatograms shows that the crudes with the highest biodegradation are found near the Serranía de la Macarena, Serranía de Lindosa, and the distal part of the foreland. EC: Eastern Cordillera.

Thus, the present-day configuration of the southern Llanos Basin, the action of hydrodynamic flow on the Basal Flow Unit, and some evidence of tilted oil-water interfaces, would indicate appropriate conditions for active biodegradation of crude oil. This biodegradation of crude oils adds to the factors that decrease the hydrocarbon retention potential, considering the increase in density generated by the biodegradation process itself.

### *5.4 Ions in Water and Regional Resistivity Analysis*

Analyses of major anions and cations ($HCO_3$, $CO_3$, $SO_4$, Cl, Na, K, Ca, Mg) in groundwaters of the southern Llanos Basin have shown the presence of freshwaters throughout the basin (e.g., Villegas et al. 1994; Person et al., 2012 and González-Penagos et al., 2014, Mora et al., 2019a). With waters dominantly fresh or slightly saline (according to Swenson and Baldwin, 1965), higher ions concentration in the Basal Flow Unit are recognized in the eastern sector, while the lowest concentrations are found in the western sector in the direction of the Serranía de la Macarena (**Figure 10**). These results coincide with the recharge zones identified for the southern Llanos Basin. Consequently, the hydrochemical facies are mainly bicarbonate-sodic and, to a lesser extent, chloride-sodic (e.g., González-Penagos et al., 2014).

Similar to the distribution of API-gravity and Compositional Trend Index, westward of the Castilla Fault, low ion concentrations are present in the formation waters samples recovered from the Basal Flow Unit from Cretaceous formations. In contrast, the formation waters from the Paleogene units (Mirador and Barco Formations) have higher ion concentrations. As explained in **Section 5.3**, this behavior is mainly attributed to the restriction of the vertical connection controlled by the aquitard of the Gachetá Formation.

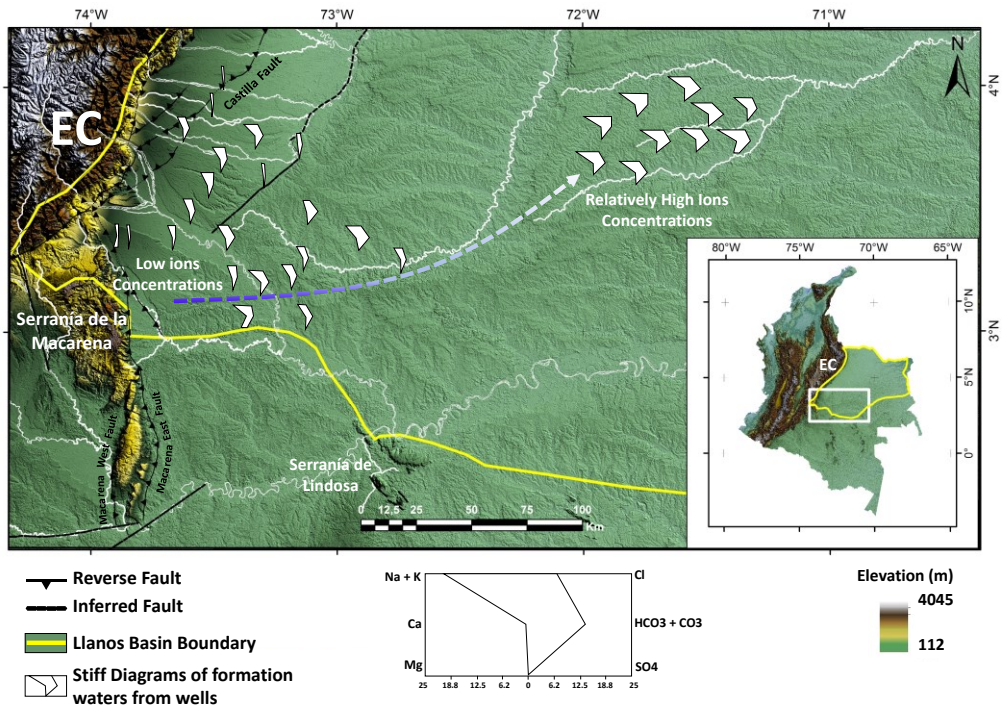


**Figure 10**. Stiff diagrams map of groundwater samples taken from the Basal Flow Unit in the southern Llanos Basin, where a decrease in the concentration of the primary ions is observed in a westward direction. The groundwater samples were taken in exploratory and producer wells in the study area. The scale of the Stiff diagram's ranges from 0 to 25 meq / L. EC: Eastern Cordillera.

Unlike the behavior of the ions concentration (**Figure 10)**, the electrical well logs show the highest deep resistivity values of the rock-fluid system (**Table 6**) towards the west-southwest sector, decreasing towards the foreland of the basin (**Figures 11 and 12**). The high resistivities are related to saturated rocks with waters of low ion concentrations (near the Serranía de la Macarena), while the lowest resistivities are related to rocks saturated with waters of relatively higher ion concentrations recognized mainly towards the foreland of the southern Llanos Basin (**Figures 10, 11 and 12**). The high deep resistivity values extending in a northward and northeast direction (dark blue colors in the maps in **Figures 11 and 12**) near the Serranía de la Macarena may be due to the proximity of the recharge zone and a better hydraulic connection in that direction. This pattern coincides with the pressure maintenance in the Cretaceous units (K2, K1) shown in the oil fields from the northwestern sector, west of the Castilla Fault, where the effect of hydrodynamic flow on the Basal Flow Unit has been confirmed (e.g., Pearson et al., 2012).

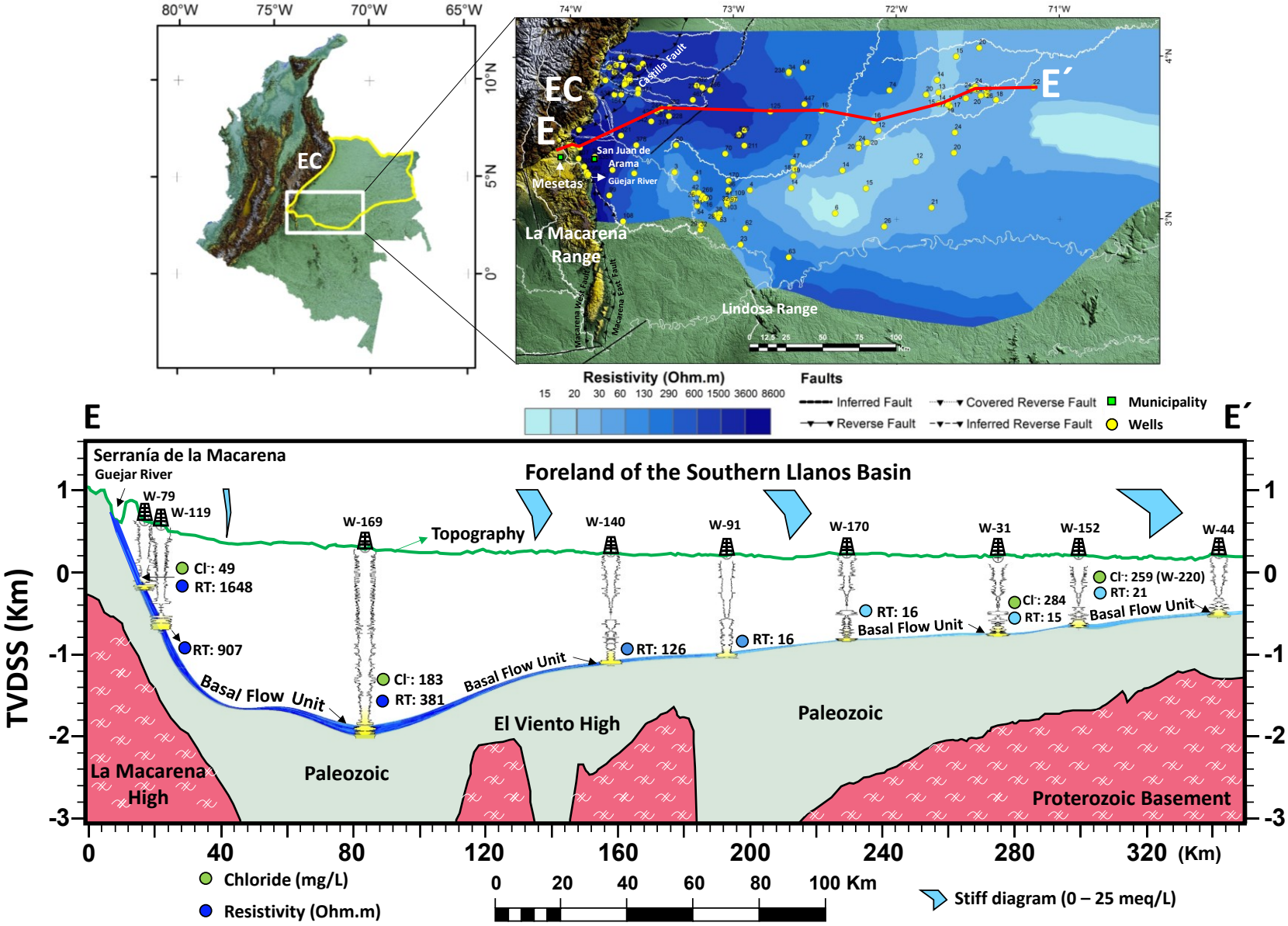


**Figure 11**. (Above) Deep resistivity map generated from electrical well logs measured in wells that reached the Basal Flow Unit in the southern Llanos Basin. (Bottom) Regional cross-section E - E' in the west-east direction showing the current configuration of the Basal Flow Unit. The blue colors of the Basal Flow Unit in the cross-section correspond to the deep resistivity values where the highest values (dark blue: freshwater) are observed to the west and the lowest values (light blue: groundwaters of relatively higher ion concentration) to the east. The gamma-ray log is shown in each well, highlighting the sands that make up the Basal Flow Unit. Green dots indicate chloride content in groundwater samples (mg/L), and blue dots indicate the average deep resistivity from well logs (Ohm.m).

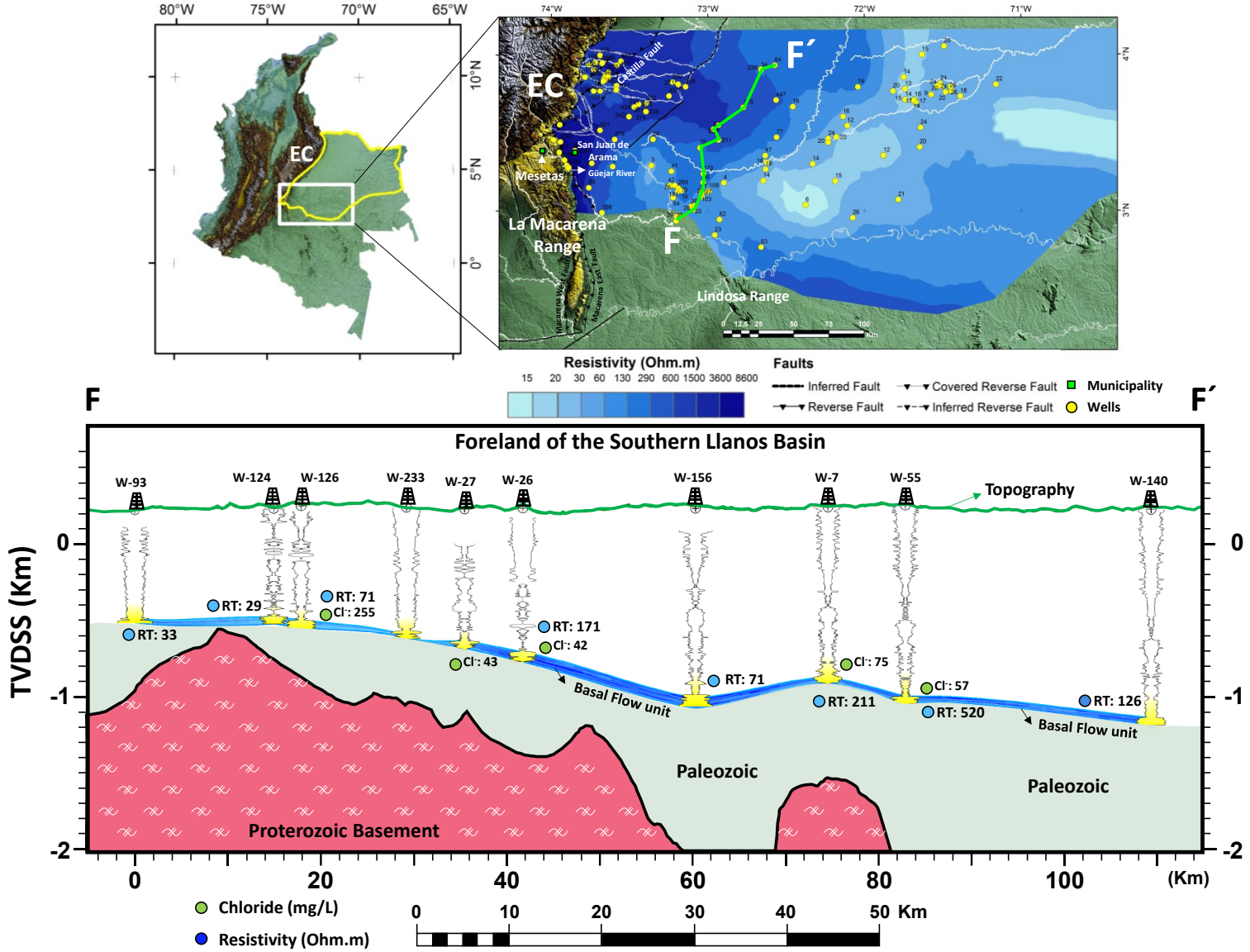


**Figure 12**. (Above) Deep resistivity map generated from electrical well logs measured in wells that reached the Basal Flow Unit in the southern Llanos Basin. (Bottom) Regional cross-section F - F' in the southwest-northeast direction showing the current configuration of the Basal Flow Unit. The blue colors of the Basal Flow Unit in the cross-section correspond to the deep resistivity values where the highest values (dark blue: freshwater) are observed to the northwest and the lowest values (light blue: groundwaters of relatively higher ions concentration) to the southwest. The gamma-ray log is shown in each well, highlighting the sands that make up the Basal Flow Unit. Green dots indicate chloride content in groundwater samples (mg/L), and blue dots indicate the average deep resistivity from well logs (Ohm.m).

Water resistivity (Rw) values will be variable in time and tend to increase as the hydrodynamic flow continues to incorporate waters of lower ion concentration (freshwater) from the west to the east. Thus, it is expected that the future behavior of resistivities over time (e.g., thousands or millions of years) will show the advance of meteoric waters towards the foreland of the basin (darker blue colors towards the east in the maps of **Figures 11** and **12**).

The regional view of the BFU in the southern Llanos Basin illustrates that the BFU gets thinner and shallower eastwards (cross-section E – E´ in **Figure 11**). It also intercepts rivers on the surface, especially from the eastern front of the northern sector of the Serranía de la Macarena. Such is the case of the Güejar River near the vilages of Mesetas and San Juan de Arama (Meta Department), where the connection between the surface and subsurface of the Basal Flow Unit is evident (**Figures 11 and 12**), as has been confirmed by recent geological mapping in that area (Arias et al., 2018). These connection zones are characterized by perennial rivers and streams flowing from the high zones of the Serranía de la Macarena and Eastern Cordillera towards the foreland of the southern Llanos Basin. The cross-section E-E´ shown in **Figure 11** reveals that in these connection zones to the north of the Serranía of Macarena, the Basal Flow Unit exhibits the highest values of formation water resistivities marked by the presence of freshwaters (dark blue in cross-section E-E´ of **Figure 11**). Gradually, the resistivities decrease towards the foreland of the basin (light blue in cross-section E-E´ of **Figure 11**), where the presence of waters with relatively higher ions concentration has been confirmed. These observations show a strong influence of meteoric waters in the BFU, preferentially towards the west, where the main recharge zone of the BFU has been identified (Arias et al., 2018; Mora et al., 2019a). It also coincides with the highest values of hydraulic head and hydraulic gradient. These patterns would explain the low potential for hydrocarbon accumulation and production confirmed with the drilling of dry or very-low hydrocarbon potential wells in the areas near the Serranía of the Macarena.

When the different maps are compared some relevant patterns are revealed:

-A region located west of the Castilla oil field where the map of API gravity in **Figure 8** shows the lightest oils of the study area. However, the resistivities are high (**Figures 11 and 12**) suggesting the presence of fresh waters, as it was also documented by Mora et al (2019a). Therefore, despite having reservoirs with fresh water these sectors do not seem to be affected by active biodegradation. Moreover, in that area there are reservoirs located deeper than the hottest lower boundary of biodegradation (80° Celsius), but they combine heavy oils with API gravities lower than 13° API, and other adjacent compartments with coeval reservoirs display API gravities higher than 20° API (e.g., Mora et al., 2019a). The heaviest oils in that area with reservoirs at current temperatures higher than 80°C suggest paleo-biodegradation (e.g., Chichimene and Castilla oil fields), a phenomenon that has been already proposed by Garcia et al. (2015).

-Our chromatograms from that area show the presence of peaks with light compounds in highly biodegraded crude oils (**Figure 9**). This suggests a second charge of lighter oils after the initial charge which is superimposed on paleo-biodegradation (Dzou et al., 1999; García et al., 2015).

-The coexistence of dominantly fresh water with lighter oils in the northwestern sector suggests active charge, which modifies the oils from those areas having deep reservoirs and paleo-biodegradation. However, we maintain that there might be shallower reservoirs receiving active hydrocarbon charge but also fresh water, which means active biodegradation. Following previous studies (e.g., Garcia et al., 2015; Mora et al 2019b), the areas not receiving modern hydrocarbon charge include most of the study area. This is supported by the fact that most of the hydrocarbons in the southern Llanos Basin come from Cretaceous marine source rocks (Garcia et al., 2015; Peters et al., 2005) which are currently located within the areas of the Eastern Cordillera which were already exhumed by the late Oligocene-early Miocene (e.g., Mora et al., 2013; Mora et al., 2015). In

contrast, the currently active kitchens are mostly related with terrigenous Cretaceous and Cenozoic source rocks located farther to the east (e.g., Garcia et al., 2015; Sanchez et al., 2015; Sanchez et al., 2021).

-Nevertheless, firstly, the fact that deep areas underwent paleo-biodegradation, and secondly the premise that the shallowest sectors not receiving active recharge from the present-day pods of active source rocks in the basin were even shallower in the past, allow us to infer that most of the petroleum charge in the study area should have happened before most of the Miocene sedimentation. Along those lines, paleo-biodegradation should be the dominant process responsible for the presence of heavy to ultraheavy oils in the study area. Therefore, the modern conditions of hydrodynamic flow can be potentially extrapolated several millions to tens of millions of years into the past. Previous works suggest similar configurations in the study area starting in the Oligocene (Mora et al., 2019b).

#### *5.5 Flow Velocity and Fluids Impact from Numerical Simulation Approach*

The approximation of groundwater velocities using numerical simulation in a 2D-realistic grid built parallel to the approximate hydrodynamic flow direction in the area allowed us to suggest the distribution and orders of magnitude of groundwater flow velocities and fluids saturation throughout the geologic structure from an oil field whose production is coming from the BFU. In **Figure 13**, we present the results of two of the simulated scenarios up to 10 My, showing the water saturation (**Figure 13a**) and groundwater flow velocities models (**Figure 13b**), considering two scenarios of OWC tilt (1° and 1.5°), with an oil density of 0.95 g/cm$^3$ and an average permeability of 2000 mD. The results of the other scenarios evaluated in the numerical simulations are summarized in **Table 7**.

The results obtained suggest that the flow velocities towards the west sector of the Castilla Fault would be around $10^{-4}$ ft/day to $10^{-3}$ ft/day (**Figure 13c** and **Table 7**). However, the most likely flow velocities in the area could be in the order of magnitude of $10^{-3}$ ft/day, considering the high permeabilities that we have experimentally measured in core samples from wells in the area from routine core analysis (e.g., plugs or Side Wall Core samples), which range from 1,000 mD to more than 10,000 mD (**Figure 13d**).

For all scenarios evaluated, the highest flow velocities are towards the central part of the structure, below the oil-water interface (**Figure 13b**). The velocities decrease towards the zones with no hydrocarbon accumulation, where the flow area is greater and remains relatively constant (**Figures 13a** and **b**). On the other hand, the groundwater flow velocities above the oil-water interface are null (V = 0) and correspond to the zone where the hydrocarbon is retained after the hydrodynamic equilibrium is reached. Unlike the null velocities above the oil-water interface, high velocities are evidenced in the central zone of the model, below the oil-water interface, due to the restriction of the area available for water flow (according to Darcy's Law equation), since the zone occupied by the hydrocarbon, acts as a vertical barrier that reduce the area exposed to the water flow (**Figure 13b**).

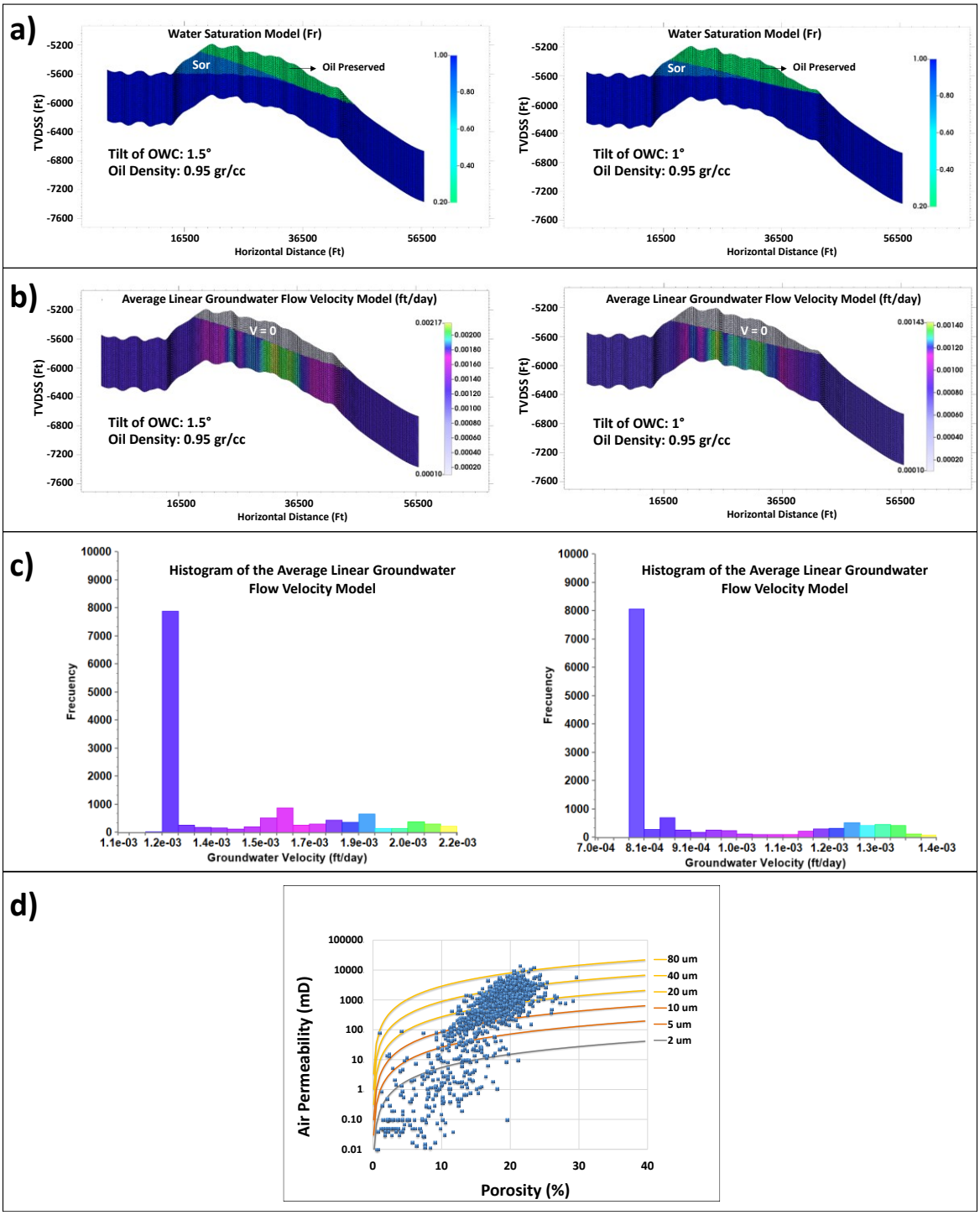


**Figure 13**. Numerical simulation results in the 2D realistic grid, from equilibrium (0 My) to 10 My, considering an average permeability of 2000 mD, oil density of 0.95 g/cm$^3$ and OWC inclinations of 1.5° (left) and 1° (right). a) Water saturation models (fr), b) Average linear groundwater flow velocity models (ft/day), c) Histograms of average linear groundwater flow velocities, and d) Porosity-Permeability plot showing typical values for Basal Flow Unit in the area (Westward of the Castilla Fault). Lines in the Porosity-Permeability plot represent different pore throat radii using the Winland Equation described by Kolodzie (1980). Sor: residual oil saturation.

This approach using numerical simulation for the estimation of groundwater velocity, using as the main constraint the tilted oil-water interface, together with petrophysical and fluids properties, may represent a more reliable approach than considering estimation of groundwater flow velocities in large-scale systems (e.g., basin-scale), due to high deviations in groundwater flow velocities calculations (Freeze and Cherry, 1979; Kreitler, 1989; Mazor and Nativ, 1992).

Finally, the 3D simulation model allows visualizing the up-dip and down-dip drainage effect of hydrodynamic flow in adjacent geologic structures with hydrocarbons usually recognized in the study area. According to the results obtained from the 3D simulation model, the down-dip flow is less critical (even favorable) than the up-dip, as reported by some authors (e.g., Hubbert, 1953; Dahlberg, 1994) (**Figure 14**). In addition, the inclination of the oil-water contact responds independently for each of the structures, even though they are affected by the same hydrodynamic flow (**Figure 14c**). This is a very important observation to keep in mind to avoid misinterpretations of regional oil-water contact across different structures, which can lead to errors in estimating the hydrocarbon potential of an area.

On the other hand, hydrocarbon retention in each of the structures will be controlled by the spill-points. Under an up-dip hydrodynamic flow, the spill-point will work the same as in a hydrostatic condition. For a down-dip hydrodynamic flow, the spill points are inverted and would be towards the lower part of the structure that retains the hydrocarbon (**Figure 14c**). In the case of the current configuration of the BFU in the southern Llanos basin (**Figure 11)**, the hydrodynamic flow in most of the basin corresponds to an up-dip flow. This configuration of BFU added to additional factors such as the high crude oil densities, poorly developed geological structures, and the presence of freshwaters, restricts the hydrocarbon retention potential in a large portion of the southern Llanos Basin. However, the down-dip structures represent an exploratory play of interest, which has confirmed its potential in some crude oil accumulations in the area (e.g., Pearson et al., 2012).

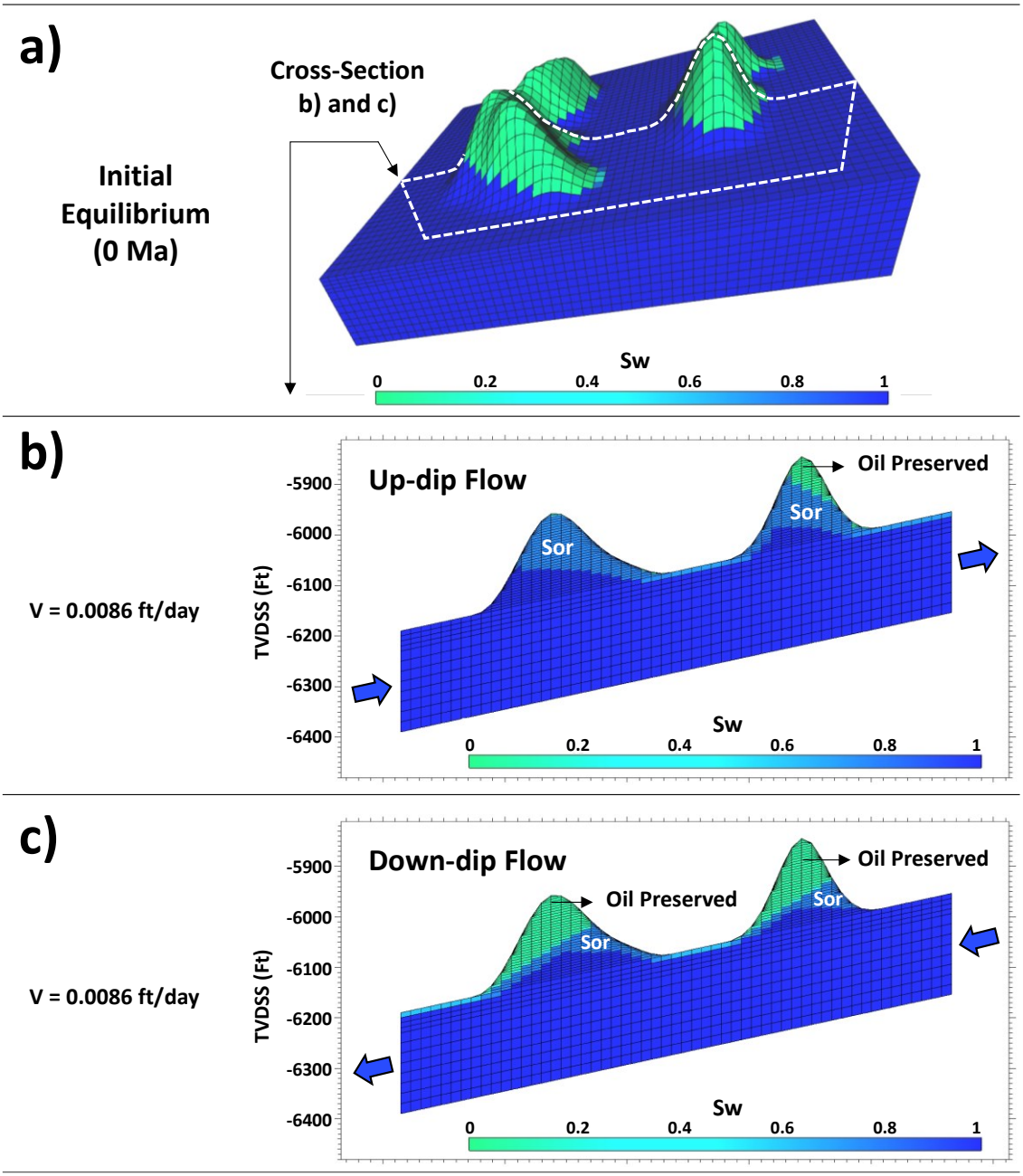


**Figure 14**. Numerical simulation results in the 3D grid, from equilibrium (0 My) to 10 My, considering an average permeability of 2000 mD, oil density of 0.95 g/cm$^3$, groundwater velocity of 0.0086 ft/day, and water flow up-dip and down dip. (a) 3D view showing the adjacent structures at the initial equilibrium, (b) cross-section at the end of the simulation in the up-dip scenario, and (c) cross-section at the end of the simulation in the down-dip scenario. Sor: Residual oil saturation.

Although hydrodynamic flow has been documented in the Llanos Basin (e.g., Villegas et al., 1994; Bachu et al., 1995; Person et al., 2012; González-Penagos et al., 2014; González-Penagos et al., 2017;

Lasso et al., 2018; Mora et al., 2018; Mora et al., 2019a), more recent approaches attribute the inclination of the water-oil contacts to active tectonic controls, associated with the current uplift of the southern area of the Rio Meta lineament (Macellari, 2021), suggesting that the OWC´s stabilization rates are slower than the uplift rate. However, although an OWC tilt of 0.3° toward the Rubiales Field is proposed (e.g., Macellari, 2021), which is low according to values reported worldwide (e.g., Wendebourg et al., 2018), there is no data of uplift rates in the southern area of the Rio Meta lineament, neither OWC stabilization times on geologic time scale. Likewise, although the hypothesis shown by Macellari (2021) deserves attention and further investigation, it would not explain the pressure support over time that has been evidenced in the reservoirs of the eastern sector of the southern Llanos Basin (e.g., Gomez et al., 2009). Moreover, as we mentioned previously, the TAF values estimated in this study towards the Rubiales Field area range between 12 and 20 and differ significantly from the value reported by Macellari (2021), who reports TAF values that would not represent the fluids in the area.

The analyzes included in this study help to explain the low potential for accumulation and production of hydrocarbons evidenced towards the southwestern corner of the Llanos basin, close to the Serranía de la Macarena. This low potential is mainly attributed to the proximity to the water recharge zone of the hydrodynamic system (Eastern Front of the Serranía de la Macarena) and the low-density contrast between water and crude oil, which has favored the drainage of accumulations of previously loaded crude. Although most of the basin would negatively affect the BFU due to the flow of groundwater, the down-dip type hydrodynamic traps represent the alternative traps to be explored with the greatest probability of exploratory success.

# 6. Conclusions

The hydrodynamic system recognized in the BFU limits the potential for hydrocarbon accumulation and production in the area. The effect of hydrodynamic flow on crude oil accumulations in the southern Llanos Basin is amplified by two main factors: the low-density contrast caused by the presence of heavy and extra-heavy oils in the presence of freshwater (high TAF values) and the presence of poorly developed structures identified in the area, with low dip angles which decreases the hydrocarbon retention potential. The southwestern corner of the southern Llanos Basin, near the Serranía de la Macarena, is recognized as the most critical area for hydrocarbon retention and coincides with the highest values of hydraulic heads, groundwaters of low ions concentration, and the presence of highly biodegraded crude oils.

The BFU is a basin-scale diachronous unit, hydraulically connected along the southern Llanos Basin, resting on Paleozoic rocks, and whose connection between surface and subsurface was favored by the uplift of the Serranía de la Macarena, close to the zones of influence of the Güejar River Fault and the Eastern Macarena Fault. Its tectonic evolution turned the eastern front of the Serranía de la Macarena into the main recharge zone and connection of the hydrodynamic system of the southern Llanos Basin as it was proposed in previous studies. This connection favors the percolation of meteoric waters from the surface up to hundreds of kilometers towards the foreland of the Llanos Basin. This has been confirmed with hydrochemical analyses of groundwater samples and deep resistivity data, which identify waters with low ions concentration along the Basal Flow Unit, recognizing a gradual decrease of ions concentration in the groundwaters from the east towards the Serranía de la Macarena.

Although the biodegradation of southern Llanos crude oils is a process that has been mainly related to past processes, the present-day hydrodynamic flow and the current configuration of the basin

may be contributing to the current biodegradation processes, coinciding these zones with the basement highs (i.e., La Macarena High, and El Viento High) and towards the forebulge of the southern Llanos Basin, in sectors where reservoirs become shallower and temperatures are reduced (<80°C). Thus, paleo-biodegradation and present-day biodegradation processes, which have produced crude oils with low API-gravity and high fractions of resins and asphaltenes, constitute an additional variable that reduces the hydrocarbon retention potential of the area, leaving crude oils of higher density that favor high TAF values (10 - 100), which under the current hydrodynamic condition limits the potential for hydrocarbon accumulation and production in the area, especially in the southwestern corner of the southern Llanos Basin towards the Serranía de la Macarena. Those areas affected by paleo-biodegradation which would be still affected by biodegradation today, should be restricted to the shallow areas with reservoirs receiving active hydrocarbon charge. Based on our new data and previous studies, we suggest that the areas undergoing active biodegradation are restricted within the study area. Therefore, most of the hydrocarbon charge must have occurred before the onset of Miocene sedimentation with concomitant early paleo-biodegradation. This means that the modern recharge zones and hydrodynamic conditions may have been persistent for several millions of years or tens of millions of years.

In hydrodynamic systems influencing hydrocarbon reservoirs, the inclination angles of the oil-water or gas-water contacts constitute a useful tool for the derivation of the groundwater flow velocities considering a field scale (e.g., oil field). According to the values of oil-water contact inclination reported in the western Castilla Fault area, and from numerical simulation models, values of groundwater flow velocities were derived and would indicate that for the BFU, the average linear groundwater flow velocity range between orders of magnitude of $10^{-3}$ ft/day and $10^{-4}$ ft/day. However, these results are only representative of the analyzed field and do not represent the flow velocities of the entire hydrodynamic system. Likewise, we suggest the future use of environmental

tracers or the use of downhole instrumentation for the calibration of flow velocities in different parts of the southern Llanos basin.

Although the hydrodynamic effect towards the eastern sector of the southern Llanos Basin is still under investigation, the data documented here suggest that the hydrodynamic effect on the Basal Flow Unit extends eastward to the distal part of the southern Llanos Basin. Pressure support over time, the presence of freshwater in the presence of heavy crude oils, and the present-day configuration of the Basal Flow Unit constitute an ideal scenario for the influence of hydrodynamic flow that in some cases may even favor the presence of hydrocarbon accumulations in specific areas. However, additional analyses are needed to establish the timing between different processes to establish whether the tilt of the OWC observed in some oil fields towards the eastern sector is a response to tectonic effects, hydrodynamics, or perhaps a mixture of these two processes.

## 7. Acknowledgments

Thanks to MINCIENCIAS in the framework of Call 758 for the financial support of the research. Thanks to EAFIT University as part of an official program agreement between ECOPETROL S.A, EAFIT University and MINCIENCIAS.

## 8. References

Arango C., J Dorado, D. Guzmán and J.F Ruiz, 2012, Climatología trimestral de Colombia Grupo de Modelamiento de Tiempo, Clima y Escenarios de Cambio Climático Subdirección de Meteorología – IDEAM.

Bata T.P., U.A. Lar, N.K. Samaila, H. U. Dibal, R.I. Daspan, L.C. Isah, A.A. Fube, S.Y. Ikyoive, E.H. Elijah and J.J. Shirputda, 2018, Effect of biodegradation and water washing on oil properties: AIMS Geosciences, v. 4, p. 21 – 35, doi: 10.3934/geosci.2018.1.21

Archie G.E., 1942, The Electrical Resistivity Log as an Aid in Determining Some Reservoir Characteristics: Trans, v. 146, p. 54 – 62, doi: https://doi.org/10.2118/942054-G.

Arias, J.P., A. Mora, D. Echeverry and G. Rodriguez, 2018, Mapping the transition between the Llanos and Caguán Basins. Impacts for the hydrocarbon exploration and basin hydrodynamics: Cumbre del Petróleo y Gas 2018, November 2018, Bogotá.

Asomaning S., and A. P. Watkinson, 2000, Petroleum Stability and Heteroatom Species Effects in Fouling of Heat Exchangers by Asphaltenes: Heat Transfer Engineering, v. 21, n. 3, p. 10 – 16, DOI:10.1080/014576300270852.

Asomaning S., 2003, Test Methods for Determining Asphaltene Stability in Crude Oils: Petroleum Science and Technology, v. 21 n. 3 & 4, p. 581-590, DOI: 10.1081/LFT-120018540.

Bachu S., J.C. Ramon, M.E. Villegas, and J.R. Underschultz, 1995, Geothermal regime and Thermal history of the Llanos Basin, Colombia: AAPG Bulletin, v. 79, n. 1, p. 116–129, https://doi.org/10.1306/8D2B14D0-171E-11D7-8645000102C1865D

Bond D.C, 1972, Hydrodynamics in Deep Aquifers of the Illinois Basin: Illinois State Geological Survey, v. 470, p. 1 – 51.

Bredehoeft J.D., K. Belitz, S. Sharp-Hansen, 1992, The Hydrodynamics of the Big Horn Basin: A Study of the Role of Faults: The American Association of Petroleum Geologists Bulletin, v. 76, n. 4, p. 530 – 546, doi.org/10.1306/BDFF8862-1718-11D7-8645000102C1865D.

Caballero V., J. Naranjo, F. De La Parra, A. Mora, A. Reyes-Harker, 2015, Estratigrafía de Secuencias de los Principales Reservorios de la Cuenca de Llanos: Momorias XV Congreso Colombiano de Geología, p. 320 – 324.

Cathles, L. M. III, 1990, Scales and effects of fluid flow in the upper crust: Science, v. 248, no. 4953, p. 323–329, doi: 10.1126/science.248.4953.323.

Chiarelli A., 1978, Hydrodynamic Framework of astern Algerian Sahara – Influence on Hydrocarbon occurrence: The American Association of Petroleum Geologists Bulletin, v. 62, n. 4, p. 667 – 685, doi.org/10.1306/C1EA4E28-16C9-11D7-8645000102C1865D.

Servicio Geológico Colombiano, 2015, Geología de la Plancha 305 San Juan de Arama – Escala 1: 100000 – Memoria Explicativa. Servicio Geológico Colombiano, p. 120.

Connan, J., 1984, Biodegradation of Crude Oils in Reservoirs, In Advances in Petroleum Geochemistry, eds. J. Brooks and D. H. Welte, Academic Press, London, vol. 1, p. 299-335. https://doi.org/10.1016/B978-0-12-032001-1.50011-0

Cortes, J., J. Rincon, J. M. Jaramillo, P. Philp, and J. Allen, 2010, Biomarkers and compound-specific stable carbon isotope of n-alkanes in crude oils from eastern Llanos Basin, Colombia: Journal of South American Earth Science, v. 29, n. 2, p. 198–213, doi:10.1016/j.jsames.2009.03.010.

Coustau H., 1977, Formation Waters and Hydrodynamics: Journal of Geochemical Exploration, v. 7, p. 213 – 241, doi.org/10.1016/0375-6742(77)90082-6.

Dahlberg E.C, 1994, Applied Hydrodiynamics in Petroleum Exploration, 2nd Ed, 295 p.

Deming, D., 1994, Fluid flow and heat transport in the upper continental crust, in J. Parnell, ed., Geofluids: Origin, migration and evolution of fluids in sedimentary basins: Geological Society, London, Special Publications 1994, v. 78, p. 27–42.

Dzou, L., A. Holba, J. Ramon, M. Moldowan, and D. Zinniker, 1999, Application of new diterpane biomarkers to source, biodegradation and mixing effects on central Llanos Basin oils, Colombia: Organic Geochemistry, v. 30, no. 7, p. 515–534, doi:10.1016/S0146-6380(99)00039-X.

Fan T., J. Wang, and J. Buckley, 2002, Evaluating Crude Oils by SARA Analysis: Society of Petroleum Engineers, Improved Oil Recovery Simposium, 13 – 17 April 2002, SPE 75228.

Freeze, R.A. and J.A. Cherry, 1979, Groundwater. Prentice-Hall, Inc., Englewood Cliffs, N. J, pp. 604.

García, D. F., E. Vaz dos Santos Neto, and H. Penteado, 2015, Controls on the petroleum composition in the Llanos Basin, Colombia: Implications for exploration: AAPG Bulletin, v. 99, no. 8, p. 1503–1535, doi:10.1306/10231411111.

Gomez, Y., F. Yoris, J. Rodriguez, F. Portillo and Y. Araujo, 2009, Aspectos hidrodinámicos, estructurales y estratigráficos del Campo Rubiales: cuenca de los Llanos Orientales, Colombia. In: X Simposio Bolivariano Exploración Petrolera en Cuencas Subandinas, July, 2009. ACGGP, Cartagena, Colombia, pp. 1–7.

González-Penagos, F., I. Moretti, C. France-Lanord, and X. Guichet, 2014, Origins of formation waters in the Llanos foreland basin of Colombia: Geochemical variation and fluid flow history: Geofluids, v. 14, n. 4, p. 443–458, https://doi.org/10.1111/gfl.12086

González-Penagos, F., I. Moretti, and X. Guichet, 2017, Fluid Flow Modeling in the Llanos Basin, Colombia: AAPG Memoir 114, p. 191–217, https://doi.org/10.1306/13602030M1143705

González-Uribe G, D. García-Bautista, L Mantilla-Figueroa, J. Rodríguez-Rincón, 2007, Hidrodinámica e hidrogeoquímica del piedemonte llanero: Hipótesis de rutas de migración a partir de técnicas hidrogeológicas. Boletín de Geología, v.29, n. 1, p. 75–84, DOI: 10.18273/revbol

Harrington, H.J., Kay, M., 1951. Cambrian and Ordovician faunas of eastern Colombia. Journal of Paleontology 25 (5), 655–668.

Hermeston, S., and M. Nemcok, 2013, Thick-skin orogen-foreland interactions and their controlling factors, northern Andes of Colombia: Geological Society, London, Special Publication v. 377, no. 1, p. 443–471, doi:10.1144/SP377.16.

Hitchon B., 1969, Fluid Flow in the Western Canada Sedimentary Basin, Effect of Topography: Water Resources Research, v. 5, n. 1, p. 186 – 195, https://doi.org/10.1029/WR005i001p00186

Hubbert M.K., 1940, The theory of ground-water motion; Journal of Geology, v. 48, n. 8, p. 785 – 944, https://doi.org/10.1086/624930

Hubbert M.K., 1953, Entrapment of petroleum under hydrodynamic condition; AAPG Bulletin, v. 37, n.8, p. 1954 – 2026, https://doi.org/10.1306/5CEADD61-16BB-11D7-8645000102C1865D

Hubbert M.K., 1967, Application of hydrodynamics to oil exploration; 7th World Petroleum Congress, Mexico City.

Ibanez-Mejia M., J. Ruiz, V. Valencia, A. Cardona, G.E. Gehrels, A. Mora, 2011, The Putumayo Orogen of Amazonia and its implications for Rodinia reconstructions: New U–Pb geochronological insights into the Proterozoic tectonic evolution of northwestern South America: Precambrian Research, v. 191, n.1-2, p. 58 – 77, https://doi.org/10.1016/j.precamres.2011.09.005

Kolodzie S, 1980, Analysis of pore throat size and use of the Waxman-Smits equation to determine OOIP in Spindle Field, Colorado: Society of Petroleum Engineers of AIME, p. 1-10, https://doi.org/10.2118/9382-MS

Kreitler, C.W., 1989, Hydrogeology of Sedimentary Basins; Journal of Hydrology, v. 106, p. 29-53, https://doi.org/10.1016/0022-1694(89)90165-0

Lafargue E. and C. Barker, 1988, Effect of Water Washing on Crude Oil Compositions: AAPG Bulletin 1988, v. 72, n. 3, p. 263 – 276. https://doi.org/10.1306/703C8C13-1707-11D7-8645000102C1865D

Lasso A., A. Mora, C. Villamizar, J. Gelvez, J. Ortiz, J. Rico, 2018, Basin scale Flow of water in southern Llanos. Impacts on petroleum exploration: Resumenes Extendidos, Cumbre del Petróleo y Gas.

Macellari C. E., 2021, Recent uplift and the origin of hydrodynamic traps in the Llanos Basin of Colombia: Marine and Petroleum Geology, v. 132, p. 1 - 12, https://doi.org/10.1016/j.marpetgeo.2021.105198

Mazor E. and R. Nativ, 1992, Hydraulic calculation of groundwater flow velocity and age: examination of the basic premises; Journal of Hydrology, v. 138, p. 211 – 222, https://doi.org/10.1016/0022-1694(92)90165-R

Mills R.V.A. & R.C. Wells, 1919, The Evaporation and Concentration of Waters Associated with Petroleum and Natural Gas: Department of Interior – United States Geological Survey, v. 693, p. 1 – 104, https://doi.org/10.3133/b693

Milner, C. W. D., M. A. Rogers and C. R. Evans, 1977, Petroleum Transformations in Reservoirs: Journal of Geochemical Exploration, v. 7, p. 101 – 153, https://doi.org/10.1016/0375-6742(77)90079-6

Montoya S., 2016, gidahatari.com: https://gidahatari.com/ih-es/como-hacer-un-diagrama-de-stiff-georeferenciado-con-python-y-qgis

Mora, A., M. Parra, M.R. Strecker, E. R. Sobel, H. Hooghiemstra, V. Torres, and J. Vallejo-Jaramillo, 2008, Climatic forcing of asymmetric orogenic evolution in the Eastern Cordillera of Colombia: Geological Society of America Bulletin, v. 120, n. 7–8, p. 930–949, https://doi.org/10.1130/B26186.1

Mora, A., V. Blanco, J. Naranjo, N. Sanchez, R. Ketcham, J. Rubiano, D. F. Stockli, I. Quintero, M. Nemcok, B.K. Horton and H. Davila, 2013, On the lag time between internal strain and basement

involved thrust induced exhumation: The case of the Colombian Eastern Cordillera: Journal of Structural Geology, v. 52, p. 96 – 118, https://doi.org/10.1016/j.jsg.2013.04.001

Mora, A., M. Parra, G. Rodriguez Forero, V. Blanco, N. Moreno and V. Caballero, 2015, What Drives Orogenic Asymmetry in the Northern Andes?: A Case Study from the Apex of the Northern Andean Orocline: in C. Bartolini and P. Mann, eds, Petroleum Geology and Potential of the Colombian Caribbean Margin: AAPG Memoir 108, p. 547 – 586, DOI:10.1306/13531949M1083652

Mora A., C. Villamizar, E. Cardozo, V. Caballero, J. Gelvez, R. Gómez, S. Lozada, S. Valencia, R. Beltran, M. Franco, M.L. Tejada, 2018, Geological Processes controlling stratigraphic traps in the southern Llanos Basin, Resúmenes Extendidos, Cumbre del Petróleo y Gas.

Mora, A., R. A. Gómez, C. Diaz, V. Caballero, M. Parra, C. Villamizar, A. Lasso, R. A. Ketcham, F. González-Penagos, J. Rico, J.P Arias-Martinez, 2019a, Water flow, oil biodegradation, and hydrodynamic traps in the Llanos Basin, Colombia: AAPG Bulletin, v. 103, no. 5, p. 1225–1264, doi:10.1306/1003 181611317237

Mora, A., García–Bautista, D.F., Reyes–Harker, A., Parra, M., Blanco, V., Sanchez, N., De la Parra, F., Caballero, V., Rodriguez, G., Ruiz, C., Naranjo, J., Teson, E., Niño, F., Quintero, I., Moreno, N., Cardozo, E., Gamba, N., Horton, B. K. & Arias–Martinez, J. P, 2019b, Tectonic evolution of petroleum systems within the onshore Llanos Basin: Insights on the presence of Orinoco heavy oil analogs in Colombia and a comparison with other heavy oil provinces worldwide. American Association of Petroleum Geologists Bulletin, 103(5): 1179–1224. https://doi. org/10.1306/1003181611417236

Moreno-Lopez, M.C., and A. Escalona, 2015, Precambrian– Pleistocene tectono-stratigraphic evolution of the southern Llanos Basin, Colombia: AAPG Bulletin, v. 99, n. 8, p. 1473–1501, https://doi.org/10.1306/11111413138

Palmer C., 1924, California Oil Field Waters: Economic Geology, v. 19, p. 623 - 635, https://doi.org/10.2113/gsecongeo.19.7.623.

Palmer S.E, 1993, Effect of Biodegradation and Water Washing on Crude Oil Composition, In Organic Geochemistry, eds. M.H. Engel and S.A. Macko, Topics in Geobiology, Springer, Boston, MA, v. 11, p. 511 – 533, https://doi.org/10.1007/978-1-4615-2890-6_23

Person, M., D. Butler, C.W. Gable, T. Villamil, D. Wavrek, and D. Schelling, 2012, Hydrodynamic stagnation zones: Anew play concept for the Llanos Basin, Colombia: AAPG Bulletin, v. 96, n. 1, p. 23–41, https://doi.org/10.1306/08101111019

Peters, K. E., C. C. Walters, and J. M. Moldowan, 2005, The biomarker guide: Biomarkers and isotopes in petroleum exploration and Earth history, 2nd ed.: New York, Cambridge University Press, v. 2, 1155 p.

Ramon, J. C., L. I. Dzou, W. B. Hughes, and A. G. Holba, 2001, Evolution of the Cretaceous organic facies in Colombia; implications for oil composition: Journal of South American Earth Sciences, v. 14, n. 1, p. 31–50, doi:10 .1016/S0895-9811(01)00010-4.

Reyes-Harker, A., C. F. Ruiz-Valdivieso, A. Mora, J. C. Ramirez-Arias, G. Rodriguez, F. De la Parra, V. Caballero, M. Parra, N. Moreno, B.K. Horton, J.E. Saylor, A. Silva, V. Valencia, D. Stockli and V. Blanco, 2015, Cenozoic paleogeography of the Andean foreland and retroarc hinterland of Colombia: AAPG Bulletin, v. 99, n. 8, p. 1407–1453, https://doi.org/10.1306/06181411110

Rozanski K., L. Araguas-Araguas and R. Gonfiantini, 1993, Isotopic patterns in modem global precipitation: In Climate Change in Continental Isotopic Records, eds. P. K. Swart, K. C. Lohman, J. Mckenzie, S. Savin, p. 1 – 36, https://doi.org/10.1029/GM078p0001

Sánchez N., A. Mora, M. Parra, D. Garcia, M. Cortes, T. M. Shanahan, R. Ramirez, O. Llamosa, and M. Guzman, 2015, Petroleum system modeling in the Eastern Cordillera of Colombia using geochemistry and timing of thrusting and deformation: AAPG Bulletin, v. 99, n. 8, p. 1537 – 1556, DOI: 10.1306/04161511107.

Sánchez N., J. Pacheco, M. A. Guzman-Vega, A. Mora and B. Horton, 2021, Timing of hydrocarbon entrapment in the eastern foothills of the Eastern Cordillera of Colombia: Interpretation, v. 9, n. 1, p. 1 – 15, https://doi.org/10.1190/INT-2020-0058.1

Saylor, J. E., Mora, A., Horton, B. K., & Nie, J. (2009). Controls on the isotopic composition of surface water and precipitation in the Northern Andes, Colombian Eastern Cordillera. Geochimica et Cosmochimica Acta, 73(23), 6999–7018, doi:10.1016/j.gca.2009.08.030

Springer, M. V., D. F. Garcia, F. T. T. Gonçalves, L. Landau, and D. A. Azevedo, 2010, Diamondoid and biomarker characterization of oils from the Llanos Orientales Basin, Colombia: Organic Geochemistry, v. 41, no. 9, p. 1013–1018, doi:10.1016/j.orggeochem.2010.03.002.

Swenson H.A., and H.L. Baldwin, 1965, A primer on water quality: Report USGS Unnumbered Series, p. 1-27, https://doi.org/10.3133/7000057

Trumpy, D., 1943, Pre-Cretaceous of Colombia: Geological Society American Bulletin, v. 54, n. 9, p. 1281–1304, https://doi.org/10.1130/GSAB-54-1281

Villegas, M. E., S. Bachu, J.C. Ramon, and J.R. Underschultz, 1994, Flow of formation waters in the Cretaceous–Miocene succession of the Llanos Basin, Colombia: AAPG Bulletin, v. 78, no. 12, p. 1843–1862, https://doi.org/10.1306/A25FF319-171B-11D7-8645000102C1865D

Washburn C.W., 1914, Chlorides in Oil-Field Waters: Transactions of AIME, v. 48, n. 1, p. 687 – 694, https://doi.org/10.2118/915687-G.

Wendebourg J., J-J Biteau and Y. Grosjean, 2018, Hydrodynamics and hydrocarbon trapping: Concepts, pitfalls and insights from case studies: Marine and Petroleum Geology, v. 96, p. 190 – 201, https://doi.org/10.1016/j.marpetgeo.2018.05.015

Wolaver B.D., J.C. Coogan, B. K. Horton, L. Suarez Bermudez, A. Y. Sun, T. F. Wawrzyniec, T. Zhang, T. M. Shanahan, D. B. Dunlap, R. A. Costley, and L. de la Rocha, 2015, Structural and hydrogeologic evolution of the Putumayo Basin and adjacent fold-thrust belt, Colombia: AAPG Bulletin v. 99, n. 10, p. 1893–1927, doi:10.1306 /05121514186.

## Tables

**Table 1**. Hydraulic Heads (Hw) estimated from initial reservoir pressure data in wells of southern Llanos Basin in the Basal Flow Unit (n=43).

| Sample ID | Long (W) | Lat (N) | Hydraulic Head (Hw) (m) |
|---|---|---|---|
| W-1 | 71.774064 | 3.846359 | 88.8 |
| W-5 | 73.943412 | 3.443077 | 409.96 |
| W-6 | 73.443317 | 3.684937 | 168.94 |
| W-7 | 72.933759 | 3.455608 | 215.23 |
| W-11 | 73.393446 | 3.689463 | 196.23 |
| W-17 | 71.818042 | 3.767322 | 84.41 |
| W-18 | 73.191202 | 3.813505 | 146.27 |
| W-19 | 71.688706 | 3.707948 | 113.51 |
| W-21 | 73.596643 | 3.458762 | 216.47 |
| W-24 | 73.226297 | 3.826055 | 131.86 |
| W-26 | 73.030112 | 3.238458 | 245.36 |
| W-27 | 73.031124 | 3.181783 | 245.29 |
| W-29 | 73.110375 | 3.028119 | 271.54 |
| W-31 | 71.739712 | 3.712175 | 114.31 |
| W-38 | 73.60964 | 3.284817 | 366.4 |
| W-39 | 73.677906 | 2.989145 | 282.25 |
| W-50 | 73.471747 | 3.66663 | 138.33 |
| W-53 | 72.634872 | 3.354711 | 167.26 |

| Sample ID | Long (W) | Lat (N) | Hydraulic Head (Hw) (m) |
|---|---|---|---|
| W-54 | 72.660242 | 3.90954 | 143.56 |
| W-55 | 72.966474 | 3.523389 | 200.82 |
| W-60 | 73.730986 | 3.769707 | 286.62 |
| W-65 | 72.700291 | 3.123672 | 203.14 |
| W-72 | 73.156969 | 3.835778 | 140.52 |
| W-78 | 73.143745 | 3.796591 | 154.43 |
| W-82 | 73.743292 | 3.305889 | 308.8 |
| W-83 | 73.465256 | 3.616413 | 144.12 |
| W-84 | 73.505136 | 3.605417 | 144.72 |
| W-85 | 73.482313 | 3.670392 | 104.8 |
| W-86 | 73.890152 | 3.278947 | 365.16 |
| W-87 | 73.775375 | 3.09621 | 254.52 |
| W-88 | 73.986479 | 3.456747 | 490.68 |
| W-89 | 72.042915 | 3.794142 | 132.57 |
| W-90 | 73.352221 | 3.459513 | 241.49 |
| W-91 | 72.458583 | 3.66802 | 127.74 |
| W-92 | 72.564819 | 3.711219 | 112.44 |
| W-93 | 73.203656 | 2.936272 | 283.71 |
| W-94 | 73.23045 | 3.192421 | 244.87 |
| W-95 | 72.836564 | 3.066075 | 294 |
| W-96 | 72.927806 | 2.945268 | 329.41 |
| W-97 | 72.994571 | 3.127304 | 273.64 |
| W-98 | 73.222927 | 3.085625 | 212.31 |
| W-99 | 73.203663 | 2.936717 | 244.05 |
| W-100 | 73.852122 | 3.376585 | 227.98 |

**Table 2**. Oil density from PVT analysis and Tilt Amplification Factor (*TAF*) values for crude oils from the southern Llanos Basin. For the estimation of TAF values, a water density of 1 g/cm$^3$ was considered.

| Sample ID | Long (W) | Lat (N) | Oil Density (g/cm$^3$) | TAF |
|---|---|---|---|---|
| W-2 | 73.6807 | 3.9794 | 0.97 | 33.3 |
| W-5 | 73.9434 | 3.4431 | 0.98 | 50 |
| W-6 | 73.4433 | 3.6849 | 0.95 | 20 |
| W-7 | 72.9338 | 3.4556 | 0.98 | 50 |

| Sample ID | Long (W) | Lat (N) | Oil Density ($g/cm^3$) | TAF |
|---|---|---|---|---|
| W-8 | 73.3984 | 3.6385 | 0.93 | 14.3 |
| W-17 | 71.8180 | 3.7673 | 0.92 | 12.5 |
| W-24 | 73.2263 | 3.8261 | 0.93 | 14.3 |
| W-26 | 73.0301 | 3.2385 | 0.97 | 33.3 |
| W-29 | 73.1104 | 3.0281 | 0.97 | 33.3 |
| W-31 | 71.7397 | 3.7122 | 0.97 | 33.3 |
| W-32 | 72.2324 | 3.4635 | 0.97 | 33.3 |
| W-36 | 71.4001 | 3.7921 | 0.962 | 26.3 |
| W-37 | 71.5379 | 3.7982 | 0.951 | 20.4 |
| W-62 | 73.9371 | 3.3500 | 0.99 | 100 |
| W-64 | 73.7473 | 3.8832 | 0.97 | 33.3 |
| W-66 | 71.5161 | 3.8155 | 0.948 | 19.2 |
| W-67 | 73.7380 | 3.9369 | 0.97 | 33.3 |
| W-68 | 72.6609 | 3.9020 | 0.9 | 10 |
| W-69 | 73.6043 | 3.8947 | 0.98 | 50 |
| W-70 | 73.6658 | 3.8367 | 0.93 | 14.3 |
| W-71 | 73.0846 | 3.0356 | 0.97 | 33.3 |
| W-72 | 73.1570 | 3.8358 | 0.97 | 33.3 |
| W-73 | 73.0841 | 3.0351 | 0.96 | 25 |
| W-74 | 73.9018 | 3.2768 | 0.99 | 100 |
| W-75 | 71.6808 | 3.7118 | 0.95 | 20 |
| W-76 | 73.1909 | 3.1479 | 0.94 | 16.7 |
| W-77 | 73.0420 | 3.1135 | 0.98 | 50 |
| W-78 | 73.1437 | 3.7966 | 0.96 | 25 |
| W-79 | 73.9863 | 3.4562 | 0.98 | 50 |
| W-80 | 71.4209 | 3.7943 | 0.961 | 25.6 |

**Table 3**. API gravity of crude oil from wells of the southern Llanos Basin (n=34)

| Sample ID | Long (W) | Lat (N) | ° API |
|---|---|---|---|
| W-1 | 71.7741 | 3.8464 | 15.02 |
| W-5 | 73.9434 | 3.4431 | 8.5 |
| W-6 | 73.4433 | 3.6849 | 11.6 |
| W-7 | 72.9338 | 3.4556 | 9.07 |

| Sample ID | Long (W) | Lat (N) | ° API |
|---|---|---|---|
| W-8 | 73.3984 | 3.6385 | 14 |
| W-10 | 73.6201 | 3.8751 | 13.5 |
| W-17 | 71.8180 | 3.7673 | 16 |
| W-18 | 73.1912 | 3.8135 | 14.1 |
| W-24 | 73.2263 | 3.8261 | 11.8 |
| W-27 | 73.0311 | 3.1818 | 10 |
| W-28 | 73.4727 | 4.0882 | 40.2 |
| W-29 | 73.1104 | 3.0281 | 10 |
| W-31 | 71.7397 | 3.7122 | 11.03 |
| W-32 | 72.2324 | 3.4635 | 10.5 |
| W-33 | 73.7475 | 3.8832 | 8.47 |
| W-36 | 71.4001 | 3.7921 | 12.4 |
| W-37 | 71.5379 | 3.7982 | 12 |
| W-39 | 73.6779 | 2.9891 | 4.9 |
| W-42 | 73.8841 | 3.2994 | 6.5 |
| W-50 | 73.4718 | 3.6667 | 11.68 |
| W-53 | 72.6349 | 3.3547 | 13 |
| W-54 | 72.6602 | 3.9095 | 18 |
| W-55 | 72.9665 | 3.5234 | 16.5 |
| W-56 | 73.3876 | 4.0648 | 16.9 |
| W-57 | 73.4548 | 4.0193 | 33.5 |
| W-58 | 73.6510 | 3.9835 | 8.93 |
| W-59 | 73.7105 | 3.9406 | 8.55 |
| W-60 | 73.7310 | 3.7697 | 10 |
| W-61 | 71.6720 | 3.6935 | 12 |
| W-62 | 73.9371 | 3.3500 | 10 |
| W-63 | 72.1813 | 3.4738 | 10 |
| W-64 | 73.7473 | 3.8832 | 8.74 |
| W-65 | 72.7003 | 3.1237 | 9 |
| W-66 | 71.5161 | 3.8155 | 12.2 |

**Table 4**. SARA Analysis fractions (Saturates, Aromatics, Resins and Asphaltenes) and Compositional Trend Index (*CTI*) of crude oils of the southern Llanos Basin.

| Sample ID | Long (W) | Lat (N) | Saturates (%) | Aromatics (%) | Resins (%) | Asphaltenes (%) | Resins + Asph (%) | Compositional Trend Index (CTI) |
|---|---|---|---|---|---|---|---|---|
| W-1 | 71.7741 | 3.8464 | 43.4 | 27.6 | - | - | 29.0 | 2.45 |
| W-2 | 73.6807 | 3.9794 | 18.8 | 31.6 | 31.6 | 17.9 | - | 1.02 |
| W-3 | 72.5187 | 3.7780 | 36.2 | 24.8 | - | - | 38.9 | 1.57 |
| W-4 | 73.3879 | 4.0816 | 41.5 | 32.0 | - | - | 26.5 | 2.77 |
| W-5 | 73.9434 | 3.4431 | 25.2 | 29.2 | - | - | 45.6 | 1.19 |
| W-6 | 73.4433 | 3.6849 | 15.3 | 29.6 | 39.7 | 15.4 | - | 0.82 |
| W-7 | 72.9338 | 3.4556 | 19.6 | 29.8 | 39.2 | 11.4 | - | 0.98 |
| W-8 | 73.3984 | 3.6385 | 30.9 | 24.3 | - | - | 44.8 | 1.23 |
| W-9 | 73.5855 | 3.7775 | 25.4 | 16.0 | - | - | 58.6 | 0.71 |
| W-10 | 73.6201 | 3.8751 | 33.4 | 29.5 | 12.2 | 25.0 | - | 1.17 |
| W-11 | 73.3935 | 3.5990 | 21.9 | 25.4 | - | - | 52.7 | 0.90 |
| W-12 | 73.1026 | 2.9927 | 38.9 | 11.4 | - | - | 49.7 | 1.01 |
| W-13 | 73.7332 | 3.9161 | 14.2 | 30.8 | 39.8 | 15.2 | - | 0.82 |
| W-14 | 73.6755 | 3.9422 | 24.6 | 29.0 | 27.9 | 18.6 | - | 1.15 |
| W-15 | 73.9167 | 3.3266 | 20.5 | 28.2 | - | - | 51.3 | 0.95 |
| W-16 | 73.9478 | 3.5535 | 19.4 | 31.0 | - | - | 49.6 | 1.02 |
| W-17 | 71.8180 | 3.7673 | 48.3 | 29.9 | - | - | 21.8 | 3.59 |
| W-18 | 73.1912 | 3.8135 | 31.7 | 30.8 | 22.1 | 15.4 | - | 1.67 |
| W-19 | 71.6887 | 3.7081 | 39.1 | 35.2 | 14.3 | 11.4 | - | 2.88 |
| W-20 | 71.6978 | 3.6952 | 46.7 | 31.0 | - | - | 22.3 | 3.48 |
| W-21 | 73.5967 | 3.4588 | 25.5 | 26.2 | - | - | 48.3 | 1.07 |
| W-22 | 73.6115 | 3.4867 | 16.6 | 22.2 | 30.6 | 30.6 | - | 0.63 |
| W-23 | 73.3686 | 4.0947 | 34.0 | 27.8 | 26.0 | 12.2 | - | 1.62 |
| W-24 | 73.2263 | 3.8261 | 34.4 | 26.0 | 22.9 | 16.7 | - | 1.53 |
| W-25 | 72.1909 | 3.4708 | 18.0 | 30.4 | - | - | 51.7 | 0.94 |
| W-26 | 73.0301 | 3.2385 | 15.2 | 34.9 | 39.1 | 10.8 | - | 1.00 |
| W-27 | 73.0311 | 3.1818 | 17.7 | 37.1 | 36.1 | 9.1 | - | 1.21 |
| W-28 | 73.4727 | 4.1063 | 71.0 | 19.0 | 6.0 | 4.0 | | 9.00 |
| W-29 | 73.1104 | 3.0281 | 27.1 | 24.7 | - | - | 48.2 | 1.07 |
| W-30 | 73.5007 | 3.8619 | 12.4 | 11.2 | - | - | 76.4 | 0.31 |
| W-31 | 71.7397 | 3.7122 | 41.4 | 28.4 | - | - | 30.2 | 2.31 |
| W-32 | 72.2324 | 3.4635 | 34.5 | 20.1 | - | - | 45.5 | 1.20 |

| Sample ID | Long (W) | Lat (N) | Saturates (%) | Aromatics (%) | Resins (%) | Asphaltenes (%) | Resins + Asph (%) | Compositional Trend Index (CTI) |
|---|---|---|---|---|---|---|---|---|
| W-33 | 73.7475 | 3.8832 | 22.4 | 23.2 | 37.8 | 16.6 | - | 0.84 |
| W-34 | 73.4985 | 3.9863 | 16.6 | 33.0 | - | - | 50.4 | 0.99 |
| W-35 | 73.5100 | 3.9746 | 13.6 | 29.4 | - | - | 57.0 | 0.76 |
| W-36 | 71.4001 | 3.7921 | 48.3 | 33.2 | - | - | 18.6 | 4.39 |
| W-37 | 71.5379 | 3.7982 | 48.4 | 27.6 | - | - | 24.0 | 3.17 |
| W-38 | 73.6096 | 3.2848 | 4.4 | 4.5 | - | - | 91.1 | 0.10 |
| W-39 | 73.6779 | 2.9891 | 27.8 | 24.4 | - | - | 47.8 | 1.09 |
| W-40 | 73.7626 | 3.1492 | 23.9 | 24.0 | - | - | 52.1 | 0.92 |
| W-41 | 73.9302 | 3.3578 | 22.0 | 21.9 | - | - | 56.1 | 0.78 |
| W-42 | 73.8841 | 3.2994 | 26.7 | 26.6 | - | - | 46.7 | 1.14 |
| W-43 | 71.0702 | 4.0338 | 51.1 | 13.1 | - | - | 36.5 | 1.76 |
| W-44 | 71.1602 | 3.8090 | 45.9 | 32.9 | 6.5 | 14.7 | - | 3.72 |
| W-45 | 73.4392 | 4.0426 | 69.3 | 20.6 | - | - | 10.1 | 8.90 |
| W-46 | 71.5160 | 3.8155 | 39.2 | 32.3 | - | - | 23.5 | 3.04 |
| W-47 | 71.6431 | 3.5332 | 16.1 | 12.3 | - | - | 71.6 | 0.40 |
| W-48 | 71.4260 | 3.6130 | 16.5 | 7.2 | - | - | 76.3 | 0.31 |
| W-49 | 71.7864 | 3.0720 | 3.6 | 5.8 | - | - | 90.6 | 0.10 |
| W-50 | 73.4717 | 3.6666 | 18.2 | 24.2 | 41.3 | 16.3 | - | 0.74 |
| W-51 | 71.4473 | 3.6358 | 56.8 | 18.0 | - | - | 25.2 | 2.97 |
| W-52 | 72.1114 | 3.5461 | 33.1 | 24.8 | - | - | 42.1 | 1.38 |
| W-53 | 72.6349 | 3.3547 | 24.3 | 27.1 | - | - | 48.6 | 1.06 |
| W-54 | 72.6602 | 3.9095 | 58.3 | 22.4 | - | - | 19.3 | 4.18 |
| W-55 | 72.9665 | 3.5234 | 28.5 | 32.6 | 25.2 | 13.7 | - | 1.57 |

**Table 5**. Anions and cations compositions (mg/L) for groundwater samples from the southern Llanos Basin (n=93).

| Sample ID | Long (W) | Lat (N) | Anion (mg/L) | | | | Cation (mg/L) | | | |
|---|---|---|---|---|---|---|---|---|---|---|
| | | | HCO3 | CO3 | SO4 | Cl | Na | K | Ca | Mg |
| W-1 | 71.7741 | 3.8464 | 671.0 | 0.0 | 4.0 | 407.0 | 431.5 | 48.1 | 52.2 | 6.8 |
| W-5 | 73.9434 | 3.4431 | 114.4 | 0.0 | 2.9 | 5.0 | 42.1 | 8.7 | 17.1 | 1.0 |
| W-6 | 73.4433 | 3.6849 | 267.0 | 0.0 | 4.0 | 183.0 | 167.0 | 3.2 | 29.0 | 4.8 |
| W-7 | 72.9338 | 3.4556 | 610.0 | 0.0 | 4.0 | 74.8 | 290.0 | 10.7 | 68.8 | 5.7 |

| Sample ID | Long (W) | Lat (N) | Anion (mg/L) | | | | Cation (mg/L) | | | |
|---|---|---|---|---|---|---|---|---|---|---|
| | | | HCO3 | CO3 | SO4 | Cl | Na | K | Ca | Mg |
| W-11 | 73.3935 | 3.6895 | 366.0 | 0.0 | 4.0 | 126.0 | 199.0 | 2.2 | 30.2 | 0.7 |
| W-17 | 71.8180 | 3.7673 | 640.5 | 0.0 | 4.0 | 334.0 | 426.0 | 15.8 | 21.5 | 5.7 |
| W-18 | 73.1912 | 3.8135 | 198.3 | 0.0 | 4.0 | 50.1 | 35.5 | 40.4 | 37.9 | 8.8 |
| W-19 | 71.6887 | 3.7079 | 732.0 | 30.0 | 1.0 | 291.0 | 588.0 | 15.0 | 41.3 | 8.6 |
| W-20 | 71.6978 | 3.6952 | 640.5 | 0.0 | 4.0 | 183.0 | 342.5 | 17.2 | 8.7 | 1.6 |
| W-21 | 73.5966 | 3.4588 | 167.8 | 0.0 | 4.0 | 91.4 | 126.9 | 2.5 | 10.2 | 0.8 |
| W-24 | 73.2263 | 3.8261 | 488.0 | 0.0 | 15.7 | 96.6 | 245.9 | 42.5 | 11.5 | 2.0 |
| W-26 | 73.0301 | 3.2385 | 285.0 | 0.0 | 1.0 | 41.8 | 166.4 | 4.5 | 19.7 | 0.9 |
| W-27 | 73.0311 | 3.1818 | 366.0 | 0.0 | 1.0 | 42.8 | 203.6 | 9.7 | 45.4 | 1.9 |
| W-31 | 71.7397 | 3.7122 | 945.5 | 0.0 | 1.0 | 284.0 | 533.0 | 11.9 | 22.5 | 4.1 |
| W-35 | 73.5100 | 3.9746 | 427.0 | 120.0 | 113.9 | 715.0 | 1128.0 | 22.0 | 9.0 | 0.1 |
| W-53 | 72.6349 | 3.3547 | 327.9 | 0.0 | 9.1 | 49.3 | 161.1 | 4.7 | 6.2 | 0.6 |
| W-55 | 72.9665 | 3.5234 | 610.0 | 0.0 | 4.0 | 57.0 | 103.0 | 6.2 | 33.0 | 10.8 |
| W-58 | 73.6771 | 3.9456 | 1159.0 | 0.0 | 17.0 | 430.0 | 500.0 | 26.6 | 93.7 | 4.2 |
| W-75 | 71.6808 | 3.7118 | 762.5 | 0.0 | 4.0 | 175.0 | 370.2 | 19.3 | 11.2 | 1.9 |
| W-78 | 73.1437 | 3.7966 | 99.1 | 15.0 | 4.0 | 6.2 | 71.0 | 3.8 | 2.9 | 0.5 |
| W-79 | 73.9863 | 3.4562 | 100.0 | 0.0 | 4.2 | 49.0 | 42.0 | 37 | 3.1 | 0.6 |
| W-83 | 73.4652 | 3.6164 | 289.8 | 0.0 | 4.0 | 58.8 | 153.0 | 2.6 | 37.8 | 2.9 |
| W-90 | 73.3522 | 3.4595 | 488.0 | 0.0 | 4.0 | 37.4 | 220.0 | 8.3 | 48.1 | 2.7 |
| W-94 | 73.2304 | 3.1924 | 266.9 | 0.0 | 0.0 | 96.3 | 146.0 | 4.4 | 37.2 | 2.0 |
| W-118 | 73.6747 | 3.9507 | 366.0 | 0.0 | 1.0 | 56.3 | 147.0 | 12.9 | 14.9 | 1.5 |
| W-125 | 73.2438 | 3.1634 | 1300.0 | 0.0 | 42.0 | 360.0 | 725.0 | 165.0 | 3.8 | 5.7 |
| W-126 | 73.1951 | 3.1257 | 515.0 | 0.0 | 31.0 | 255.0 | 330.0 | 14.0 | 1.5 | 54.0 |
| W-127 | 73.2138 | 3.1642 | 780.0 | 0.0 | 57.0 | 490.0 | 735.0 | 66.0 | 3.7 | 17.0 |
| W-128 | 73.1890 | 3.1451 | 490.0 | 8.1 | 14.0 | 84.0 | 260.0 | 37.0 | 1.2 | 4.8 |
| W-134 | 71.6720 | 3.6935 | 701.5 | 30.0 | 4.0 | 147.0 | 399.0 | 10.5 | 15.5 | 2.0 |
| W-141 | 73.0420 | 3.1135 | 475.0 | 0.0 | 2.0 | 50.0 | 180.0 | 7.3 | 0.0 | 8.7 |
| W-144 | 71.7402 | 3.7122 | 793.0 | 0.0 | 4.0 | 210.0 | 404.0 | 10.4 | 6.1 | 1.6 |
| W-147 | 73.2494 | 3.7373 | 106.8 | 0.0 | 4.0 | 35.8 | 40.0 | 16.9 | 11.9 | 0.6 |
| W-153 | 71.4483 | 3.7964 | 988.4 | 0.0 | 9.1 | 90.3 | 409.9 | 10.0 | 7.3 | 0.0 |
| W-154 | 71.4831 | 3.7599 | 695.0 | 0.0 | 27.0 | 127.0 | 351.0 | 6.0 | 6.1 | 0.0 |
| W-174 | 73.6702 | 3.9482 | 30.5 | 0.0 | 3.1 | 5.8 | 4.7 | 4.3 | 5.9 | 1.2 |
| W-175 | 73.6825 | 3.9355 | 38.1 | 0.0 | 2.1 | 35.7 | 15.0 | 7.8 | 13.7 | 1.6 |
| W-176 | 73.6825 | 3.9332 | 53.4 | 0.0 | 4.8 | 22.8 | 20.7 | 5.7 | 8.3 | 1.6 |

| Sample ID | Long (W) | Lat (N) | Anion (mg/L) | | | | Cation (mg/L) | | | |
|---|---|---|---|---|---|---|---|---|---|---|
| | | | HCO3 | CO3 | SO4 | Cl | Na | K | Ca | Mg |
| W-177 | 73.6690 | 3.9520 | 45.8 | 0.0 | 1.0 | 8.9 | 10.8 | 5.2 | 6.6 | 1.0 |
| W-178 | 73.6839 | 3.9385 | 46.0 | 0.0 | 3.8 | 9.8 | 10.5 | 5.9 | 6.5 | 1.3 |
| W-179 | 73.6781 | 3.9354 | 274.5 | 0.0 | 9.6 | 195.0 | 170.4 | 14.7 | 32.2 | 4.1 |
| W-180 | 73.6727 | 3.9504 | 83.9 | 0.0 | 9.0 | 19.6 | 29.7 | 7.5 | 10.4 | 1.2 |
| W-181 | 73.6774 | 3.9453 | 61.0 | 0.0 | 3.7 | 6.4 | 14.8 | 6.2 | 6.8 | 1.2 |
| W-182 | 73.7146 | 3.9192 | 2120.0 | 0.0 | 0.0 | 1267.0 | 1589.0 | 118.8 | 110.8 | 8.0 |
| W-183 | 73.6899 | 3.9981 | 854.0 | 0.0 | 33.6 | 806.0 | 1032.0 | 18.9 | 35.5 | 3.8 |
| W-184 | 73.6899 | 3.9981 | 793.0 | 0.0 | 4.0 | 359.0 | 575.0 | 24.6 | 59.5 | 4.6 |
| W-185 | 73.6899 | 3.9981 | 762.5 | 0.0 | 4.0 | 369.0 | 578.0 | 29.6 | 17.4 | 3.4 |
| W-186 | 73.6899 | 3.9981 | 777.8 | 0.0 | 4.0 | 370.0 | 575.0 | 25.6 | 19.8 | 3.6 |
| W-187 | 73.6899 | 3.9981 | 732.0 | 0.0 | 8.0 | 403.0 | 566.0 | 25.9 | 17.5 | 3.9 |
| W-188 | 73.6899 | 3.9981 | 732.0 | 0.0 | 114.0 | 400.0 | 599.0 | 25.8 | 16.4 | 4.0 |
| W-189 | 73.6899 | 3.9981 | 732.0 | 0.0 | 7.0 | 413.0 | 558.0 | 25.7 | 15.6 | 3.5 |
| W-190 | 73.6899 | 3.9981 | 915.0 | 0.0 | 3.9 | 628.7 | 874.0 | 25.4 | 39.2 | 4.1 |
| W-191 | 73.6899 | 3.9981 | 976.0 | 0.0 | 7.5 | 629.0 | 887.0 | 29.0 | 38.8 | 4.6 |
| W-192 | 73.7624 | 3.9388 | 1159.0 | 0.0 | 34.8 | 672.0 | 876.0 | 12.3 | 33.8 | 1.7 |
| W-193 | 73.7624 | 3.9388 | 1260.0 | 0.0 | 117.0 | 513.0 | 808.2 | 14.5 | 32.3 | 2.8 |
| W-194 | 73.7624 | 3.9388 | 1159.0 | 0.0 | 135.0 | 563.0 | 1016.0 | 18.0 | 43.6 | 1.9 |
| W-195 | 73.7624 | 3.9388 | 1555.5 | 0.0 | 89.0 | 1080.0 | 1749.0 | 19.1 | 75.4 | 3.3 |
| W-196 | 73.6899 | 3.9981 | 732.0 | 0.0 | 8.0 | 403.0 | 566.0 | 25.9 | 17.5 | 3.9 |
| W-197 | 73.6899 | 3.9981 | 732.0 | 0.0 | 7.0 | 413.0 | 558.0 | 25.7 | 15.6 | 3.5 |
| W-198 | 73.3756 | 4.0737 | 244.0 | 0.0 | 38.9 | 823.0 | 625.0 | 15.7 | 28.1 | 5.1 |
| W-199 | 73.3773 | 4.0702 | 153.0 | 0.0 | 11.8 | 178.0 | 136.5 | 10.7 | 34.0 | 2.0 |
| W-200 | 73.4034 | 4.0881 | 549.0 | 0.0 | 17.6 | 113.9 | 186.0 | 53.8 | 27.7 | 2.8 |
| W-201 | 73.3751 | 4.0862 | 73.3 | 0.0 | 33.6 | 25.0 | 42.0 | 6.3 | 13.7 | 0.9 |
| W-202 | 73.6274 | 3.8684 | 122.0 | 0.0 | 16.1 | 6.8 | 50.9 | 3.6 | 8.3 | 1.0 |
| W-203 | 73.3810 | 4.0710 | 259.3 | 0.0 | 90.2 | 318.0 | 239.0 | 18.6 | 78.7 | 6.2 |
| W-204 | 73.3715 | 4.1006 | 628.3 | 0.0 | 160.0 | 585.0 | 825.0 | 41.4 | 8.0 | 4.0 |
| W-205 | 73.3894 | 4.0833 | 183.0 | 0.0 | 134.0 | 490.0 | 396.0 | 16.4 | 52.1 | 4.9 |
| W-206 | 73.3898 | 4.0792 | 70.2 | 0.0 | 20.7 | 10.9 | 20.5 | 5.6 | 13.9 | 1.1 |
| W-207 | 73.3731 | 4.0871 | 88.5 | 0.0 | 25.1 | 28.9 | 41.9 | 7.0 | 21.0 | 1.6 |
| W-208 | 73.4512 | 4.0224 | 198.3 | 0.0 | 0.0 | 533.0 | 230.8 | 13.9 | 57.1 | 6.7 |
| W-209 | 73.4450 | 4.0252 | 91.5 | 0.0 | 11.6 | 13.7 | 31.0 | 7.0 | 10.2 | 1.0 |
| W-210 | 73.4505 | 4.0290 | 1281.0 | 0.0 | 34.6 | 1278.0 | 1333.3 | 17.9 | 53.0 | 8.8 |

| Sample ID | Long (W) | Lat (N) | Anion (mg/L) | | | | Cation (mg/L) | | | |
|---|---|---|---|---|---|---|---|---|---|---|
| | | | HCO3 | CO3 | SO4 | Cl | Na | K | Ca | Mg |
| W-211 | 73.4499 | 4.0235 | 61.0 | 0.0 | 17.4 | 502.0 | 154.4 | 32.1 | 136.0 | 13.1 |
| W-212 | 73.4553 | 4.0283 | 213.5 | 0.0 | 32.7 | 447.0 | 295.2 | 21.8 | 65.6 | 6.8 |
| W-213 | 73.4434 | 4.0354 | 213.5 | 0.0 | 0.0 | 685.0 | 233.0 | 13.5 | 57.6 | 6.7 |
| W-214 | 73.4524 | 4.0465 | 175.4 | 0.0 | 1.0 | 31.0 | 57.0 | 20.4 | 25.9 | 1.6 |
| W-215 | 73.4407 | 4.0382 | 70.0 | 0.0 | 4.1 | 6.9 | 14.2 | 4.6 | 10.3 | 1.0 |
| W-216 | 73.4297 | 4.0483 | 53.4 | 7.5 | 4.0 | 4.1 | 20.5 | 5.8 | 12.6 | 1.0 |
| W-217 | 73.4420 | 4.0410 | 61.0 | 7.5 | 4.0 | 11.9 | 23.4 | 18.2 | 10.7 | 1.1 |
| W-218 | 71.7526 | 3.7414 | 915.0 | 0.0 | 4.0 | 251.0 | 395.0 | 10.6 | 6.7 | 1.8 |
| W-219 | 71.7556 | 3.7684 | 1281.0 | 0.0 | 4.0 | 541.0 | 889.0 | 22.8 | 43.5 | 3.8 |
| W-220 | 71.4287 | 3.7928 | 549.0 | 0.0 | 4.5 | 259.5 | 340.1 | 20.0 | 7.3 | 0.0 |
| W-221 | 71.4898 | 3.7665 | 943.0 | 0.0 | 1.0 | 260.0 | 483.0 | 7.5 | 1.2 | 12.5 |
| W-222 | 71.4442 | 3.7817 | 641.0 | 0.0 | 1.0 | 221.0 | 385.0 | 13.0 | 2.5 | 12.8 |
| W-223 | 71.4146 | 3.8307 | 1050.0 | 0.0 | 6.0 | 240.0 | 815.0 | 42.0 | 9.9 | 20.0 |
| W-224 | 71.3441 | 3.8330 | 610.0 | 0.0 | 4.5 | 200.0 | 320.0 | 14.0 | 2.5 | 7.0 |
| W-225 | 71.5156 | 3.9043 | 950.0 | 4.0 | 3.1 | 165.0 | 440.0 | 43.0 | 5.1 | 11.0 |
| W-226 | 71.4711 | 3.8859 | 835.0 | 0.0 | 0.0 | 72.0 | 340.0 | 18.0 | 3.5 | 6.9 |
| W-227 | 71.5547 | 3.7493 | 825.0 | 0.0 | 8.1 | 195.0 | 395.0 | 25.0 | 4.6 | 9.7 |
| W-228 | 71.4178 | 3.7502 | 750.0 | 34.0 | 72.0 | 245.0 | 495.0 | 17.0 | 26.0 | 44.0 |
| W-229 | 71.5233 | 3.7362 | 590.0 | 0.0 | 11.0 | 110.0 | 310.0 | 7.1 | 1.9 | 7.4 |
| W-230 | 71.4629 | 3.8383 | 985.0 | 0.0 | 2.0 | 125.0 | 400.0 | 35.0 | 4.8 | 8.3 |
| W-232 | 73.3586 | 4.0786 | 549.0 | 0.0 | 1.0 | 1177.0 | 993.8 | 11.1 | 38.0 | 1.2 |

**Table 6**. Deep resistivity – RT (ohm.m), temperature (°C), effective porosity (fr), and formation water resistivity-Rwa (ohm.m) estimated from well logs of southern Llanos Basin (n=128).

| Sample ID | Long (W) | Lat (N) | Depth Interval (ft) | | Average RT (ohm-m) | Average Temperatura (°C) | Efective Porosity (Frac) | Rwa (ohm-m) m = 1.8 |
|---|---|---|---|---|---|---|---|---|
| | | | Top | Bottom | | | | |
| W-5 | 73.9434 | 3.4431 | 3868 | 4305 | 2007.67 | 49.37 | 0.15 | 65.23 |
| W-6 | 73.4433 | 3.6849 | 7436 | 7787 | 403.82 | 84.53 | 0.19 | 20.71 |
| W-7 | 72.9338 | 3.4556 | 3647 | 3770 | 211.11 | 47.27 | 0.15 | 7.03 |
| W-8 | 73.3984 | 3.6385 | 6957 | 7269 | 228.41 | 55.07 | 0.20 | 12.16 |
| W-9 | 73.5855 | 3.7775 | 5542 | 5820 | 52.66 | 58.23 | 0.24 | 4.16 |
| W-11 | 73.3934 | 3.6895 | 6813 | 7031 | 382.33 | 65.12 | 0.19 | 19.97 |
| W-15 | 73.9167 | 3.3266 | 781 | 1499 | 5306.33 | 33.00 | 0.18 | 252.04 |

| Sample ID | Long (W) | Lat (N) | Depth Interval (ft) | | Average RT (ohm-m) | Average Temperatura (°C) | Efective Porosity (Frac) | Rwa (ohm-m) m = 1.8 |
|---|---|---|---|---|---|---|---|---|
| | | | Top | Bottom | | | | |
| W-16 | 73.9479 | 3.5535 | 3862 | 4437 | 787.56 | 49.72 | 0.14 | 21.42 |
| W-17 | 71.8180 | 3.7673 | 3271 | 3399 | 20.61 | 45.19 | 0.27 | 1.98 |
| W-18 | 73.1912 | 3.8135 | 7395 | 7663 | 271.42 | 81.44 | 0.20 | 15.52 |
| W-19 | 71.6887 | 3.7079 | 2912 | 3032 | 19.95 | 43.18 | 0.27 | 1.93 |
| W-21 | 73.5966 | 3.4588 | 6655 | 6935 | 378.35 | 64.42 | 0.22 | 25.40 |
| W-24 | 73.2263 | 3.8261 | 7577 | 7881 | 282.97 | 80.38 | 0.22 | 18.09 |
| W-26 | 73.0301 | 3.2385 | 3090 | 3270 | 170.72 | 63.24 | 0.26 | 15.21 |
| W-27 | 73.0311 | 3.1818 | 2873 | 2978 | 36.13 | 65.62 | 0.27 | 3.49 |
| W-29 | 73.1104 | 3.0281 | 2572 | 2671 | 38.16 | 41.23 | 0.30 | 4.26 |
| W-31 | 71.7397 | 3.7122 | 3010 | 3256 | 15.21 | 44.07 | 0.31 | 1.79 |
| W-32 | 72.2324 | 3.4635 | 3330 | 3362 | 24.83 | 45.26 | 0.29 | 2.66 |
| W-37 | 71.5379 | 3.7982 | 2882 | 3017 | 24.97 | 43.05 | 0.27 | 2.33 |
| W-38 | 73.6096 | 3.2848 | 4206 | 4784 | 4.45 | 49.82 | 0.25 | 0.36 |
| W-39 | 73.6779 | 2.9891 | 4931 | 4960 | 108.45 | 54.14 | 0.27 | 10.00 |
| W-40 | 73.7626 | 3.1492 | 5601 | 5738 | 99.48 | 58.16 | 0.22 | 6.25 |
| W-44 | 71.1602 | 3.8090 | 2536 | 2629 | 22.26 | 41.01 | 0.30 | 2.49 |
| W-46 | 71.5160 | 3.8155 | 2906 | 3033 | 24.75 | 43.16 | 0.26 | 2.24 |
| W-47 | 71.6431 | 3.5332 | 2818 | 2893 | 24.36 | 42.53 | 0.26 | 2.14 |
| W-49 | 71.7864 | 3.0720 | 2099 | 2219 | 21.71 | 38.66 | 0.28 | 2.25 |
| W-50 | 73.4717 | 3.6666 | 7564 | 7721 | 244.93 | 84.92 | 0.20 | 13.40 |
| W-52 | 72.1114 | 3.5461 | 3182 | 3279 | 12.82 | 44.61 | 0.30 | 1.44 |
| W-53 | 72.6349 | 3.3547 | 2781 | 2857 | 47.08 | 42.33 | 0.29 | 5.07 |
| W-54 | 72.6602 | 3.9095 | 5466 | 5937 | 238.99 | 58.34 | 0.07 | 2.20 |
| W-55 | 72.9665 | 3.5234 | 4144 | 4260 | 520.08 | 74.06 | 0.06 | 3.39 |
| W-60 | 73.7310 | 3.7697 | 7191 | 7851 | 538.38 | 68.45 | 0.15 | 16.86 |
| W-61 | 71.6720 | 3.6935 | 2803 | 3028 | 17.69 | 42.87 | 0.29 | 1.92 |
| W-63 | 72.1813 | 3.4738 | 3360 | 3433 | 20.93 | 45.53 | 0.30 | 2.37 |
| W-66 | 71.5161 | 3.8155 | 2907 | 3033 | 24.52 | 43.17 | 0.25 | 2.01 |
| W-68 | 72.6609 | 3.9020 | 5420 | 6957 | 34.93 | 61.05 | 0.05 | 0.16 |
| W-70 | 73.6658 | 3.8367 | 2093 | 2224 | 682.96 | 38.66 | 0.12 | 14.36 |
| W-71 | 73.0846 | 3.0356 | 2480 | 2512 | 53.01 | 73.90 | 0.29 | 5.57 |

| Sample ID | Long (W) | Lat (N) | Depth Interval (ft) | | Average RT (ohm-m) | Average Temperatura (°C) | Efective Porosity (Frac) | Rwa (ohm-m) m = 1.8 |
|---|---|---|---|---|---|---|---|---|
| | | | Top | Bottom | | | | |
| W-75 | 71.6808 | 3.7118 | 2855 | 3171 | 18.58 | 43.41 | 0.32 | 2.39 |
| W-76 | 73.1909 | 3.1479 | 4474 | 4867 | 269.06 | 52.61 | 0.30 | 31.37 |
| W-78 | 73.1437 | 3.7966 | 6893 | 7044 | 266.23 | 65.38 | 0.20 | 14.17 |
| W-79 | 73.9863 | 3.4562 | 3997 | 4201 | 1647.65 | 49.44 | 0.22 | 111.51 |
| W-82 | 73.7433 | 3.3059 | 6261 | 6507 | 1952.56 | 62.13 | 0.21 | 119.68 |
| W-84 | 73.5051 | 3.6054 | 7280 | 7676 | 542.14 | 77.80 | 0.19 | 26.00 |
| W-86 | 73.8902 | 3.2789 | 1383 | 1934 | 8600.00 | 35.88 | 0.18 | 373.22 |
| W-88 | 73.9865 | 3.4567 | 2653 | 2886 | 982.72 | 42.05 | 0.17 | 38.78 |
| W-89 | 72.0429 | 3.7941 | 3906 | 3939 | 74.67 | 48.46 | 0.17 | 2.95 |
| W-90 | 73.3522 | 3.4595 | 5738 | 5769 | 50.97 | 85.84 | 0.20 | 2.92 |
| W-91 | 72.4586 | 3.6680 | 4092 | 4252 | 16.27 | 49.85 | 0.27 | 1.58 |
| W-92 | 72.5648 | 3.7112 | 5508 | 5618 | 447.85 | 57.57 | 0.02 | 0.39 |
| W-93 | 73.2037 | 2.9363 | 2361 | 2424 | 32.46 | 39.96 | 0.21 | 1.97 |
| W-96 | 72.9278 | 2.9453 | 2084 | 2112 | 62.50 | 38.32 | 0.13 | 1.66 |
| W-97 | 72.9946 | 3.1273 | 2529 | 2921 | 109.49 | 41.80 | 0.05 | 0.52 |
| W-98 | 73.2229 | 3.0856 | 3194 | 3279 | 54.19 | 44.65 | 0.26 | 4.80 |
| W-101 | 73.7624 | 3.9388 | 3024 | 3150 | 170.99 | 43.82 | 0.16 | 6.17 |
| W-102 | 73.6899 | 3.9981 | 9110 | 9400 | 105.27 | 78.08 | 0.18 | 4.62 |
| W-100 | 73.8521 | 3.3766 | 6314 | 6833 | 3351.26 | 63.19 | 0.16 | 125.17 |
| W-103 | 73.7201 | 3.9517 | 2762 | 2811 | 159.43 | 42.15 | 0.17 | 6.78 |
| W-104 | 73.6905 | 3.5175 | 2137 | 2300 | 521.91 | 38.99 | 0.16 | 18.42 |
| W-105 | 72.6621 | 2.7677 | 1187 | 1328 | 63.98 | 33.65 | 0.21 | 3.85 |
| W-106 | 72.8999 | 3.1810 | 2283 | 2643 | 4.42 | 40.35 | 0.26 | 0.39 |
| W-107 | 73.3968 | 3.6370 | 6940 | 7032 | 374.54 | 90.47 | 0.24 | 28.06 |
| W-108 | 73.6376 | 3.8896 | 7664 | 7931 | 298.45 | 69.99 | 0.19 | 14.45 |
| W-109 | 73.6390 | 3.8679 | 7736 | 7887 | 572.70 | 70.07 | 0.17 | 23.59 |
| W-110 | 73.6638 | 3.8517 | 6823 | 7539 | 366.05 | 39.15 | 0.15 | 12.18 |
| W-111 | 73.6638 | 3.8658 | 2197 | 2297 | 387.94 | 39.17 | 0.18 | 17.53 |
| W-112 | 73.6601 | 3.8398 | 6538 | 7016 | 725.67 | 64.32 | 0.16 | 26.50 |
| W-113 | 73.6542 | 3.8720 | 2177 | 2325 | 606.26 | 39.17 | 0.18 | 26.31 |
| W-114 | 73.6363 | 3.8569 | 6356 | 7311 | 562.23 | 64.63 | 0.16 | 20.76 |
| W-115 | 73.6697 | 3.8332 | 6663 | 7092 | 830.28 | 64.87 | 0.16 | 29.30 |

| Sample ID | Long (W) | Lat (N) | Depth Interval (ft) | | Average RT (ohm-m) | Average Temperatura (°C) | Efective Porosity (Frac) | Rwa (ohm-m) m = 1.8 |
|---|---|---|---|---|---|---|---|---|
| | | | Top | Bottom | | | | |
| W-116 | 73.7300 | 3.9074 | 8807 | 8999 | 505.31 | 76.13 | 0.13 | 13.38 |
| W-117 | 73.6771 | 3.9456 | 8545 | 8701 | 2606.02 | 85.12 | 0.18 | 123.78 |
| W-118 | 73.6747 | 3.9507 | 8603 | 8938 | 661.51 | 75.39 | 0.16 | 23.34 |
| W-119 | 73.9508 | 3.3757 | 918 | 1627 | 907.15 | 33.74 | 0.15 | 29.47 |
| W-120 | 73.8514 | 3.3868 | 3795 | 3967 | 361.94 | 48.23 | 0.28 | 35.43 |
| W-121 | 73.9027 | 3.2940 | 767 | 1387 | 4090.38 | 32.65 | 0.19 | 200.02 |
| W-122 | 73.8934 | 3.2708 | 444 | 979 | 7859.78 | 30.62 | 0.21 | 481.74 |
| W-123 | 73.9001 | 3.2792 | 300 | 896 | 4589.60 | 29.99 | 0.20 | 251.02 |
| W-124 | 73.0907 | 3.0097 | 2335 | 2488 | 28.45 | 70.99 | 0.22 | 1.82 |
| W-125 | 73.2438 | 3.1634 | 3767 | 3852 | 42.16 | 65.13 | 0.31 | 5.00 |
| W-126 | 73.1951 | 3.1257 | 3321 | 3347 | 70.90 | 45.19 | 0.30 | 8.22 |
| W-127 | 73.2138 | 3.1642 | 3692 | 3765 | 26.31 | 47.38 | 0.26 | 2.36 |
| W-128 | 73.1890 | 3.1451 | 3464 | 3507 | 131.25 | 87.21 | 0.31 | 16.31 |
| W-129 | 73.1985 | 2.9649 | 2458 | 2524 | 29.10 | 76.05 | 0.20 | 1.58 |
| W-130 | 73.0433 | 3.1202 | 2689 | 2780 | 38.14 | 41.86 | 0.21 | 2.26 |
| W-131 | 73.0389 | 3.0930 | 2568 | 2586 | 32.56 | 61.41 | 0.27 | 3.06 |
| W-132 | 73.0054 | 3.1250 | 2396 | 2501 | 41.04 | 104.74 | 0.21 | 2.49 |
| W-133 | 72.6331 | 3.2673 | 2684 | 2776 | 19.38 | 41.83 | 0.25 | 1.58 |
| W-134 | 71.6720 | 3.6935 | 3969 | 4043 | 17.06 | 48.92 | 0.24 | 1.32 |
| W-135 | 73.5848 | 3.8037 | 8871 | 9172 | 371.05 | 76.79 | 0.16 | 14.17 |
| W-136 | 73.1708 | 3.1305 | 3201 | 3221 | 16.97 | 44.51 | 0.25 | 1.44 |
| W-137 | 73.7861 | 3.8584 | 8248 | 9246 | 140.74 | 75.26 | 0.10 | 2.03 |
| W-138 | 72.9584 | 2.8460 | 1166 | 1238 | 23.45 | 33.34 | 0.21 | 1.37 |
| W-139 | 72.2335 | 3.4391 | 3209 | 3305 | 20.60 | 44.76 | 0.27 | 1.99 |
| W-140 | 72.7742 | 3.6642 | 4477 | 4618 | 125.71 | 51.93 | 0.28 | 12.47 |
| W-141 | 73.0420 | 3.1135 | 2659 | 2685 | 97.50 | 41.51 | 0.29 | 10.63 |
| W-142 | 73.0422 | 3.1135 | 2662 | 2695 | 103.99 | 41.55 | 0.29 | 11.06 |
| W-143 | 73.5832 | 3.9350 | 8637 | 8864 | 417.02 | 75.28 | 0.18 | 19.23 |
| W-144 | 71.7402 | 3.7122 | 3004 | 3244 | 14.94 | 44.02 | 0.33 | 2.01 |
| W-145 | 72.5733 | 3.9336 | 5641 | 5987 | 64.71 | 58.97 | 0.22 | 4.17 |
| W-146 | 71.4920 | 4.0550 | 3266 | 3406 | 20.69 | 45.20 | 0.26 | 1.88 |
| W-147 | 73.2494 | 3.7373 | 6971 | 7140 | 462.44 | 88.85 | 0.22 | 30.55 |
| W-148 | 71.7417 | 3.7808 | 3173 | 3429 | 13.92 | 45.01 | 0.27 | 1.33 |

| Sample ID | Long (W) | Lat (N) | Depth Interval (ft) | | Average RT (ohm-m) | Average Temperatura (°C) | Efective Porosity (Frac) | Rwa (ohm-m) m = 1.8 |
|---|---|---|---|---|---|---|---|---|
| | | | Top | Bottom | | | | |
| W-149 | 71.6335 | 4.0014 | 3403 | 3648 | 15.92 | 46.25 | 0.26 | 1.38 |
| W-150 | 71.5742 | 3.7442 | 2409 | 2495 | 9.48 | 40.29 | 0.34 | 1.38 |
| W-151 | 71.4449 | 3.7670 | 2707 | 2768 | 26.50 | 41.87 | 0.29 | 2.77 |
| W-152 | 71.5085 | 3.7962 | 2834 | 2964 | 20.74 | 42.77 | 0.26 | 1.77 |
| W-153 | 71.4484 | 3.7964 | 2746 | 2858 | 23.07 | 42.23 | 0.30 | 2.66 |
| W-154 | 71.4832 | 3.7599 | 2733 | 2852 | 20.27 | 42.18 | 0.27 | 1.91 |
| W-155 | 71.3881 | 3.7336 | 2407 | 2553 | 18.78 | 40.45 | 0.28 | 1.94 |
| W-156 | 73.0516 | 3.4051 | 4052 | 4117 | 70.76 | 49.36 | 0.25 | 5.63 |
| W-157 | 73.2344 | 3.2545 | 4401 | 4481 | 41.34 | 51.34 | 0.25 | 3.51 |
| W-158 | 73.3618 | 3.2920 | 3744 | 4910 | 3.41 | 50.70 | 0.19 | 0.18 |
| W-159 | 72.1884 | 3.1908 | 2384 | 2497 | 15.31 | 40.22 | 0.26 | 1.37 |
| W-160 | 72.6471 | 3.1935 | 2755 | 2829 | 14.01 | 42.18 | 0.17 | 0.57 |
| W-161 | 72.6245 | 3.3110 | 2820 | 2867 | 18.89 | 42.46 | 0.24 | 1.39 |
| W-162 | 72.3322 | 3.3015 | 2809 | 2828 | 14.89 | 42.32 | 0.24 | 1.14 |
| W-163 | 72.3776 | 3.0376 | 1507 | 2073 | 6.95 | 36.61 | 0.20 | 0.37 |
| W-164 | 71.7499 | 3.8563 | 3350 | 3665 | 14.31 | 46.15 | 0.26 | 1.29 |
| W-165 | 72.0766 | 2.9557 | 1840 | 1985 | 26.46 | 37.29 | 0.28 | 2.71 |
| W-166 | 71.8802 | 3.3551 | 2597 | 2711 | 12.20 | 41.41 | 0.29 | 1.34 |
| W-167 | 71.6485 | 3.4084 | 2597 | 2835 | 20.17 | 41.75 | 0.27 | 1.92 |
| W-168 | 73.4718 | 3.6667 | 8083 | 8525 | 426.88 | 88.75 | 0.17 | 17.40 |
| W-169 | 73.4434 | 3.6848 | 7754 | 8245 | 381.43 | 88.48 | 0.20 | 21.43 |
| W-170 | 72.1382 | 3.6042 | 3525 | 3612 | 16.18 | 46.49 | 0.29 | 1.79 |
| W-171 | 72.9329 | 3.5507 | 5103 | 5136 | 200.92 | 55.11 | 0.01 | 0.04 |
| W-172 | 73.5562 | 3.9612 | 9315 | 9546 | 495.31 | 79.06 | 0.15 | 15.90 |
| W-173 | 73.6887 | 3.7700 | 6860 | 7218 | 164.94 | 65.77 | 0.12 | 3.85 |

**Table 7**. Summary of estimated average linear groundwater velocities considering different ranges of oil densities, tilt of OWC and Permeabilities. The average porosity for each scenario was 20%.

| Oil Density ($g/cm^3$) | Tilt of OWC (degrees) | Permeability (mD) | Average Linear Groundwater Velocity (ft/day) (min - max) |
|---|---|---|---|
| 0.92 | 1° | 500 | 0.00033 - 0.00063 |
| | | 2000 | 0.0014 - 0.0025 |
| | | 5000 | 0.0034 - 0.0063 |
| | 1.5° | 500 | 0.00045 - 0.00086 |
| | | 2000 | 0.0019 - 0.0034 |
| | | 5000 | 0.0049 - 0.0086 |
| 0.95 | 1° | 500 | 0.00018 - 0.00036 |
| | | 2000 | 0.00076 - 0.0015 |
| | | 5000 | 0.0019 - 0.0035 |
| | 1.5° | 500 | 0.00028 - 0.00054 |
| | | 2000 | 0.0012 - 0.0022 |
| | | 5000 | 0.0030 - 0.0053 |

# 3. APORTES A LA INVESTIGACIÓN-2

## Decoding of Groundwater Recharge in Deep Aquifers of Foreland Basins Using Stable Isotopes ($\delta^{18}O$ and $\delta D$) and Anion-Cation Analysis: A Case Study in the Southern Llanos Basin, Colombia.

Ricardo Andrés Gómez-Moncada[a,b], Andrés Mora[c], Marcela Jaramillo[b], Henry Mayorga[d], Andrés Martínez[d], Mauricio Parra[e], Davis Suárez[a], Jorge Sandoval-Muñoz[a], Jose Sandoval-Ruiz[a], Víctor Caballero[a], Miguel Jiménez[a], Ricardo Bueno[a], Joel Edward Saylor[f].

[a]*Innovation and Technology Center of ECOPETROL S.A - ICP, Santander, Colombia.*

[b]*EAFIT University, Medellín, Colombia.*

[c]*Ecopetrol Oleo E Gas Do Brasil Ltda, Rio de Janeiro, Brasil.*

[d]*TIP Colombia, Santander, Colombia.*

[e]*Institute of Geosciences, University of Sao Paulo, Brasil.*

[f]*University of British Columbia. Vancouver, Canada.*

Corresponding author (ricardoandres.gomez@ecopetrol.com.co)

Corresponding author address: Ricardo Gómez-Moncada, Innovation and Technology Center of ECOPETROL S.A - ICP, Km. 7 via Piedecuesta, Santander, Colombia.

# Abstract

The topographic and structural configuration of the deformation front in foreland basins has implications in the process of hydrologic recharge of deep aquifer systems. Deep aquifer systems are favored when tectonic deformation has exhumed aquifer units to the surface, creating a connection between the surface and subsurface. The indirect water recharge processes established by this connection allow meteoric water to infiltrate and travel long distances through a basin. Therefore, establishing recharge zones and determining the influence of meteoric waters in deep aquifers represents a challenge to understand the dynamics and hydraulic potential of this type of system. This study presents new oxygen and hydrogen isotopic data from 162 samples of surface water and 109 samples from groundwater. Groundwater samples were taken from deep wells (700 m to 4000 m deep) that penetrated the aquifer units that make up the *Basal Flow Unit (BFU)* present in the southern Llanos basin in Colombia. In addition, anion (-) and cation (+) analysis ($HCO_3^-$, $CO_3^{-2}$, $SO_4^{-2}$, $Cl^-$, $Na^+$, $K^+$, $Ca^{+2}$, $Mg^{+2}$) was performed on 67 surface water samples and 93 groundwater samples from wells to evaluate their composition and existing relationship with the recharge areas. We used these isotope compositions ($\delta^{18}O$ - $\delta D$) and hydrochemical data to identify the provenance and degree of influence of meteoric waters in the Basal Flow Unit. Thus, we evaluated the isotopic behavior of the Andean Foreland in Colombia. These data allowed us to propose the altitude ranges of the recharge zones for a deep regional aquifer (BFU) that extends along the southern Llanos basin in Colombia. The $\delta^{18}O$ and $\delta D$ values from surface water sources showed consistency with respect to the isotopic behavior reported in global datasets (GMWL), the Local Meteoric Water Line (LMWL) established for Llanos basin, and data from IAEA-GNIP stations examined in this study. The new $\delta^{18}O$ and $\delta D$ analysis, together with datasets from previous studies carried out in the area, made it possible to establish the Local Meteoric Water Line for the Llanos basin following the equation $\delta D = 7.8 (\pm 0.10) \times \delta^{18}O + 11.66 (\pm 0.75)$. $\delta^{18}O$ and $\delta D$ values of groundwater samples taken in the deep wells follow the proposed Llanos Local Meteoric Water Line. It supports a high influence of meteoric waters in the *Basal Flow Unit*, from areas close to the recharge zones up to more than 300 km away to the east of the basin and suggesting its origin from approximate altitude ranges that vary between 580 m and 2060 m, related to the La Macarena Range and the eastern flank of the Eastern Cordillera. The physicochemical data was used as an additional proxy and showed the lowest ion concentrations in proximity to the recharge zones, recognizing in general groundwater with low concentrations of $Cl^-$ (4.1 - 1278 mg/L) and Na (4.7 – 1749 mg/L) along the BFU present in the southern Llanos basin.



**Keywords:** Deep aquifers, stable isotopes, $\delta^{18}O$ - $\delta D$, anions (-), cations (+), water recharge.

## 1. Introduction

Identifying the recharge areas of a hydrogeological system is essential for the understanding of the dynamics and characteristics of groundwater in a given region. Two main types of recharge are recognized: direct recharge that occurs by direct percolation of precipitation, and indirect recharge, which occurs following runoff or through the beds of surface watercourses (Lerner et al., 1990; Simmers, 1997; Lloyd, 1986). However, the recognition of these recharge zones is theoretically simple and relatively intuitive (but by no means easy to quantify) when it comes to a recharge controlled mainly by precipitation (Lerner et al., 1990). When the recharge is indirect (e.g., river-aquifer), the determination of the recharge zones represents an additional challenge in the characterization of the aquifer systems, especially when it comes to connected aquifers from the surface to depths of the order of thousands of meters. In addition, the challenge becomes greater when considering groundwater flow paths of hundreds of kilometers (Alley, 2009). Many authors have reported the water recharge analysis in deep aquifers referring to depths that do not exceed on average 500 meters (e.g., Sharma and Huges, 1985; Yang et al., 1999; De Vries et al., 2000; Alley 2009; Currell et al., 2010; Xu et al., 2017; Tirumalesh et al., 2017; Guo et al., 2019; Huang et al., 2019). However, recharge processes of aquifers connected with the surface become efficient even at depths of the order of kilometers (Bair et al., 1985; Garven, 1985; Hitchon, 1969).

Stable isotopes of water are useful in determining groundwater's provenance, revealing the mixing processes, and tracing the isotopic evolution of groundwater (Kong et al., 2017). These isotopes are commonly used to identify linkages between the surface water and the groundwater systems and provide insights into water movements (Kendall and Caldwell, 1998). The integration of stable isotopes (e.g., δD, $\delta^{18}O$) and chemical tracers (e.g., $HCO_3^-$, $CO_3^{-2}$, $SO_4^{-2}$, $Cl^-$, $Na^+$, $K^+$, $Ca^{+2}$, $Mg^{+2}$), constitute a powerful tool for the understanding of recharge processes and residence times of

groundwater (Edmunds and Wright, 1979; Edmunds et al., 2003; Negrel et al., 2011; Monjerezi et al., 2011; Negrel et al., 2012; Carucci et al., 2012; Giambastiani et al., 2013; Zabala et al., 2015).

This research focuses on the Llanos basin, which is located in the central-eastern sector of Colombia (**Figure 1**). Previous research has documented the flow directions in the Llanos Basin by correlating zones of water with low concentrations of anions (-) and cations (+) in the basin which match with regions with high hydraulic head associated with the Eastern Cordillera and La Macarena Range in the orogenic belt (Villegas et al., 1994; Bachu et al., 1995; González-Uribe et al., 2007; Person et al., 2012; González-Penagos et al., 2014; González-Penagos et al., 2017; Mora et al., 2019; Gómez-Moncada et al., 2022). (See **Figure 1** for location).

The isotopic analyses presented by González-Penagos et al. (2014) show that meteoric waters already influence some reservoirs of the central and northern Llanos basin. On the other hand, González-Uribe et al. (2007) show that towards the foothills of the Eastern Cordillera, the influx of meteoric waters is not as efficient as towards the adjacent foreland basin. It was confirmed with the presence of high concentrations of ions in groundwater, and isotopic concentrations of groundwater that move away from the local Colombian meteoric water line presented by Rodriguez (2004), or even in the global datasets (e.g., Craig, 1961; Rozanski et al., 1993)

The main goal of this study is to focus on identifying the provenance and ionic concentrations of groundwater in deep aquifers that are connected from the surface to more than -3,000 m.a.s.l deep, along the southern Llanos basin. Moreover, we evaluate the degree of influence of meteoric water in different structural styles. We document that water would be traveling long distances from the elevated zones related with the deformation front to the distal part of the basin (>300 Km) and passing through high pressure (600 - 4500 Psi) and high temperature (58° - 126°C) conditions.

Stable isotopes ($\delta^{18}O$ and $\delta D$) and a complete characterization of anions (-) ($HCO_3^-$, $CO_3^{-2}$, $SO_4^{-2}$, $Cl^-$) and cations (+) ($Na^+$, $K^+$, $Ca^{+2}$, $Mg^{+2}$) were used to understand the recharge process of these deep groundwater, which has reached different stratigraphic units along the southern Llanos basin. Likewise, we compare the isotopic composition of groundwaters with the isotopic signal of meteoric waters, comparing how deviated is the isotopic signal from groundwater with respect to the Local Meteoric Water Line (Llanos LMWL) and the Global Meteoric Water Lines (GMWL) (e.g., Craig, 1961; Rozanski et al., 1993). An additional important goal of the isotopic study was to propose altitude ranges for the different isotopic values obtained from groundwater samples. These altitude ranges were estimated using the altitude model proposed by Saylor et al. (2009). The key outcome of these analyses would be to associate the isotopic values coming from groundwater, whose waters have a potential provenance from meteoric waters, with altitude ranges of the recharging zones. The isotopic analysis was integrated with the results reported in the northwestern part of the basin (e.g., González-Uribe et al., 2007; González-Penagos et al., 2014; Saylor et al., 2009), allowing us to establish the Llanos Meteoric Water Line, and likewise propose the potential recharge areas of the Basal Flow Unit.

## 2. Regional Setting

### *2.1. Geology*

The study area is located in the northwestern corner of South America, in the southern Llanos basin of eastern Colombia. This sedimentary basin is a foreland basin bounded by the Eastern Cordillera fold-thrust belt to the northwest, La Macarena Range to the southwest, and the Precambrian basement of the Guyana Shield to the east (Moreno-López and Escalona, 2015) (**Figure 1**).

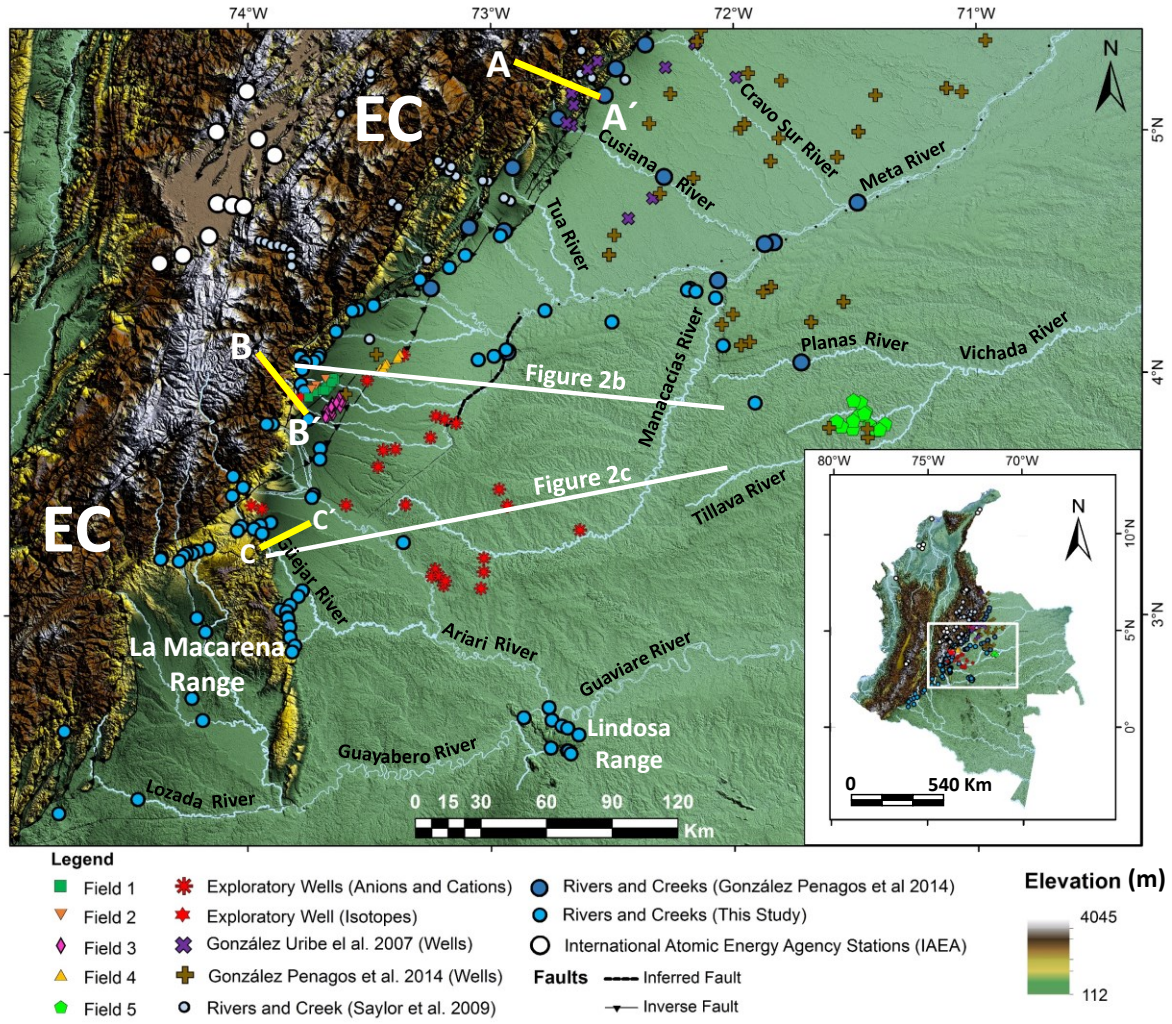


**Figure 1**. Digital elevation model (from the Shuttle Radar Topography Mission-SRTM) of central Colombia showing regional hydrology and sample locations. EC: Eastern Cordillera. Cross-sections A-A', B-B', and C-C' are showed in **Figure 11**. All samples except for those represented by the red asterisk [anions (-) and cations (+)] correspond to isotopic analysis.

The sedimentary record of the Llanos basin was controlled by the tectonics associated with the Northern Andean orogeny (Cooper et al., 1995; Parra et al., 2009, 2010; Mora et al., 2010b; Mora et al., 2013), and corresponds to siliciclastic deposits from the Paleozoic (undifferentiated), Mesozoic and Cenozoic Eras. Ages of stratigraphic units from Mesozoic and Cenozoic eras range from the Upper Cretaceous (Une, Gachetá, and Guadalupe Formations), Paleogene (Barco, Cuervos, Mirador, and Carbonera (C8-C7) Formations), Neogene (Carbonera (C6-C1), León and Guayabo Formations) and Quaternary deposits (**Figure 2**, from Reyes-Harker et al., 2015). In the southern

Llanos basin, towards La Macarena Range, the Paleocene stratigraphic units (Barco and Cuervos Formations) are absent, since these units are restricted to the deep western sector of the basin, but no including La Macarena Range (e.g., Reyes-Harker et al., 2015; Mora et al., 2019).

Along-strike of western boundary of Llanos basin, changes in structural style impact the degree of connectivity between the surface and sub-surface aquifers. In the eastern flank of the Eastern Cordillera, the complexity of the style of deformation decreases to the southwest toward La Macarena Range. The decreased structural complexity and outcropping areas favors direct connection between surface water and rocks of the Upper Cretaceous and Paleogene with aquifer potential (e.g., Mora et al., 2010a, 2010b; Mora et al., 2013, Moreno et al., 2013; Jimenez et al., 2013; Mora et al., 2014; Mora et al., 2019; Gómez-Moncada et al., 2022). (**Figures 2b, 2c**).

***2.2. Hydrogeology***

Aquifer potential is related to the sandstones and minor conglomerates of the Une, Guadalupe, Barco, Mirador, and Carbonera formations, while the main aquitards correspond to the Gachetá Formation and the muddy sediments of the Eocene and Oligocene (**Figure 3**). These units onlap Paleozoic strata to the east, forming an amalgamated high porosity and permeability flow unit, directly above the Paleozoic strata, and which is referred to in the present study as the *Basal Flow*

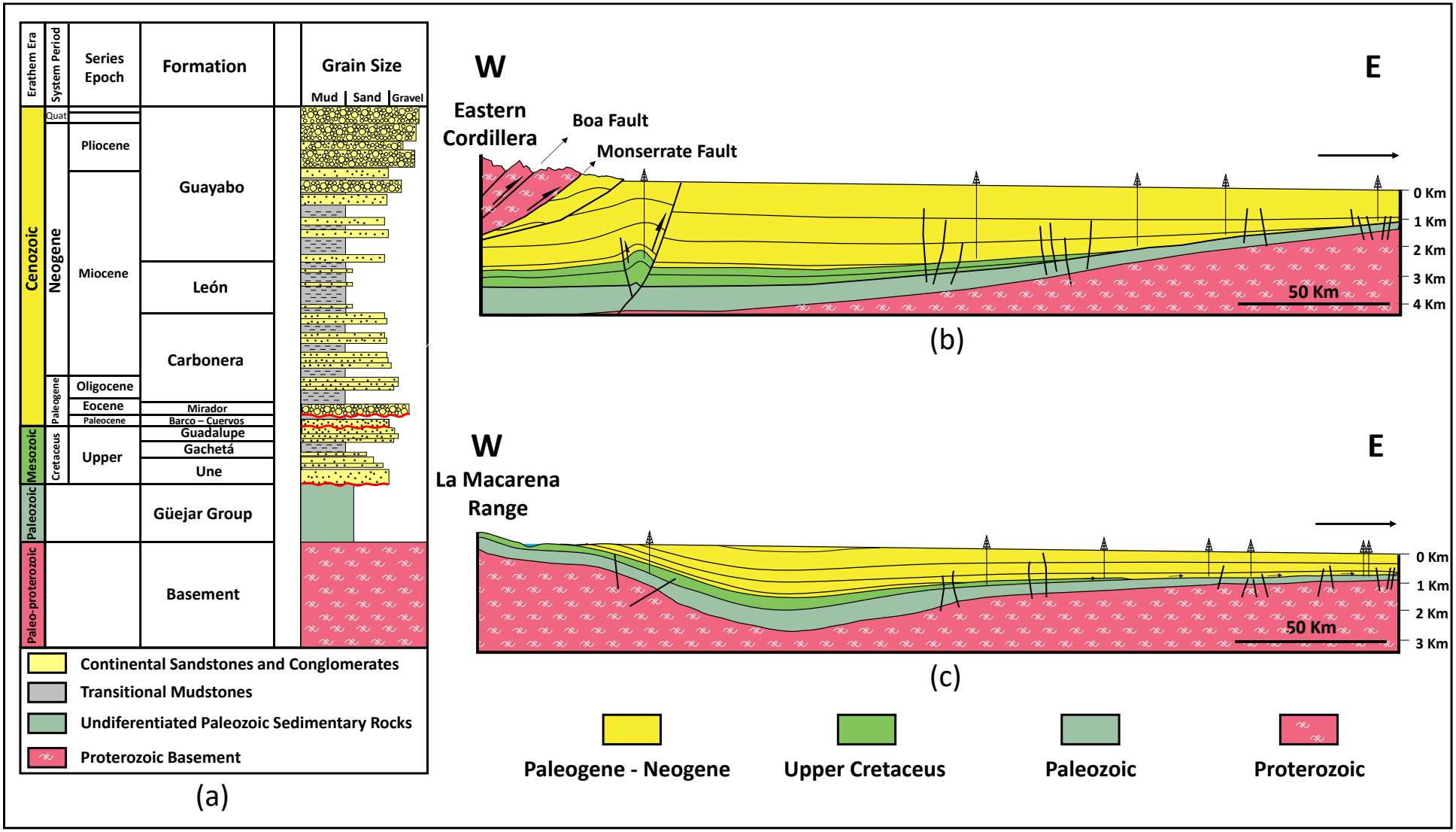


**Figure 2**. (a) Stratigraphic Chart for Southern Llanos Basin (From Reyes-Harker et al., 2015). (b) Illustrative cross section of the regional configuration of Southern Llanos Basin from the Eastern Cordillera to the foreland and (c) Illustrative cross section of the regional configuration of Southern Llanos Basin from La Macarena Range to the foreland. For location of cross sections (b) and (c), see **Figure 1**.

*Unit*. (**Figure 3**). The aquitard associated with the Gachetá Formation is restricted to the western sector of the study area (**Figure 3**). It controls westward the vertical connection between the basal Cretaceous aquifer (Une Formation) and the Paleogene and Neogene aquifer units. In turn, the thickness of the Gachetá Formation varies drastically, generating two different hydrological configurations. In the northwestern the Gachetá Formation aquitard is >150 meters thick and restricts the vertical connection between the Une Formation and the Guadalupe, Barco, and Mirador formations (**Figure 3a**). In contrast, in the south, adjacent to the La Macarena Range, the thickness of the Gachetá Formation aquitard is drastically reduced (< 30 meters), and even it gets to be absent in some places, favoring the vertical connection between the Une Formation and the Mirador Formation (**Figure 3b**, Wells: LLS-2, LLS-3, and LLS-4). The largest aquitards covering the most area that overlie and confine the Basal Flow Unit are made up of the muddy sediments from the Eocene, Oligocene, and Miocene, which extend throughout the southern sector of the Llanos basin.

***2.3 Physiography and Hydroclimatology***

The area of interest is located in the Llanos foreland basin and is part of the eastern topographically flat-lying sectors of Colombia which are adjacent (east) to the Eastern Cordillera. The Eastern Cordillera has an average altitude of 2600 m.a.s.l with mountain peaks that exceed 5300 m.a.s.l, whereas La Macarena Range, has an average altitude of 800 m.a.s.l with peaks of 1600 m.a.s.l. In comparison, the Llanos foreland plain towards the Orinoco has low altitudes, on average 200 m.a.s.l., and continues to decrease eastward. Rivers that drain the Eastern Cordillera, including the Meta, Ariari, Guayabero, and Manacacias, ultimately flow northward to the Orinoco River and the Caribbean Sea.

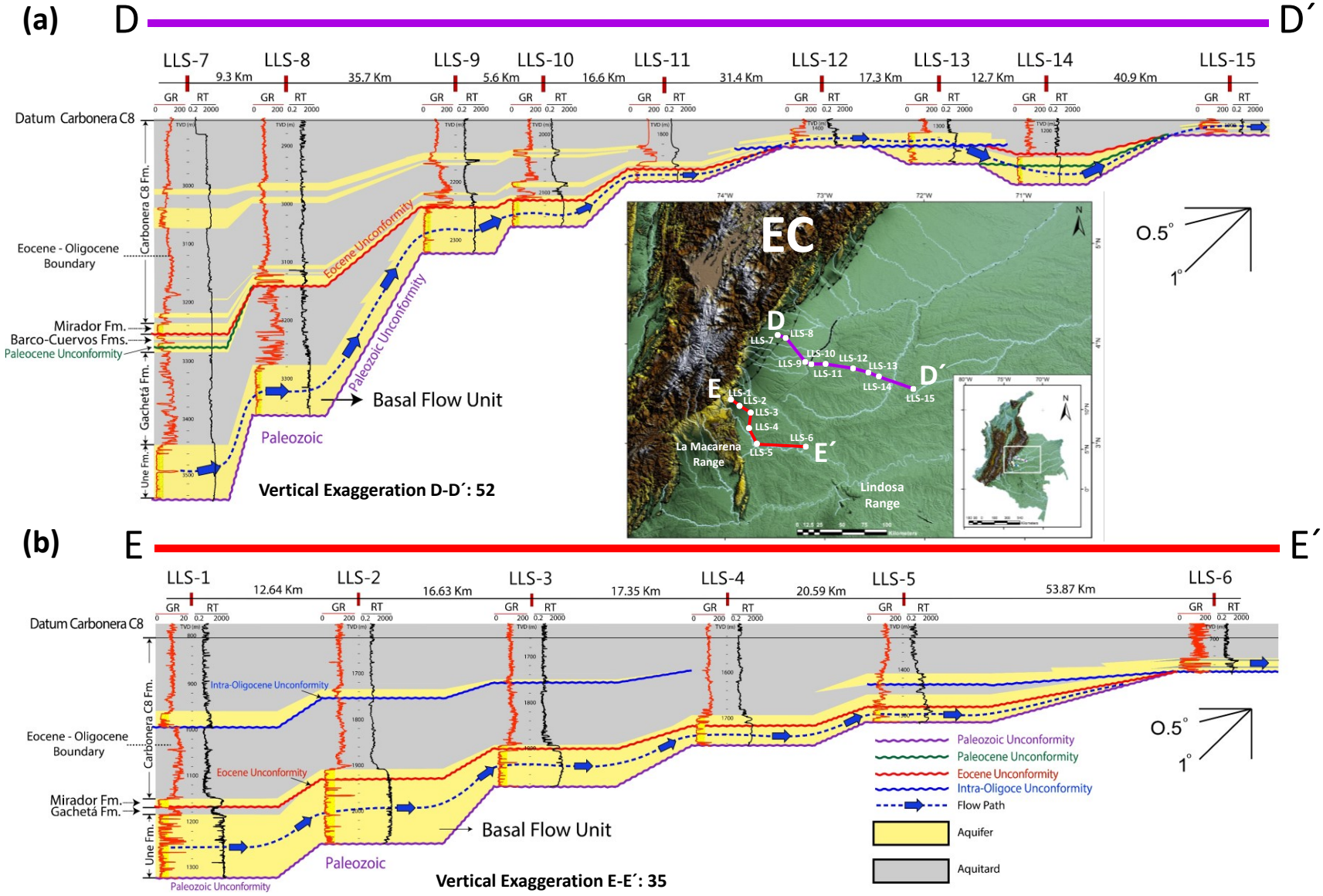


**Figure 3**. Stratigraphic correlations through the southern Llanos Basin. Gamma Ray (GR) and Resistivity (RT) logs are presented per well a) D-D´, NW-SE correlation showing the Basal Flow Unit and thicker aquitard of the Gachetá Formation. b) E-E´, NW-SE correlation showing the Basal Flow Unit and thinner aquitard of the Gachetá Formation. EC: Eastern Cordillera. Modified from Gómez-Moncada et al. (2022).

The Eastern Cordillera forms an efficient orographic barrier that favors high rainfall across the eastern flank of the range (Mora et al., 2008). Precipitation varies between 2000 mm/yr to 3500 mm/yr towards the central and eastern sectors of the Orinoco River basin, and up to 7000 mm/yr towards the eastern flank of Eastern Cordillera (Arango et al., 2012). The annual cycle of rainfall along north tropical South America is dominated by the latitudinal oscillation of the Intertropical Convergence Zone (ITCZ) (Mejía et al., 1999; Poveda et al., 2006; Espinoza et al., 2009, Sierra et al., 2015; Espinoza et al., 2020). The annual cycle of precipitation in western and central Colombia exhibits a mostly bimodal behavior with two wet seasons (March-April-May and September-October-November) and two drier seasons (December-January-February and June-July-August) (Bendix and Lauer, 1992; Poveda et al., 2001; Poveda, 2004; Rodriguez, 2004; Saylor et al., 2009; Ricaurte et al., 2019; Espinoza et al., 2020).

The orography of the Andes is a key factor controlling the initiation and evolution of the convective precipitation system that dominates the tropical and subtropical Andes (Arias et al., 2021). The Amazon-Andes transition region constitutes a biogeophysical system that controls the hydrology of this region, resulting from interactions between climates and the complexity of Andean topography (Hoorn et al., 2010; Rangel et al., 2018; Espinoza et al., 2020). The eastern Andes and Amazon basin constitute an interconnected system, where de Amazon region favors the contribution de water vapor to the Andes through the moisture-laden trade winds (e.g., Garreaud, 1999; Poveda et al., 2006; Zemp et al., 2017; Espinoza et al., 2020). This phenomenon favors high-intensity rainfall rates over the eastern foothills of the Andes (Espinoza et al., 2009; Espinoza et al., 2015; Chavez and Takahashi, 2017; Kumar et al., 2019; Espinoza et al., 2020).

The eastern flank of tropical Andes (which includes the eastern flank of Eastern Cordillera in Colombia) is the wettest region in Amazonia (e.g., Figueroa and Nobre, 1990; Espinoza et al., 2009;

Espinoza et al., 2020). The rainfall variability in the Amazon-Andes transition region is interpreted as a conjunction of processes such as the regional atmospheric circulation, temperature contrast (lowland-highland), and Andean topography (Ronchail and Gallaire, 2006; Espinoza et al., 2015; Segura et al., 2016; Junquas et al., 2018; Espinoza et al., 2020). These processes produce high rainfall rates of around 6000 - 7000 mm/year (Johnson, 1976; Giovannettone and Barros, 2009; Poveda et al., 2014; Espinoza et al., 2015; Chavez and Takahashi, 2017; Espinoza et al., 2020).

The main oceanic and continental atmospheric moisture sources for most of the north tropical Andes are the Atlantic Ocean and the Amazon rainforest, respectively (Arias et al., 2015; Hoyos et al., 2017; Zemp et al., 2017; Espinoza et al., 2020). This area which includes the Andes-Amazon transition zone in Colombia is dominated by the physiographic contrast between the Eastern Cordillera and the Llanos Basin. The Amazon rainforest is the main supply of humidity for tropical South America (Espinosa et al., 2020). Recent estimations show that around 25-50% of total annual rainfall in the tropical Andes is originated from Amazon forest transpiration, moisture that is subsequently transported westward by trade winds (Staal et al., 2018; Espinoza et al., 2020). This water vapor evapotranspired by the Amazonian rainforest is transported by the trade winds from eastern to western Amazonia, is lifted by the orography of the Andes, and then condensed and converted into rainfall. These processes of condensation and conversion to rainfall occur several times in the region, favoring precipitation recycling (Espinoza et al., 2020). This behavior is the explanation for why the rainiest areas are related to the foothills of the Andes of Colombia, Ecuador, Peru, and Bolivia (Espinoza et al., 2009; Espinoza et al., 2020) and high precipitation recycling rates in the Andes (Zemp et al., 2014; Staal et al., 2018; Espinoza et al., 2020) (**Figure 4**).

Alvarez-Villa et al. (2011) present these orographic effects, who explicitly relate the relationship between the long-term mean annual precipitation and the topography through regional cross-

sections (for latitudes 2°N, 4°N, 6°N, and 8°N) that cross from the Orinoco basin to the Pacific Ocean (**Figure 4**). Alvarez-Villa et al. (2011) show the low values of long-term mean annual precipitation over the flat terrain of the Orinoco region in Colombia (Llanos basin), which contrasts with the significant increase in long-term mean annual precipitation in the Eastern Cordillera (around 4°N) (**Figure 4**).

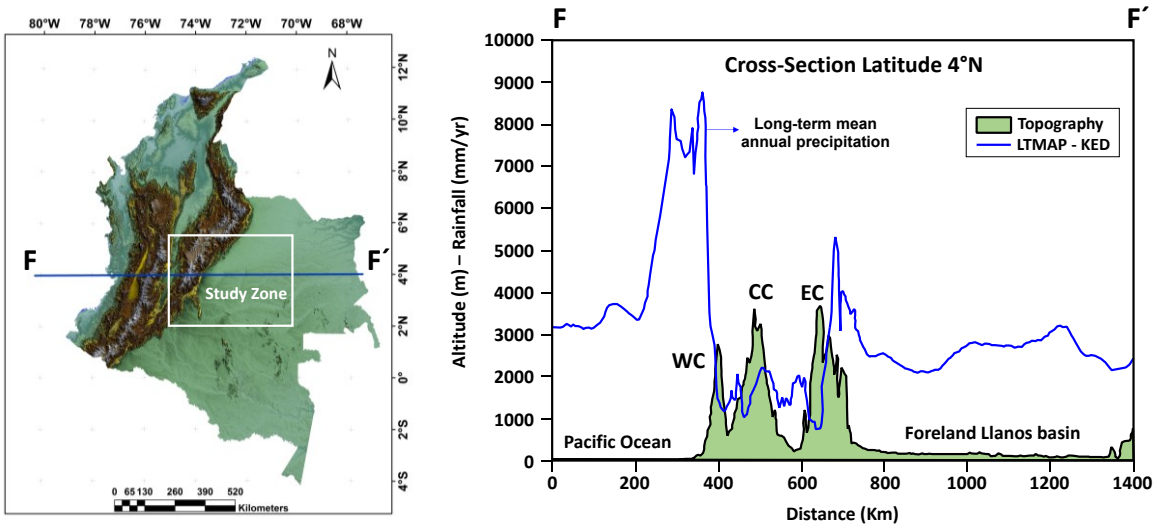


**Figure 4**. (Left) Digital Elevation Model (SRTM) of Colombia showing the location of the cross-section F-F´ for latitude 4°N through the foreland Llanos basin and the Colombian Andes to the Pacific Ocean. (Right) Cross-section F-F´ showing the topography (green shading) and kriging-estimated long-term mean annual precipitation (blue line) at latitude 4°N. WC: Western Cordillera, CC: Central Cordillera, EC: Eastern Cordillera. LTMAP-KED: Long Term Mean Annual Precipitation using Kriging with an External Drift. Modified from Alvarez-Villa et al. (2011).

## 3. Methods

### *3.1. Sampling Methods*

To calibrate the LMWL we analyzed 162 samples from the main surface water bodies (rivers and streams) (**Figure 1**). Surface water samples were taken both in the dry period (January-February 2018) and in the rainy period (April-May 2019), in order to cover the isotopic variations of the hydrological cycle documented in Colombia (e.g., Bendix and Lauer, 1992; Poveda et al., 2001; Poveda, 2004; Rodriguez, 2004; Rodriguez, 2004; Saylor et al., 2009; Ricaurte et al., 2019; Espinoza

et al., 2020). We included samples from the main rivers of the Orinoco River basin, as well as some creeks with lower flow, covering the area of the deformation front associated with the topographic highs of the Eastern Cordillera, La Macarena Range, La Lindosa Range and samples at lower elevations within the lowlands in the foreland Llanos basin. To complement information to the east and south of Colombia and compare the local trend of the southern Llanos basin with the regional trend of Colombia, we also examined IAEA-GINP data from 33 stations in Colombia, 2 stations from Brazil, 1 from Perú, and 1 from Ecuador.

### *3.2. Stable Isotope Analysis (Surface water and Groundwater)*

The samples for isotopic analysis were packed in glass vials with a septa-type hermetic cap (20 ml). Before the isotopic analysis, all samples were filtered using glass microfiber filters (0.45 µm) and a volume of 2 ml was transferred to a glass vial to be subsequently analyzed in the spectrometer. Measurements of oxygen isotopes ratios ($^{18}O/^{16}O$) and ($^{2}H/^{1}H$) are in parts per thousand (‰) relative to the international standard VSMOW (Vienna Standard Mean Oceanic Water) (±1σ). Water samples were measured on a Picarro A2120i High Precision Cavity Ring-Down spectrometer using VSMOW, GISP, and V-SLAP standard reference materials for calibration.

We compare the LMWL based on the surface water samples to the $\delta^{18}O$ and δD values of groundwater from petroleum wells included 109 samples from five producing oil fields and 2 exploratory wells. Sampled wells have depths approximately between -600 m.a.s.l to -3000 m.a.s.l.

To establish the provenance of the groundwater present Basal Flow Unit, we used the altitude model proposed by Saylor et al. (2009) and the $\delta^{18}O$ and δD groundwater compositions (only groundwater samples from this study) to estimate the elevations where the waters are coming from. For the use of the altitude model, the delta values of $\delta^{18}O$ ($\Delta\delta^{18}O$) and delta of δD (ΔδD) were estimated for all groundwater samples, which consists of a normalization of the $\delta^{18}O$ and δD

compositions to be able to make comparative analyses with paleoelevation studies (Saylor et al., 2009).

### *3.3. Physicochemical analysis (Surface water and Groundwater)*

The samples for physicochemical analysis were stored in 1000 ml plastic bottles with a hermetic seal. All samples were transported and refrigerated (2°C to 5°C) before analysis. For each sample for physicochemical analysis, two plastic bottles were taken: one for anion (-) analysis ($HCO_3^-$, $CO_3^{-2}$, $SO_4^{-2}$, and $Cl^-$) and the other for cation (+) analysis ($Na^+$, $K^+$, $Ca^{+2}$, $Mg^{+2}$). The samples for cation (+) analysis were preserved with $HNO_3$ with a pH < 2.0. Physicochemical analyses were completed on 67 of the 162 surface water samples where isotopic analyses were performed. The idea of conducting this type of analysis was to characterize the water samples regarding the abundance of different anions (-) and cations (+) in Sitff and Pipper diagrams which would allow to understand the lateral variations of groundwater in different locations and correlate them with potential influence from meteoric waters. In the case of groundwater samples, 93 physicochemical analyses were carried out, which included 69 samples from oil producing wells (from Fields 1, 2, 4, 5) and 24 additional samples from exploratory wells. The physicochemical analysis used in this study corresponded to the main anions (-) ($HCO_3^-$, $CO_3^{-2}$, $SO_4^{-2}$, $Cl^-$) and cations (+) ($Na^+$, $K^+$, $Ca^{+2}$, $Mg^{+2}$). Sampling elevations are referred to a digital elevation model (DEM) from the Shuttle Radar Topography Mission (SRTM), of 12 meters resolution, according to coordinates of a handheld GPS with an accuracy of 7 meters in the horizontal plane and 14 meters in vertical plane (altitude).

## 4. Results

Stable isotope compositions of surface water samples collected in this study range from -9.56 ‰ to -1.99 ‰ VSMOW for $\delta^{18}O$ and -60.5 ‰ to -5.90 ‰ VSMOW for δD (**Table 1**). Precipitation $\delta^{18}O$ values for the IAEA/GNIP stations in Colombia (33), and additional stations from Brasil (2), Ecuador

(1) and Perú (1) range from -11.98 ‰ VSMOW to -4.55 ‰ VSMOW and -81.02 ‰ VSMOW to -26.93 ‰ VSMOW for δD.

In the case of groundwater samples from oil fields, $\delta^{18}O$ values range from -8.45 ‰ VSMOW to -6.06 ‰ VSMOW and from -55.6 ‰ VSMOW to -33.8 ‰ VSMOW for δD (**Table 2**), showing less variation of isotope compositions than data from surface water samples. The depths of the open flow intervals in the sampled oil producing wells range from -600 m.a.s.l. to -3000 m.a.s.l. The temperature conditions of the reservoirs from different wells vary between 58° C to 126° C, with the lowest temperatures in Field 5, located to the East of the basin and the highest in the fields close to the Eastern Cordillera (Fields 1, 2, 3 and 4) (**Table 3**). The same behavior in pressure is observed with variations between 600 Psi and 4500 Psi.

Physicochemical analysis of groundwater samples generally showed low concentrations of NaCl, which varied between 39 ppm and 3718 ppm, corresponding to fresh and slightly saline waters (according to Swenson and Baldwin, 1965). The anion (-) concentrations for groundwater range between 4.1 ppm to 1278 ppm for $Cl^-$, 30.5 ppm to 2120 ppm for $HCO_3^-$, 0 ppm to 160 ppm for $SO_4^-$ and 0 ppm to 120 ppm for $CO_3^{-2}$. Cation (+) concentrations for groundwater ranged from 4.7 ppm to 1589 ppm for $Na^+$, 2.2 ppm to 165 ppm for $K^+$, 0 ppm to 136 ppm for $Ca^{+2}$ and 0 ppm to 54 ppm for $Mg^{+2}$ (**Table 3**). For surface water samples the anion (-) concentrations range between 0.51 ppm to 92.1 ppm for $Cl^-$, 0 ppm to 174 ppm for $HCO_3^-$, 0.51 ppm to 408 ppm for $SO_4^-$ and 0 ppm for $CO_3^{-2}$. For cations (+), the concentrations for surface water range from 1.14 ppm to 12.58 ppm for $Na^+$, 0.87 ppm to 7.01 ppm for $K^+$, 0.22 ppm to 183 ppm for $Ca^{+2}$, and 0.01 ppm to 63 ppm for $Mg^{+2}$ (**Table 3**).

## 5. Discussion

### *5.1 Llanos Local Meteoric Water Line*

The least-square fit of $\delta^{18}O$ and $\delta D$ isotope compositions of surface water sources from southern Llanos basin, including additional data from previous research (**Figure 5**) (e.g., González-Uribe et al., 2007; González-Penagos et al., 2014; Saylor et al., 2009) results in the following the **Equation 1**:

$$\delta D = 7.8\ (\pm 0.10) \times \delta^{18}O + 11.66\ (\pm 0.75)\ (R2 = 0.96)\ n = 260 \qquad (1)$$

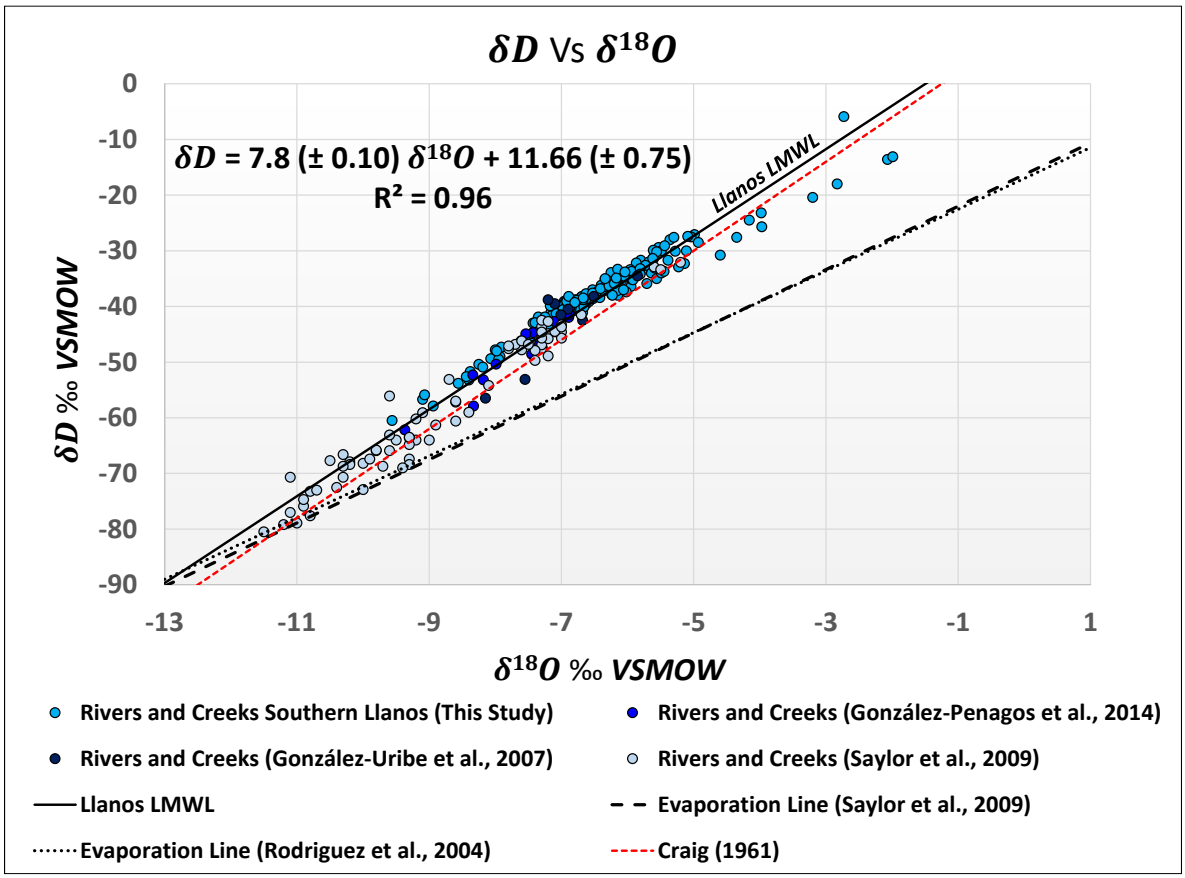


**Figure 5**. (A) $\delta^{18}O$ and $\delta D$ compositions and Local Meteoric Water Line (LMWL) for surface water samples of the southern Llanos basin (including data from González-Uribe et al. (2007), Saylor et al. (2009), and González-Penagos et al. (2014). Evaporation lines are from Rodriguez (2004), and Saylor et al. (2009).

The model for southern Llanos basin differs slightly from the model proposed for Colombia by Rodriguez (2004), as seen in **Equation 2**:

$$\delta D = 8 \times \delta^{18}O + 9.6 \qquad (2)$$

and the main difference, like the model proposed by Craig (1961), lies in the excess of deuterium, which in this work is 11.66 ‰ VSMOW (± 2.66 ‰ VSMOW) and take values of 13.12 ‰ VSMOW (± 2.68 ‰ VSMOW) using the model proposed by Dansgaard (1964), which defines the d-excess for each pair of points with respect to the GMWL ($\delta D - 8\ \delta^{18}O$).

The Local Meteoric Water Line for the southern Llanos basin is also similar to the Local Meteoric Line proposed by Saylor et al. (2009), whose data come mainly from the eastern flank of the Eastern Cordillera (**Equation 3**):

$$\delta D = 8.02 \times \delta^{18}O + 12.12\ (\pm 1.8)\ (R2 = 0.95)\ n = 76 \qquad (3)$$

The surface water isotopic compositions ($\delta^{18}O$ and $\delta D$) analyzed in this study were also compared with isotopic IAEA-GNIP stations. The $\delta^{18}O$ and $\delta D$ values fall on the LMWL from Colombia. The model that describes the local meteoric water line for Colombia integrating the 37 IAEA-GNIP stations follow the **Equation 4**:

$$\delta D = 7.9\ (\pm 0.03) \times \delta^{18}O + 9.4\ (\pm 0.27)\ (R2 = 0.99)\ n = 1011 \qquad (4)$$

which becomes very similar to LMWL proposed for Colombia by Rodriguez (2004), even in the d-excess value (9.6 ‰ VSMOW).

***5.2 Comparison to GMWL***

Llanos LMWL is very similar to the GMWL proposed by Rozanski et al. (1993) based on the long-term annual precipitation-amount weighted mean stable isotope composition from the IAEA/WMO global network (including the Bogota station in Colombia 4.70°N, 74.13°W) as seen in **Equation 5**:

$$\delta D = 8.20\ (\pm 0.07) \times \delta^{18}O + 11.27\ (\pm 0.65). \qquad (5)$$

Rozanski et al. (1993) present a small variation with respect to the Global Meteoric Water Line (GMWL) proposed by Craig (1961) described in **Equation 6**:

$$\delta D = 8 \times \delta^{18}O + 10 \qquad (6)$$

Saylor et al. (2009), explains that waters recovered in the Eastern Cordillera have suffered a minimal isotopic modification since their evaporation from the Atlantic Ocean. Rozanski et al. (1993), attributes this behavior to the barrier effect that the Andes exerts on the air currents that come from the Atlantic, making the continental and altitude effect substantially less, and therefore causing less isotopic depletion. On the other hand, the d-excess values that have been recognized in the study area are relatively higher compared to the GMWL proposed by Craig (1961). However, this behavior has been documented in IAEA / WMO stations with continental influence from different latitudes worldwide (e.g., Rozanski et al., 1993).

We identify the isotope signal of meteoric water from the southern Llanos basin as a transition zone. The average value of $\delta^{18}O$ in meteoric water indicates an isotopic depletion in comparison with $\delta^{18}O$ values from the Amazon basin stations located in the east of Colombia (e.g., Manaos and Sao Gabriel stations from the IAEA / WMO global network). In turn, $\delta^{18}O$ compositions of meteoric water from the southern Llanos basin become higher than the annual average reported at the Bogotá station (**Figure 6**). Bogotá station reveals much higher isotope depletion than meteoric water samples from the southern Llanos basin. This isotope depletion would be attributed mainly to the altitude effect due to the orographic uplift of the air masses on the Eastern flank of the Andes (Rozanski et al., 1993). The average value of $\delta^{18}O$ in surface water of the southern Llanos basin becomes 6.4 ‰ VSMOW (dry season and rainy season data sets), representing an intermediate value between the average annual values reported by Rozanski et al. (1993) at the Sao Gabriel stations in Brazil (0.13° S, 67.08° W) in the Amazon basin and the Bogotá station in the Colombian Andes (**Figure 6**). The average of the $\delta^{18}O$ composition of meteoric water from the southern Llanos basin, which represents an intermediate $\delta^{18}O$ composition between the behavior of the stations of the Amazon basin and the Andes, coincides with the inflection point between the foreland and the Colombian Andes domains.

According to Salati et al. (1979), Gat and Matsui (1991), and Rozanski et al. (1993), the Colombian Amazon basin has a reduced continentality effect from the Manaus station (3.12 ° S, 60.02 ° W) to the west (including the Colombian foreland), which is attributed to the high intensity of recycling of moisture by evapotranspiration of Amazon Basin. This can be recognized in the continental gradient of $\delta^{18}O$ in precipitation, which becomes very small to the west of Manaus Station in Brazil (Rozanski et al., 1993) (**Figure 6**).

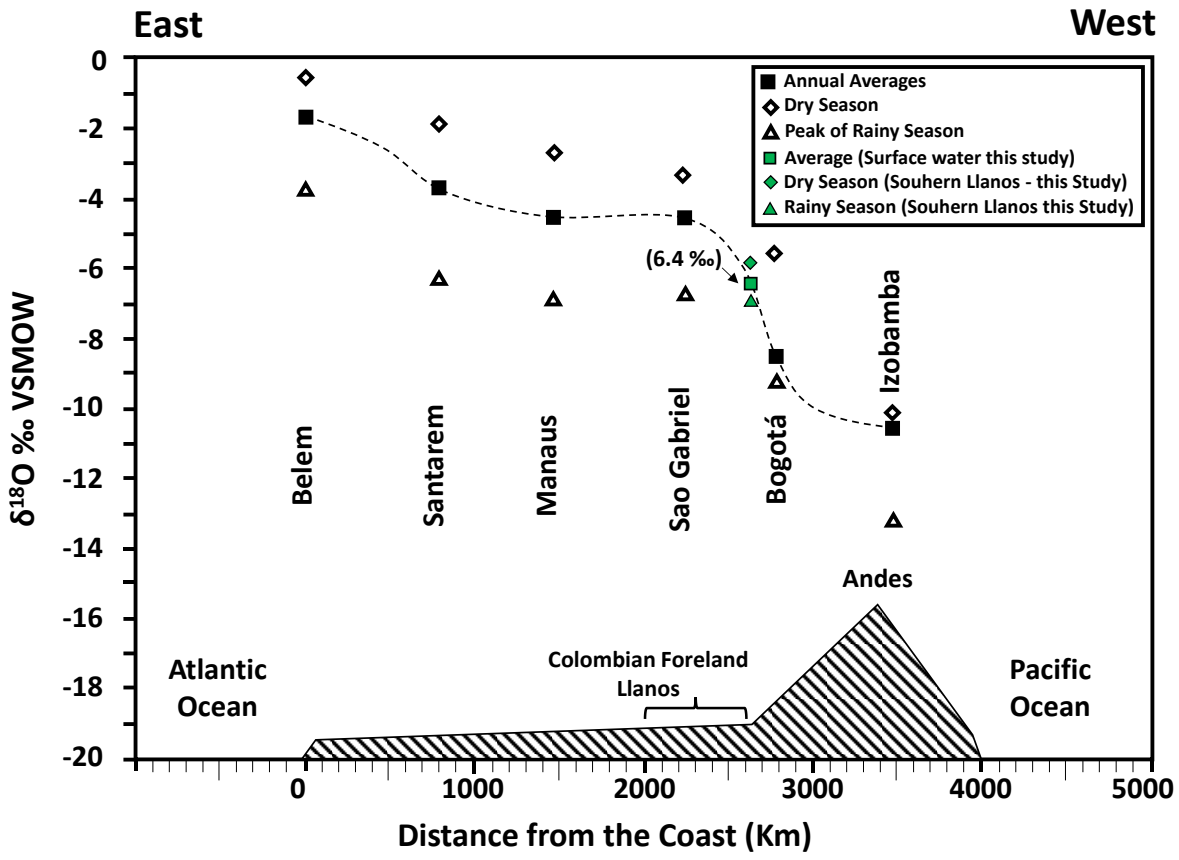


**Figure 6**. $\delta^{18}O$ isotope composition in precipitation as a function of the distance from Atlantic Ocean for selected stations located in the Amazon Basin in Brazil (Belem, Santarem, Manaus and Sao Gabriel Stations) and Colombian Andes (Bogotá Station). Green square is the average of $\delta^{18}O$ isotope composition of meteoric water from the southern Llanos basin data, including dry and rainy seasons (Modify from Rozanski et al. 1993).

***5.3 Isotope Compositions in Groundwater (wells)***

The groundwater samples recovered from oil fields show particular pressure and temperature conditions (**Table 3**). Fields closer to the eastern flank of Eastern Cordillera (Field-1, 2, 3 and 4) exhibit the highest pressure and temperature conditions due to its proximity to the Llanos basin foredeep, while the Field-5, which is located towards the Llanos foreland, it is the shallowest and has the lowest pressures and temperatures (**Table 3**).

Craig (1961) has documented that a plot of the isotopic content of $\delta^{18}O$ versus $\delta D$ follows a very well defined pattern for meteoric waters, that is even valid worldwide. That plot was defined as the Global Meteoric Water Line (GMWL) and from that general trend, also Local Meteoric Water Lines (LMWL, e.g. see the one for the southern Llanos in **Figure 5**) can be derived. In contrast, Clayton et al. (1966), show that water from selected oil fields do not follow that pattern but they yield lines of different slopes (**Figure 7A**). These cases were associated by Clayton et al. (1966) to waters with enrichment of $\delta^{18}O$ by effect of isotopic exchange between water and reservoir rocks, especially in waters of higher salinity, which can be interpreted as a disconnection with meteoric water influx and considerable transit times.

The groundwater samples from the southern Llanos basin of this study all follow the trend of the LMWL and the GMWL (**Figure 7B**). Projecting the $\delta^{18}O$ and $\delta D$ compositions of groundwater from the southern Llanos basin onto the plot of Clayton et al. (1966) suggests that our groundwater samples (southernmost sector of Llanos) show no influence by the oxygen exchange between water and rock like the groundwater samples taken from different oil fields described by Clayton et al. (1966) (**Figure 7A**). This observation is of interest when considering that the depositional environments of the formations that make up the Basal Flow Unit involved saline waters and brackish waters (marine environments), suggesting a dilution of ions in the water due to the

percolation of meteoric waters over time (González-Penagos et al., 2014; Caballero et al., 2015; Gómez-Moncada et al., 2022).

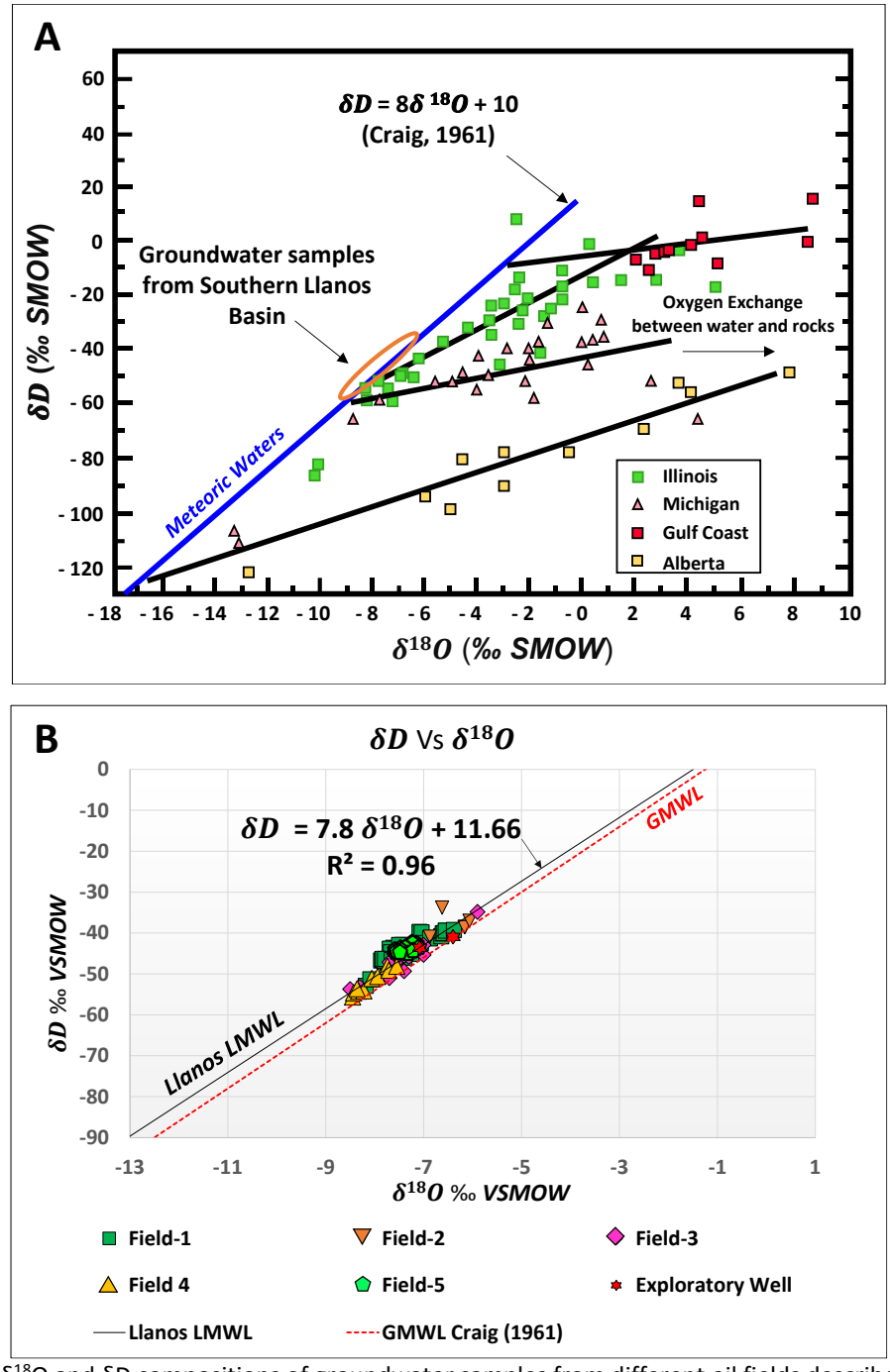


**Figure 7**. (A) $\delta^{18}O$ and $\delta D$ compositions of groundwater samples from different oil fields described by Clayton et al. (1966), showing an extensive oxygen exchange by effect of interaction between groundwater and reservoir rocks (modified from Clayton et al. (1966)). (B) $\delta^{18}O$ and $\delta D$ compositions for groundwater samples from different oil fields and exploratory wells in the southern Llanos basin. The orange closed polygon showed in (A) corresponds to the isotope composition of the groundwater from southern Llanos basin.

Spatial variability in d-excess values from groundwater samples (from this study) suggests a greater degree of connectivity between meteoric water recharge zones and deep aquifers in the southern Llanos Basin than in the central or northern Llanos Basin. All groundwater samples from the oil fields (Field-1, 2, 3, 4, and 5) fall on the proposed Local Meteoric Water Line of the southern Llanos basin and Colombian Local Meteoric Water Line, showing similar trend and isotope compositions compared with surface waters (**Figures 8A-1, 8A-2 and 8C**). The mean estimated for d-excess in groundwater samples (this study) is 14.44 ‰ VSMOW (± 1.75‰) and it is similar to the mean estimated to meteoric waters in the westernmost sector of the study area which is 14.69 ‰ VSMOW (± 1.27 ‰), close to La Macarena Range and the eastern flank of Eastern Cordillera (**Figure 9**). The groundwater samples with the least variation in isotopic composition is the Field-5. These groundwater samples have a mean $\delta^{18}O$ value of -7.36 ‰ VSMOW (± 0.13 ‰ VSMOW) and a mean δD value of -43.69 ‰ VSMOW (± 0.65 ‰ VSMOW) and its composition is very similar to meteoric waters from the southern Llanos basin.

Although some variation of the isotope concentration is observed for the groundwater samples, the data is consistent with influence of meteoric waters, even for fields far from the deformation front (e.g., Field 5). In contrast, part of the data reported by González-Uribe et al. (2007) and González-Penagos et al. (2014), related with groundwater samples show significant deviation from the Llanos LMWL (**Figure 8B-1 and 8B-2**). According to the data reported by González-Uribe et al. (2007), it is observed that 66% of the groundwater samples taken in wells from Cretaceous and Cenozoic formations, move away from the Llanos LMWL (**Figure 10**). Most of these groundwater samples are associated with the zone of greatest structural deformation, between segments limited by reverse faults that border the deformation front of the Eastern Cordillera. In turn, the data from González-Uribe et al. (2007) show that towards the foreland of the Llanos basin, the groundwater samples tend to follow the Llanos LMWL (**Figure 10**).

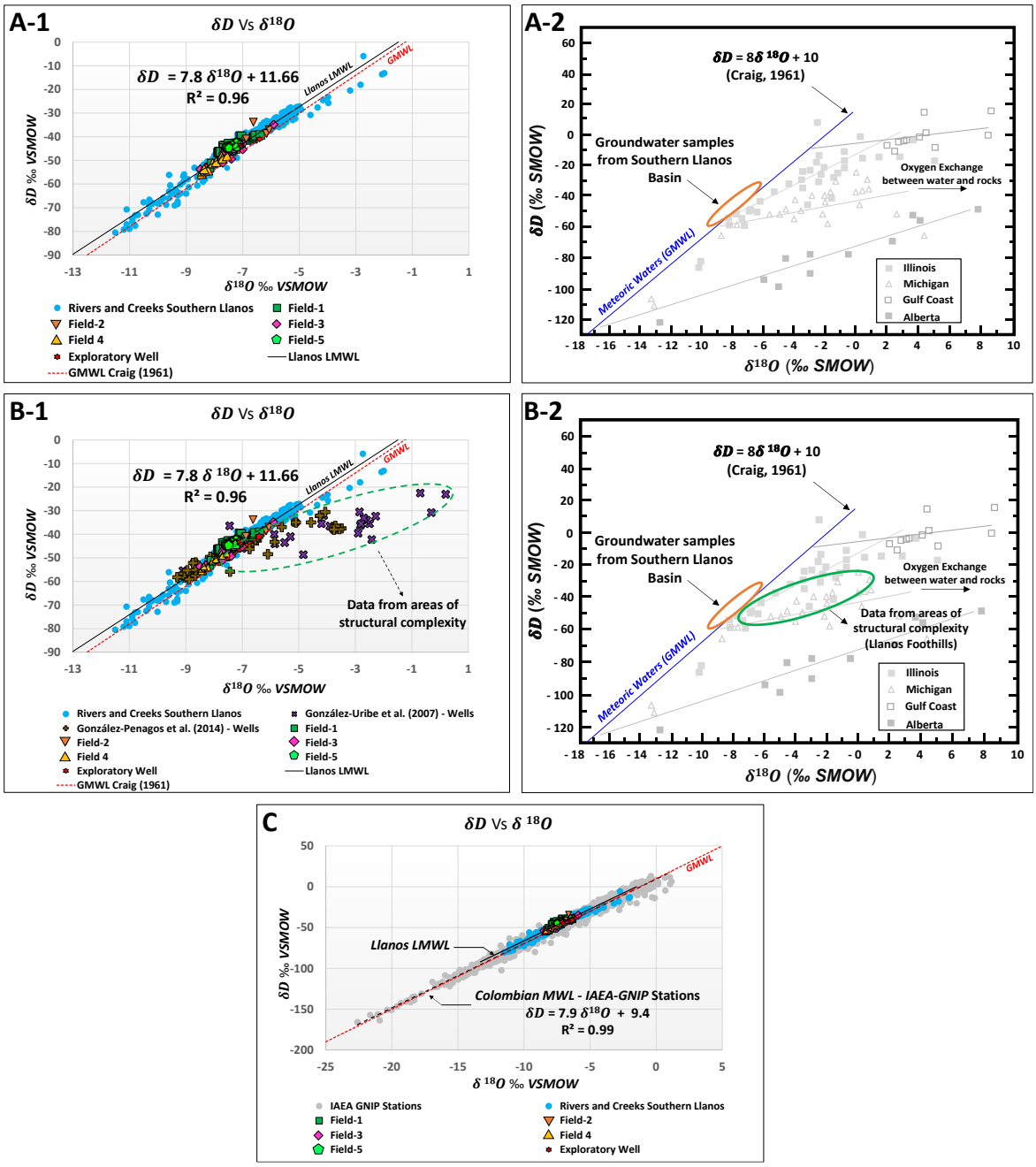


**Figure 8**. (A-1) $\delta^{18}O$ and δD compositions for groundwater samples from different oil fields, exploratory wells and surface waters (blue dots) in the southern Llanos basin. (B-1) $\delta^{18}O$ and δD compositions for groundwater samples including information from González-Uribe et al. (2007) and González-Penagos et al. (2014) and surface waters (blue dots). C) $\delta^{18}O$ and δD compositions from southern Llanos basin (surface water and groundwater from this study) and in the background the data from 37 IAEA-GNIP stations (grey dots). (A-2) Comparison between the isotope compositions ($\delta^{18}O$ and δD) of the groundwater samples from the southern Llanos basin (without oxygen enrichment) in contrast with the samples reported by Clayton et al. (1966) where the oxygen enrichment of the waters is evidenced. (B-2) Comparison between the isotope compositions ($\delta^{18}O$ and δD) of the groundwater samples from the areas of structural complexity in the Llanos foothills (data from González-Uribe et al. (2007) and González-Penagos et al. (2014)), and the samples reported by Clayton et al. (1966), where the oxygen enrichment of the waters is evidenced.

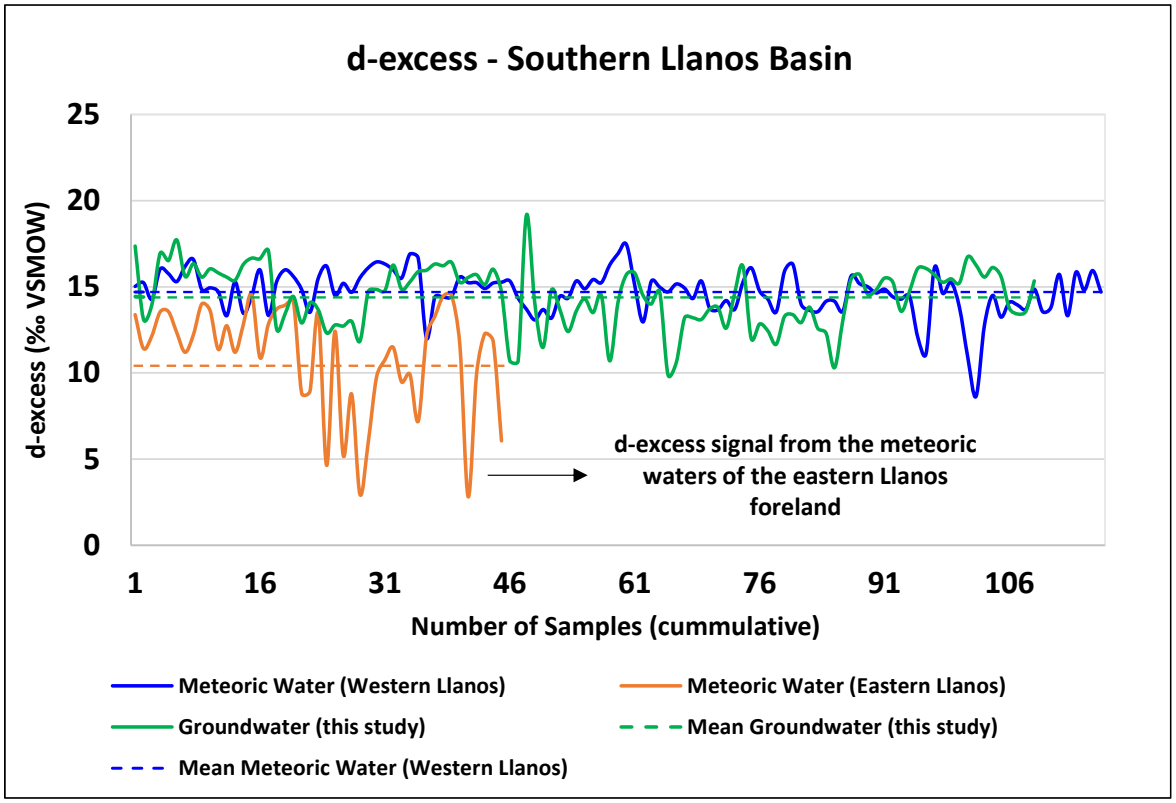


**Figure 9**. d-excess signal from the meteoric water of southern Llanos basin. Groundwater (green lines) The groundwater of the southern Llanos basin (This study) correlates with the meteoric waters of the westernmost sector of the study area (blue lines).

In the case of the data published by González-Penagos et al. (2014), it was not possible to spatially relate the groundwater samples since the coordinates or the name of the oil wells are not reported in the publication. However, according to the spatial distribution of the data shown by González-Penagos et al. (2014), and the data obtained in the present study, we interpreted that the groundwater samples from González-Penagos et al. (2014) that are far from the Llanos LMWL (20% of the total samples) are related to the central and northern sector, near the eastern flank of the Eastern Cordillera (**Figure 10**).

In the northern and central foothills exhumation is driven by reverse faulting which severs the hydrologic connection to the deep aquifers. However, to the south Paleogene and Upper Cretaceous strata are exposed adjacent to La Macarena Range as the western limb of a basin-scale syncline. The lack of faulting in the southern region means that the hydrologic connection between the surface

and the deep aquifers is maintained and meteoric water rapidly recharges the deep aquifer (e.g., Mora et al., 2019; Gómez-Moncada et al., 2022).

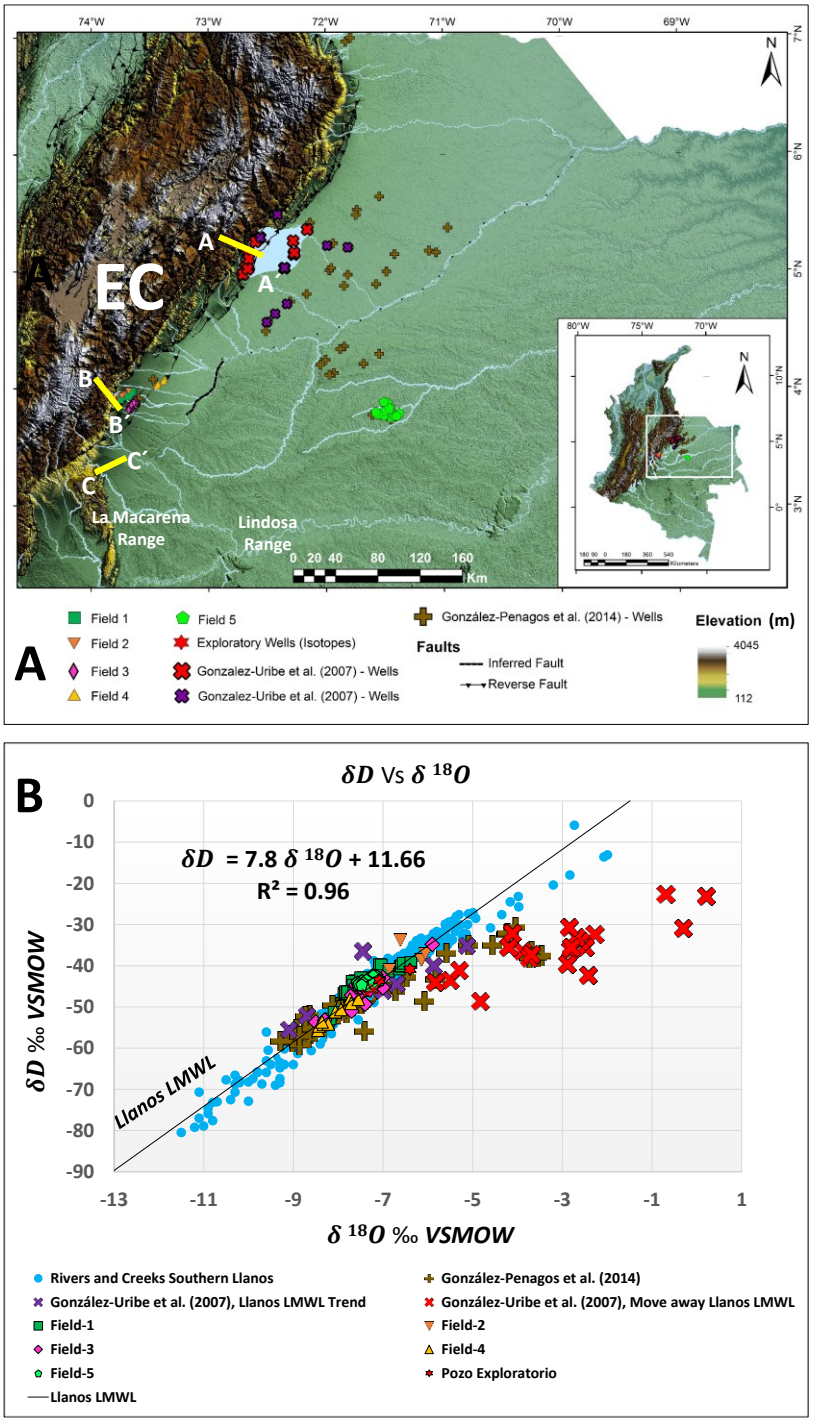


**Figure 10**. (A) Digital elevation model (SRTM) showing the location of groundwater samples and plot (B) of isotopic composition ($\delta^{18}O$ - $\delta D$) reported from González-Uribe et al. (2007), González-Penagos et al. (2014) and data from the present study. Note that the data that move away from the Llanos LMWL correspond mostly to samples located close to the deformation front of the eastern flank of the Eastern Cordillera. EC: Eastern Cordillera.

The isotopic compositions of the groundwater samples that move away from the Llanos LMWL presented by González-Uribe et al. (2007) and González-Penagos et al. (2014) (**Figures 8B-1, 8B-2 and 10**) are found in a zone of hydrogeological disconnection due to the structural complexity of the area. Isotopic compositions show an oxygen enrichment attributed to the oxygen exchange by the effect of interaction between water and reservoir rocks (e.g., Clayton et al., 1966). This, in turn, allows us to deduce that there would be longer transit times towards those parts of the deformation front, which allows the observed oxygen enrichment. In **Figure 11**, three structural sections are shown to summarize the changes in the structural complexity of different areas along the eastern flank of Eastern Cordillera and La Macarena Range and their relationship with the groundwater isotopic compositions of $\delta^{18}O$ and $\delta D$. As shown in **Figure 11**, the structural complexity increases drastically in a northeasterly direction in the eastern foothills of the Eastern Cordillera. It is mainly controlled by the fault system of Guaicaramo (in the northernmost sector) and Algeciras (to the south, near the Macarena mountain range). This increase in structural complexity to the north (e.g., section A-A´ in **Figure 11**) limits the recharge in the deepest aquifer levels, preserving the salinities of the connate waters, and at the same time favors the oxygen exchange that causes oxygen enrichment as observed in the reported datasets of González-Uribe et al. (2007) and González-Penagos et al. (2014) (**Figures 8B-1, 8B-2, 10 and 11**). This complexity decreases towards the La Macarena Range sector (e.g., section C-C´ in **Figure 11**), having an additional relevant factor: the exposure of rock units on the surface (Mesozoic and Cenozoic units). This factor favors the percolation of meteoric waters from the surface to high depths. This condition would explain both the low salinities and the isotopic compositions ($\delta^{18}O$ and $\delta D$) of the groundwaters of the southern Llanos basin shown in this study, where oxygen enrichment in the water is not observed.

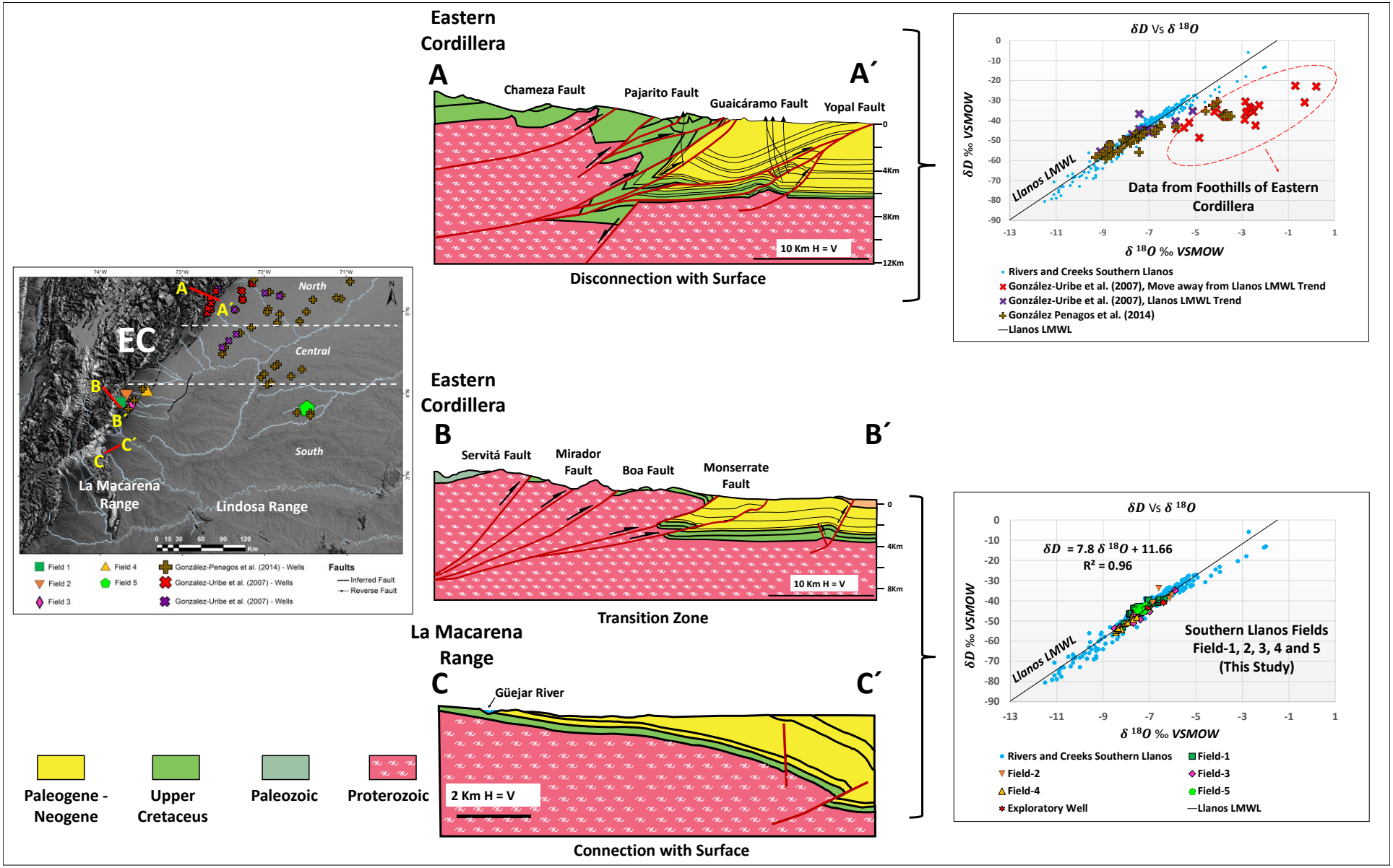


**Figure 11**. Gradual changes in structural complexity from northeast to southwest in southern Llanos basin and its correlation with isotope behavior. Section A – A´ (modify from Mora et al., 2010a), Section B – B´ (modified from Mora et al., 2010b), Section C – C´ (Modify from Arias-Martínez et al., 2018). All samples taken in this study, from Fields 1, 2, 3, 4 and 5, near to B-B´ follow the Llanos LMWL. 66% of samples from González-Uribe et al. (2007) move away from Llanos LMWL trend and is related with high structural complexity on eastern flank of the Eastern Cordillera. EC: Eastern Cordillera.

The intersection between these outcropping rock units on the surface and the drainages of surface water sources (e.g., Güejar River in section C-C´ - **Figure 11**) that border the eastern front of the La Macarena Range favors the recharge of meteoric waters in the Basal Flow Unit of the southern Llanos basin.

***5.4 Recharge Areas – Provenance of Groundwater***

The provenance of the groundwaters present in the Basal Flow Unit was established from the isotope compositions of $\delta^{18}O$ and $\delta D$ using samples from oil fields, of the proximal sector of the eastern deformation front of the La Macarena Range and the eastern flank of Eastern Cordillera, and some samples from the oil field in the easternmost sector of the Llanos foreland.

The models used to estimate the altitude ranges for the groundwater samples as a function of $\Delta\delta^{18}O$ and $\Delta\delta D$ with their respective associated 2σ uncertainties were for $\Delta\delta^{18}O$ (**Equations 7 and 8**):

$$\text{Elevation} = -565.1\ (\pm 50.37) \times \Delta\delta^{18}O\ (\pm 455.6) \quad (7)$$

And for $\Delta\delta D$:

$$\text{Elevation} = -68.63\ (\pm 6.67) \times \Delta\delta D\ (\pm 405.4) \quad (8)$$

The results suggest that the groundwater associated with deep aquifers present an isotopic footprint associated with altitude ranges between 580 m.a.s.l and 2060 m.a.s.l. according to the most likely model proposed by Saylor et al., 2009 (**Figure 12**).

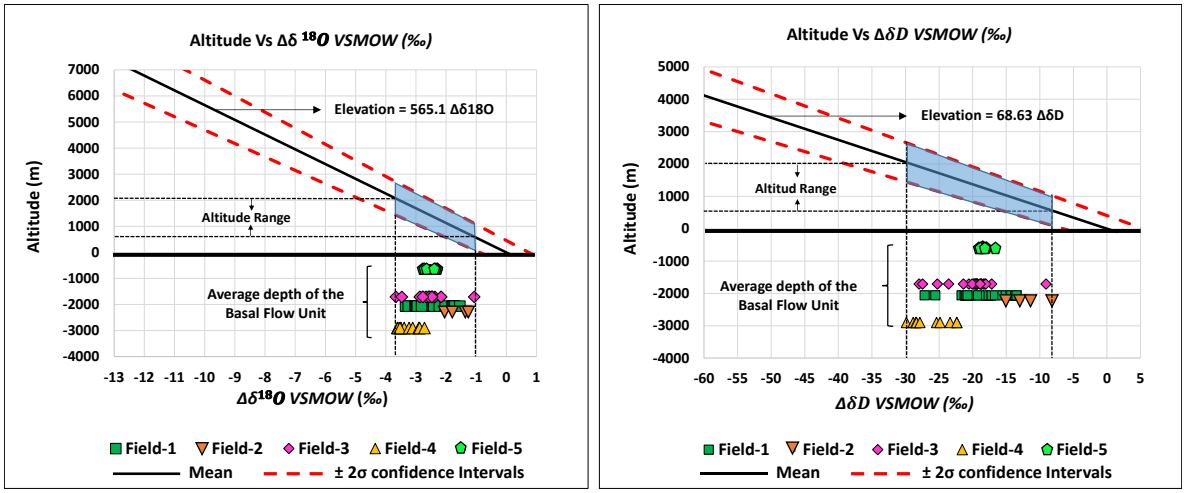


**Figure 12**. Altitude ranges estimated using the altitude model proposed by Saylor et al. (2009). Sampling depths (m.a.s.l) of the groundwater from the oil fields corresponds to the average depth of the reservoirs.

This range represent the altitude ranges reported in the western boundary of the basin, associated with the eastern foothills of the Eastern Cordillera and la Macarena Range. To visualize these altitude ranges, the area associated with those elevations was extracted from a digital elevation model. Based on that, we identified the eastern foothills of the Eastern Cordillera and la Macarena Range as the main recharge areas of the system. (**Figure 13**).

The defined altitude ranges suggest that the origin of the groundwater has followed a flow path from the recharge zones on the western boundary of the Llanos basin (Eastern Cordillera Foothills and the La Macarena Range), to distal areas of the Llanos foreland basin. However, according to the structural styles recognized in the western limit of the Llanos basin, we interpret as the main recharge zone La Macarena Range area due to the most effective hydraulic connection between the Basal Flow Unit and surface (e.g., Güejar River in section C-C´ **Figure 11**).

In the foothills of Eastern Cordillera, although there may be recharge, there is a greater degree of lateral disconnection, attributed mainly to the more complex structural styles (**Figure 11**) documented in this area (Mora et al., 2010a; Mora et al., 2010b; Arias-Martínez et al., 2018; Mora et al., 2019). Thus, the flow path that the meteoric water follows from the surface through the Basal

Flow Unit in the basin is established by the lateral connection of hydraulically connected diachronous rock units resting on Paleozoic rocks throughout the basin. (**Figure 13**).

The findings presented in this study limit the recharge zones to the southwestern edge of the Llanos basin, which contrasts some hypotheses where it is proposed that the water recharge of this deep aquifer system would be towards the eastern sector (e.g., González-Penagos et al., 2014). However, additional geological and isotopic analyzes of the easternmost sector of Colombia would allow establishing the existence (or not) of recharge zones to the east of the foreland of the southern llanos basin.

The results and approach of this study are similar to those proposed by Springer et al. (2016), who determined the origin of the recharge for groundwater in western North America using stable isotopes, suggesting that a regional source of water recharge is expected towards the plains whereas the recharge for the high elevation zones has a more significant local influence. In our case, the recharge of the Basal Flow Unit is interpreted as regionally sourced (from La Macarena Range) because a large part of the foreland of the basin is isolated from the influence of local precipitation (or surface water sources) by the aquitards confining the Basal Flow Unit. On the other hand, the recharge of the BFU is mainly attributed to the contribution of surface water sources in the La Macarena Range area (rivers and creeks). A more detailed analysis could show the contribution of the different sources to the recharge of the Basal Flow Unit using approaches such as those shown by Liu and Yamanaka (2012). They estimate the contribution to the recharge from different surface water sources. However, our approach using the altitude model from stable isotopes ($\delta^{18}O$ - $\delta D$) allowed us to interpret that the recharge is mainly influenced by the deformation front of the La Macarena Range.

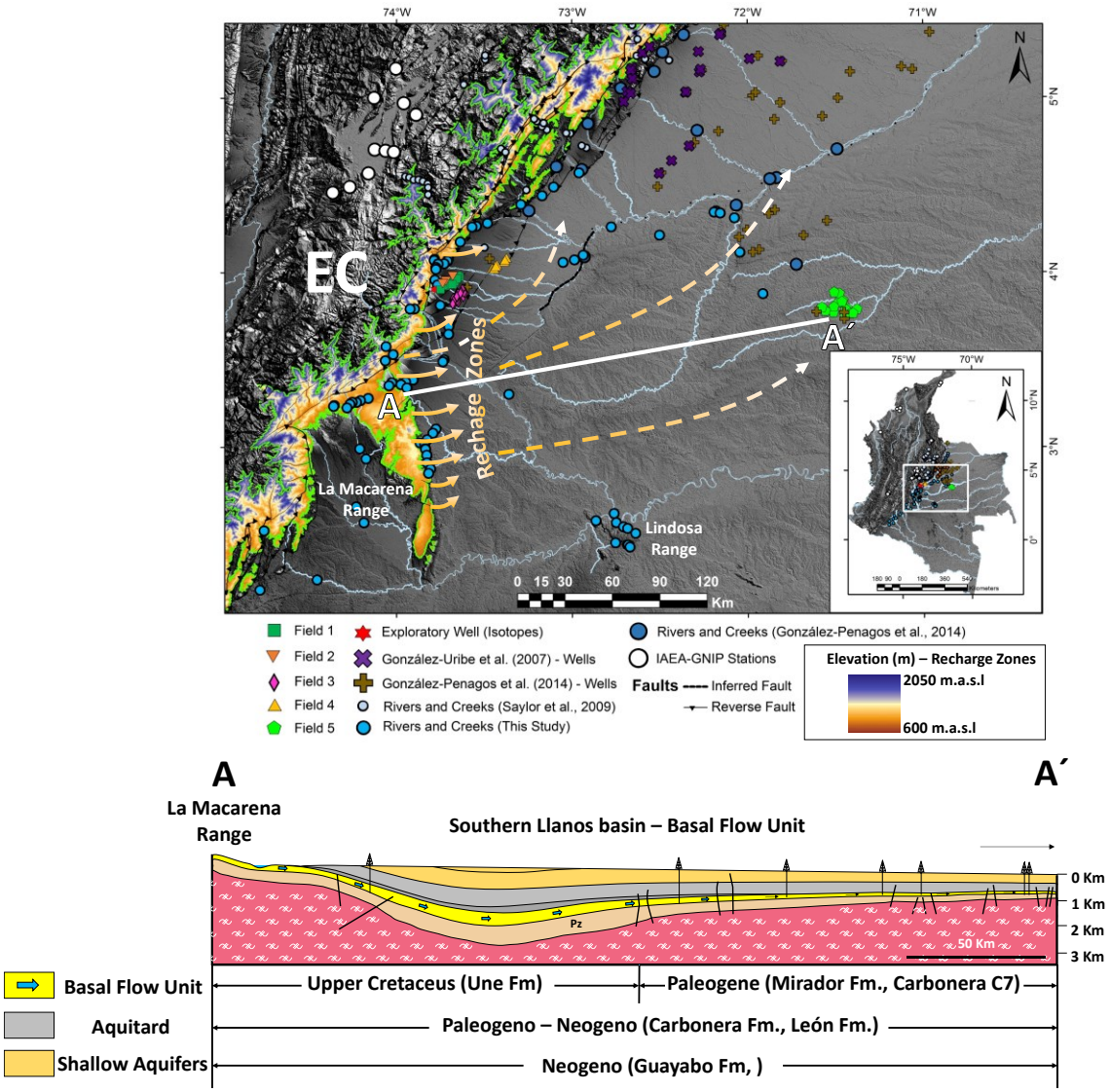


**Figure 13**. (Above) The map shows the recharge areas (shaded areas with warm colors) identified using the altitude model proposed by Saylor et al. (2009). The range of altitudes was extracted from 12 meters DEM (SRTM). (Below) An illustrative section A-A´ with the configuration of the Basal Flow Unit (Yellow unit and blue arrows), aquitards (grey), and shallow aquifers (orange). Below the illustrative section A-A´, is the schematic extension of the formations that make up the Basal Flow Unit. EC: Eastern Cordillera.

### *5.5. Anions (-) and Cations (+) in Groundwater*

From the analysis of anions (-) and cations (+) carried out in surface water and groundwater samples, Stiff and Piper diagrams were constructed to facilitate the visualization of compositional variations throughout the study area. Stiff diagrams were constructed using $HCO_3^-$, $CO_3^{-2}$, $SO_4^{-2}$, and $Cl^-$ for the anions (-) and $Na^+$, $K^+$, $Ca^{+2}$, and $Mg^{+2}$ for the cations (+), using a scale of 0 to 25 meq/L, considering

the highest concentrations recognized in the area. Stiff diagrams represent concentrations of anions (-) to the right of the mid-line, and concentrations of cations (+) to the left of the mid-line. A very narrow Stiff diagram indicates low mean anion (-) and cation (+) concentrations whereas a wide Stiff diagram indicates highly saline waters.

The presence of low salinities in the foreland and in proximity to la Macarena Range has been documented in previous works (e.g., Villegas et al. 1994; Person et al., 2012; González-Penagos et al., 2014; Gómez-Moncada et al., 2022). On the other hand, it is recognized that the highest concentrations of anions (-) and cations (+) (moderately saline and very saline, according to Swenson and Baldwin, 1965), are restricted to the western sector of the basin (González-Penagos et al., 2014), close to the deformation front of Eastern Cordillera, while towards the southern Llanos basin, groundwaters with low ion concentrations are recognized. The behavior observed in the composition of the groundwater samples along the southern Llanos basin allows us to see the transition in the dilution processes throughout the basin. The eastern area corresponds to the relatively highest concentrations of ions (See Field-5 in **Figure 14**). In contrast, the western area, towards the recharge zones (La Macarena Range), corresponds to the sector where the dilution of ions by effect of meteoric waters is more efficient (**Figure 14**).

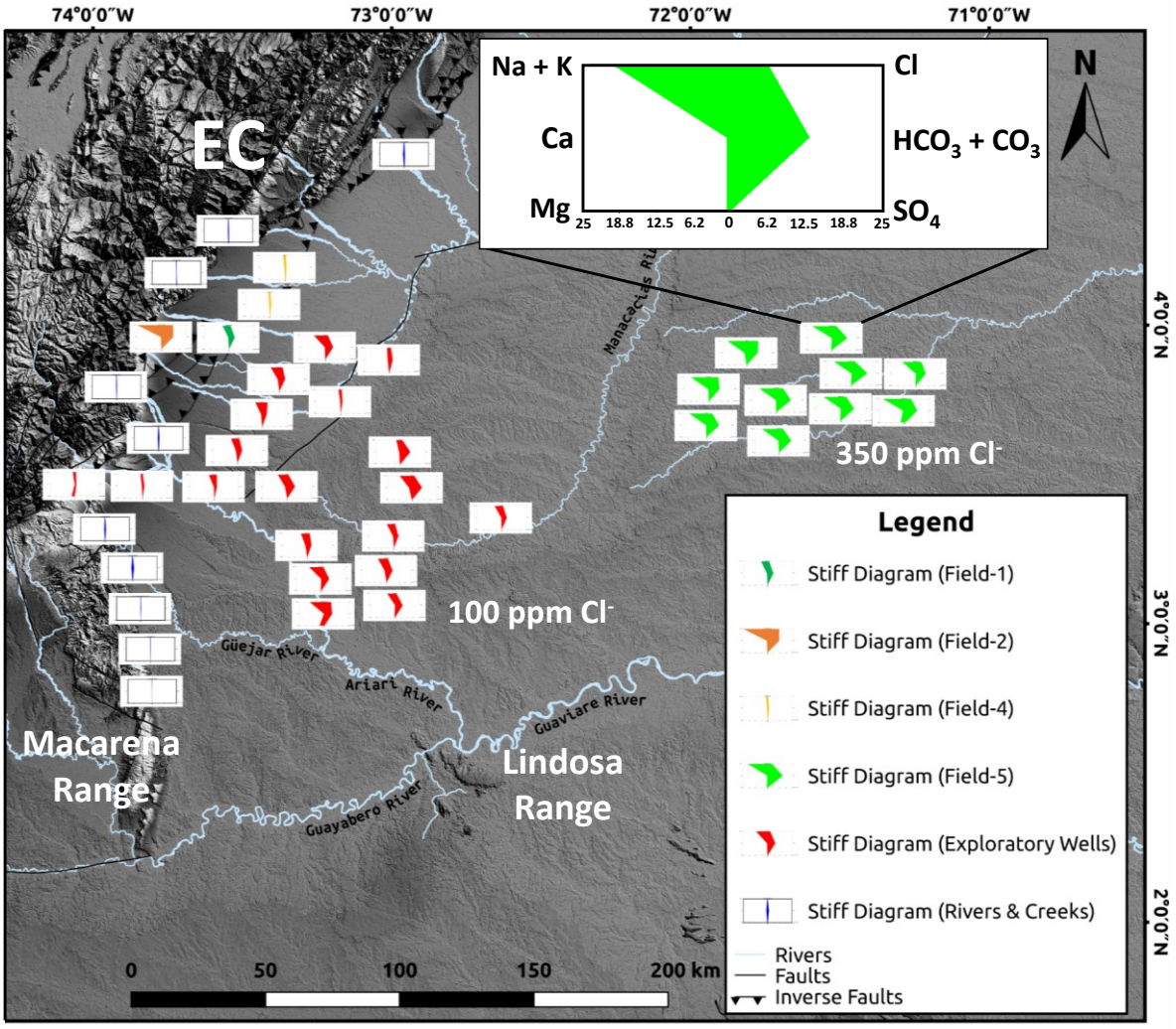


**Figure 14.** Stiff diagrams from surface waters (blue) and groundwater (other colors) of the Southern Llanos basin. The map shows the reduction of ion concentrations in the direction East-West. Low concentrations are correlated with the proximity to the recharge zones identified with the altitude model (La Macarena Range). Modify from Gómez-Moncada et al. (2022).

Although the eastern sector is the one with the highest ion preservation, the groundwater of this sector corresponds to freshwaters and slightly saline waters according to the classification of Swenson and Baldwin (1965).

Moreover, ion concentrations are highly variable in the western sector (Fields 1, 2, 3, and 4 in **Figure 14**). One factor controlling variability is attributed mainly to the restriction of the vertical connection controlled by the Gachetá Formation (aquitard), which acts as a vertical barrier between the Basal

Flow Unit (Une Formation) and the Paleogene (Barco, Mirador and Guadalupe Formations). The second factor corresponds to the lateral changes of the structural style itself (**Figure 11**). The anion (-) and cation (+) analysis of southern Llanos basin shows correspondence with the recharge zones established from the presented altitude model, which confirms the influence of meteoric waters in a west-east direction, from La Macarena Range and Eastern Cordillera to the foreland of Llanos basin. Nevertheless, considering the differences found in the structural configuration of the southernmost sector, we attribute to La Macarena Range as the main recharging area, which may even be influencing the northernmost sector (Fields 1, 2, 3, and 4 in **Figures 11** and **14**). The above can be confirmed in the exploratory wells that were drilled to the southwest, especially those that were drilled close to La Macarena Range, which report low ion concentrations. $Cl^-$ concentrations on average considering all exploratory wells is 176.3 ppm. However, very close to La Macarena Range, there are wells that have reported concentrations as low as those recognized in surface water sources that border La Macarena Range, as in the case of Güejar River (See Section C – C´ **Figure 11**, and **Figure 14**).

Similarly, Piper diagrams made for the area show that 97.7% of the samples are located in area 2 of the Piper diagrams (Piper, 1944), recognizing that the alkaline components (Na, K) exceed the alkaline terrestrial components (Ca, Mg) (**Figure 15**). According to Back (1966), hydrogeochemical facies classification, approximately 65 % of the samples are located in the Sodium-Potassium zone (90 - 100% of $Na^+$ and $K^+$) (Field-1, Field-4 and exploratory wells of the central part of southern Llanos basin). Concerning anion (-) content, and according to the classification of Back (1966), approximately 70% of the samples are located in the Bicarbonate-Chloride-Sulfate facies (50 - 90% of $HCO_3^-$ and $CO_3^{-2}$) and 26% in the Chloride-Sulfate-Bicarbonate facies (10 - 50 % of $HCO_3^-$ and $CO_3^{-2}$). This defines that the waters of the southern Llanos basin are mainly bicarbonate, in transitions between sodium bicarbonate and sodium chloride.

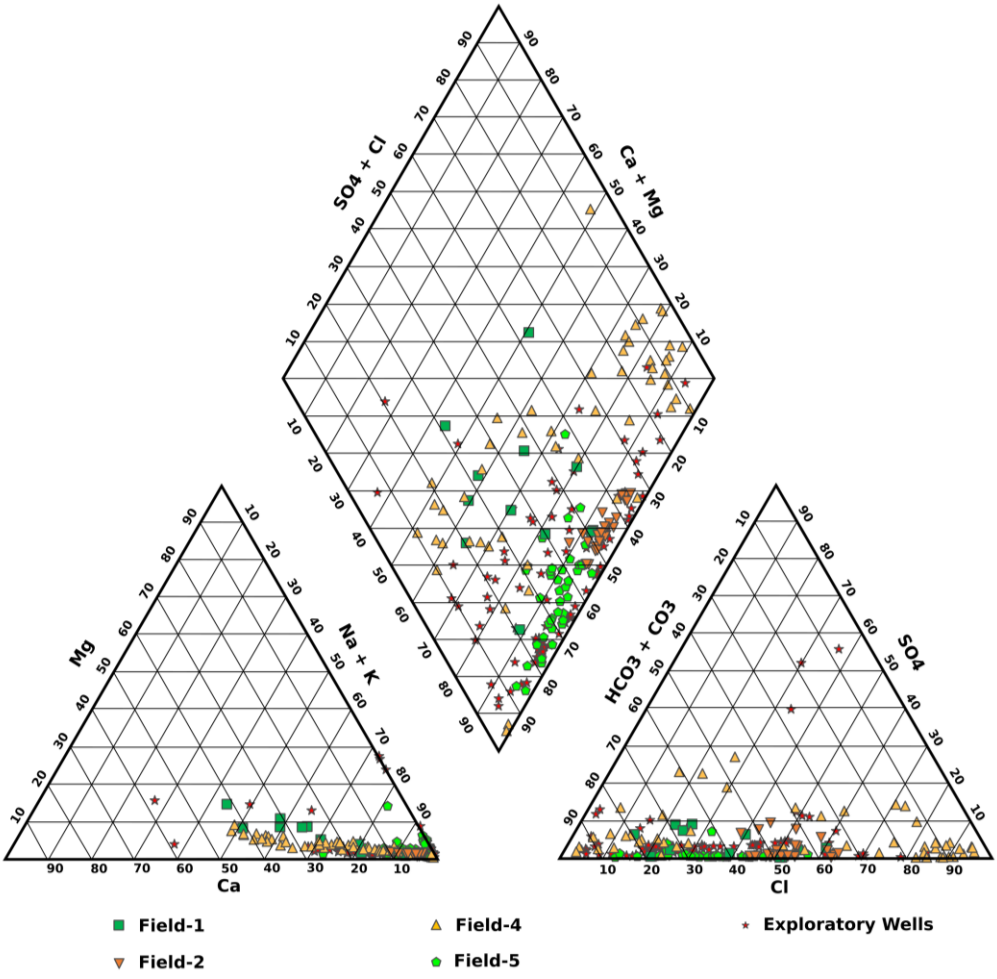


**Figure 15**. Piper diagram from groundwaters samples of southern Llanos basin generated from anions ($HCO_3^-$, $CO_3^{-2}$, $SO_4^{-2}$, and $Cl^-$) and cations ($Na^+$, $K^+$, $Ca^{+2}$, and $Mg^{+2}$).

This behavior of the groundwater composition in the southern Llanos basin confirms that the influx of meteoric waters from the surface has reached deep aquifers (-0.6 km to -4.0 km) in the area. The above-mentioned points agree with the analyses reported by González-Penagos et al. (2014). However, and in contrast to what is proposed by González-Penagos et al. (2014), the results of the altitude model built with isotopic analyses and considering the structural configuration of La Macarena Range sector, support that the recharge of the Basal Flow Unit is limited to the west of the basin and corresponds mainly to La Macarena Range.

## 6. Conclusions

We integrated 162 new and 98 previously published stable isotope analyses from surface water samples taken along the main rivers and creeks of the Orinoco River basin to develop a Local Meteoric Water Line (LMWL) for the Llanos basin in Colombia. The Llanos LMWL is similar to the Global Meteoric Water Line of Craig (1961) and Rozanski et al. (1993) but with slightly higher deuterium excess. The d-excess value of meteoric waters from the southern Llanos basin is close to the global datasets and can be attribute to non-equilibrium fractionation during evaporation processes (Dansgaard, 1964; Rozanski et al., 1993; Saylor et al., 2009).

The isotope compositions of surface waters and groundwater in the southern sector of the Llanos basin are best represented by the long-term annual weighted mean model proposed by Rozanski et al. (1993), while the trend of isotopic behavior for Colombia, considering all IAEA- GNIP stations present in Colombia is represented by the GMWL.

A reduced continentality effect is interpreted for Llanos basin in Colombia according to what is observed from the central zone of the Amazon basin westward Manaus station, where the $\delta^{18}O$ gradient become very small in response to recycling of moisture by evapotranspiration (Salati et al., 1979; Gat and Matsui, 1991; Rozanski et al., 1993). The isotopic compositions ($\delta^{18}O$ and $\delta D$) of meteoric water from the southern Llanos basin reflect a transition zone of isotopic behavior, expressed in terms of isotope depletion, which coincides with the change in topography between the Amazon basin and the Colombian Andes. This isotope depletion observed in the surface water samples from southern Llanos is interpreted as a response of altitude effect which is exerted from orographic uplift of Eastern Cordillera.

100% of groundwater samples (n=109) from different oil fields confirmed the influence of meteoric waters in the reservoirs along the southern Llanos basin. This showed an isotope composition similar to the surface water samples. The $\delta^{18}O$ and $\delta D$ compositions of the groundwater in the Southern Llanos suggest that the groundwater is not influenced by oxygen exchange between the water and the reservoir rocks. The groundwater reveals average values of d-excess of 14.44 ‰ VSMOW (±1.75), similar to average values of d-excess in meteoric waters of 13.66‰ VSMOW (±2.55) when all samples are considered, or a d-excess of 14.69 ‰ VSMOW (±1.27) when we compare only with the samples of the most western sector. From the La Macarena Range northwards and along the foothills of the Eastern Cordillera, the isotopic compositions move away from the GMWL and Llanos LMWL, correlating this behavior with the structural complexity of those areas. Those data that move away from LLanos LMWL reveal average d-excess values of -2.91 ‰ VSMOW (±14.25) (data from González-Uribe et al., 2007). However, some isotopic analyses ($\delta^{18}O$ and $\delta D$) carried out in the north sector show that meteoric water has reached some reservoirs even in the most structural complexity areas (e.g., González-Uribe et al., 2007; González-Penagos et al., 2014; Mora et al., 2019).

The altitude ranges estimated from the values of $\Delta\delta^{18}O$ and $\Delta\delta D$ for the evaluation of the provenance of the groundwater in the southern Llanos basin range approximately between 580 m.a.s.l to 2060 m.a.s.l. These altitudes are related with the elevations of the foothills along the Eastern Cordillera and La Macarena Range (**Figure 13**). However, the structural configuration in the surroundings of La Macarena Range, which is a continuous monoclinal configuration with rivers in direct connection with surface exposures of the reservoir units, favors that most of the recharge for the subsurface aquifers may be focused on this structural domain. Moreover, the Lindosa Range sector, which corresponds to an elevated area towards the southern sector of the basin, presents a

lower probability of being an active recharge area considering the area exposed to recharge, which is approximately ¼ compared to the area of La Macarena Range.

The low salinities (freshwaters to slightly saline) and the alkaline character associated with bicarbonate groundwater of the southern Llanos basin, correlate with the location of the recharge zones identified from the isotope analysis. Thus, the data suggests that the dilution process of ions in the groundwater has been more efficient in proximity to the main recharge zone of the system corresponding to La Macarena Range. On the other hand, the western sector where Fields 1, 2, 3, and 4 are located (**Figure 14**), is segmented by complex structures that complicate the direct connection with the surface. In this sector a bimodal behavior is observed in the concentration of anions (-) and cations (+), finding a more significant influence of meteoric waters in the Upper Cretaceous units (Une and Guadalupe Formations) than in Paleocene formations.

From the results obtained, we suggest that the pathway followed by the water from the surface corresponds to a combination of different factors. However, two conditions have favored the hydric recharge of the Basal Flow unit in the southern Llanos: 1) The presence of laterally continuous (i.e., hydraulically connected) sandy formations with high permeability configured the flow path through the Llanos basin. 2) The recent tectonics of the deformation front of the La Macarena Range and the evolution of the Colombian Andes allowed the exhumation of rock units (outcrops) currently intersected by surface water sources, which generate water recharge in this type of system associated with deep aquifer levels.

## 7. Acknowledgments

Thanks to MINCIENCIAS in the framework of Call 758 for the financial support of the research. Thanks to EAFIT University as part of an official program agreement between ECOPETROL S.A, EAFIT University and MINCIENCIAS.

## 8. References

Alley W.M, 2009, Ground Water: in E. Likens, ed., Encyclopedia of Inland Waters, Elsevier, p. 684-690, https://doi.org/10.1016/B978-012370626-3.00015-6.

Alvarez-Villa O. D., J. I. Vélez, and G. Poveda, 2011, Improved long-term mean annual rainfall fields for Colombia: International Journal of Climatology, v. 31, p. 2194 – 2212, doi:10.1002/joc.2232

Arango C., J Dorado, D. Guzmán and J.F Ruiz, 2012, Climatología trimestral de Colombia Grupo de Modelamiento de Tiempo, Clima y Escenarios de Cambio Climático Subdirección de Meteorología – IDEAM

Arias, P. A., J. A. Martínez, and S. C. Vieira, 2015, Moisture sources to the 2010-2012 anomalous wet season in northern South America: Climate Dynamics, v. 45, p. 2861 – 2884, https://doi.org/10.1007/s00382-015-2511-7

Arias P.A., R. Garreaud, G. Poveda, J.C. Espinoza, J. Molina-Carpio, M. Masiokas, M. Viale, L. Scaff and P.J. van Oevelen, 2021, Hydroclimate of the Andes Part II: Hydroclimate Variability and Sub-

Continental Patterns: Frontiers in Earth Science, v. 8:505467, p. 1 – 25, doi: 10.3389/feart.2020.505467

Arias-Martínez J.P., A. Mora, D. Echeverry and G. Rodríguez, 2018, Nuevo Mapa de la Transición entre las cuencas Llanos y Caguán - Impactos para la Exploración y el Flujo Hidrodinámico de la Cuenca: I Cumbre del Petróleo y Gas, Bogotá, Colombia, 14 – 16 November 2018.

Bachu S., J.C. Ramon, M.E. Villegas, and J.R. Underschultz, 1995, Geothermal regime and Thermal history of the Llanos Basin, Colombia: AAPG Bulletin, v. 79, n. 1, p. 116–129, https://doi.org/10.1306/8D2B14D0-171E-11D7-8645000102C1865D

Back, W., 1966, Hydrochemical facies and ground-water flow patterns in Northern part of Atlantic Coastal Plain: Hydrology of aquifer systems, U.S. Geological Survey, p. A1 – A42, https://doi.org/10.3133/pp498A

Bair E. S., T.P. O´Donnell, L.W. Picking, 1985, Potentiometric mapping from incomplete drill-steem test data: Palo Duro Basin area, Texas and New Mexico: Ground Water, v. 23, n. 2, p. 198 – 211, https://doi.org/10.1111/j.1745-6584.1985.tb02793.x

Bendix, J., and W. Lauer, 1992, Die Niederschlagsjahreszeiten in Ecuador undihre klimadynamische Interpretation (Rainy Seasons in Ecuador and Their Climate-Dynamic Interpretation): Erdkunde v.46: 2, p.118–134, https://www.jstor.org/stable/25646379

Caballero V., J. Naranjo, F. De La Parra, A. Mora, A. Reyes-Harker, 2015, Estratigrafía de Secuencias de los Principales Reservorios de la Cuenca de Llanos: Memorias XV Congreso Colombiano de Geología, p. 320 – 324.

Carucci, V., M. Petitta, & R. Aravena, 2012, Interaction between shallow and deep aquifers in the Tivoli Plain (Central Italy) enhanced by groundwater extraction: a multi-isotope approach and geochemical modeling: Applied Geochemistry, v. 27, n.1, p. 266–280, https://doi.org/10.1016/j.apgeochem.2011.11.007

Chavez, S. P., and K. Takahashi, 2017, Orographic rainfall hotspots in the Andes-Amazon transition according to the TRMM precipitation radar and in situ data: Journal of Geophysical Research: Atmospheres, v. 122, p. 5870 – 5882, doi: 10.1002/2016JD026282

Clayton R.N., I. Friedman, D.L. Graf, T.K. Mayeda, W.F. Meents, N.F. Shimp, 1966, The origin of saline formation waters. 1. Isotopic composition, Journal of Geophysical Research, v. 71, n. 16, p. 3869 – 3882, https://doi.org/10.1029/JZ071i016p03869

Cooper, M. A., F.T. Addison, R. Alvarez, M. Coral, R.H. Graham, A.B. Hayward, S. Howe et al., 1995, Basin development and tectonic history of the Llanos Basin, Eastern Cordillera, and Middle Magdalena Valley, Colombia: AAPG Bulletin, v. 79, n. 10, p. 1421–1443, https://doi.org/10.1306/7834D9F4-1721-11D7-8645000102C1865D

Craig H., 1961, Isotopic variations in meteoric waters: Science v. 133, p. 1702–1703, http://dx.doi.org/10.1126/science.133.3465.1702

Currell M.J., I. Cartwright, D.C. Bradley & D. Han, 2010, Recharge history and controls on groundwater quality in the Yuncheng Basin, north China: Journal of Hydrology v. 385, n. 1-4, p. 216–229, https://doi.org/10.1016/j.jhydrol.2010.02.022

Dansgaard W., 1964, Stable isotopes in precipitation: Tellus, v. 16, p. 436-468, https://doi.org/10.1111/j.2153-3490.1964.tb00181.x

De Vries J.J, E.T. Selaolob and H.E. Beekmanc, 2000, Groundwater recharge in the Kalahari, with reference to paleo-hydrologic conditions: Journal of Hydrology, v. 238, n. 1-2, p. 110 – 123, https://doi.org/10.1016/S0022-1694(00)00325-5

Edmunds, W.M., A.H. Guendouz, A. Mamou, A. Moulla, P. Shand, and K. Zouari, 2003, Groundwater evolution in the Continental Intercalaire aquifer of southern Algeria and Tunisia: trace element and isotopic indicators. Applied Geochemistry, v.18, n. 6, p. 805–822, https://doi.org/10.1016/S0883-2927(02)00189-0

Edmunds W.M., and E.P. Wright, 1979, Groundwater recharge and palaeoclimate in the Sirte and Kufra basins, Libya: Journal of Hydrology, v. 40, n. 3-4, p. 215–241, https://doi.org/10.1016/0022-1694(79)90032-5

Espinoza, J. C., J. Ronchail, J. L. Guyot, G. Cochonneau, F. Naziano, W. Lavado, E. De Oliveira, R. Pombosa, 2009, Spatio-temporal rainfall variability in the Amazon basin countries (Brazil, Peru,

Bolivia, Colombia, and Ecuador): International Journal of Climatology, v. 29, p. 1574–1594, doi: 10.1002/joc.1791.

Espinoza, J. C., S. Chavez, J. Ronchail, C. Junquas, K. Takahashi, and W. Lavado, 2015, Rainfall hotspots over the southern tropical Andes: spatial distribution, rainfall intensity and relations with largescale atmospheric circulation: Water Resources Research, v. 51, p. 3459 – 3475, doi: 10.1002/2014wr016273

Espinoza J.C., R. Garreaud, G. Poveda, P.A. Arias, J. Molina-Carpio, M. Masiokas, M. Viale and L. Scaff, 2020, Hydroclimate of the Andes Part I: Main Climatic Features: Frontiers in Earth Science, v. 8:64, p. 1 – 20, doi: 10.3389/feart.2020.00064.

Figueroa, S. N., and C. A. Nobre, 1990, Precipitation distribution over central and western tropical South America: Climanálise, v. 5: 6, p. 36 – 45.

Garreaud, R. D., 1999, Multiscale analysis of the summertime precipitation over the Central Andes: American Meteorological Society, v. 127, p. 901–921. https://doi.org/10.1175/1520-0493(1999)127<0901:MAOTSP>2.0.CO;2

Garven G., 1985, The Role of Regional Fluid Flow in the Genesis of the Pine Point Deposit, Western Canada Sedimentary Basin: Economic Geology, v. 80, p. 307 – 324, https://doi.org/10.2113/gsecongeo.80.2.307

Gat, J.R., and E. Matsui, 1991, Atmospheric Water Balance in the Amazon Basin: An Isotopic Evapotranspiration Model: Journal of Geophysical Research, v. 96, n. D7, p. 13,179 – 13,188, https://doi.org/10.1029/91JD00054

Giambastiani, B.M.S., N. Colombani, M. Mastrocicco, and M.D. Fidelibus, 2013, Characterization of the lowland coastal aquifer of Comacchio (Ferrara,Italy): Hydrology, hydrochemistry and evolution of the system: Journal of Hydrology, v. 501, p. 35–44, https://doi.org/10.1016/j.jhydrol.2013.07.037

Giovannettone, J. P., and A. P. Barros, 2009, Probing regional orographic controls of precipitation and cloudiness in the central Andes using satellite data: Journal of Hydrometeorology, v. 10, p. 167 – 182, doi: 10.1175/2008jhm973.1

Gómez-Moncada R.A, A. Mora, M. Jaramillo, M. Parra, A. Martínez, H. Mayorga, J.E. Sandoval, A. Cuy-Cipamocha, D. Suárez, J.R. Sandoval-Ruiz, R. Ramírez, R. Márquez and R. Bueno, 2022, Implications of groundwater flow on preservation of heavy and extra-heavy oil accumulations in Southern Llanos Basin, Colombia: Journal of South American Earth Sciences, v. 119, p. 1 – 24, https://doi.org/10.1016/j.jsames.2022.104013

González-Penagos, F., I. Moretti, C. France-Lanord, and X. Guichet, 2014, Origins of formation waters in the Llanos foreland basin of Colombia: Geochemical variation and fluid flow history: Geofluids, v. 14, n. 4, p. 443–458, https://doi.org/10.1111/gfl.12086

González-Penagos, F., I. Moretti, and X. Guichet, 2017, Fluid Flow Modeling in the Llanos Basin, Colombia: AAPG Memoir 114, p. 191–217, https://doi.org/10.1306/13602030M1143705

González-Uribe G, D. García-Bautista, L Mantilla-Figueroa, J. Rodríguez-Rincón, 2007, Hidrodinámica e hidrogeoquímica del piedemonte llanero: Hipótesis de rutas de migración a partir de técnicas hidrogeológicas. Boletín de Geología, v.29, n. 1, p. 75–84, DOI: 10.18273/revbol

Guo, X., Q. Feng, J. Si, H. Xi, Y. Zhao and R.C Deo, 2019, Partitioning groundwater recharge sources in multiple aquifers system within a desert oasis environment: Implications for water resources management in endorheic basins, Journal of Hydrology, v. 579, https://doi.org/10.1016/j.jhydrol.2019.124212

Hitchon B., 1969, Fluid Flow in the Western Canada Sedimentary Basin 1. Effect of Topography: Water Resources Research, v. 5, n. 1, p. 186 – 195, https://doi.org/10.1029/WR005i001p00186

Hoorn, C., P. Wesseling, H. ter Steege, M. A. Bermudez, A. Mora, J. Sevink, et al., 2010, Amazonia through time: andean uplift, climate change, landscape evolution, and biodiversity: Science, v. 330, 927–931, doi: 10.1126/science.1194585

Hoyos, F. I, J. Dominguez, J. A. Cañón-Barriga, R. Martínez, L. Nieto, L. Gimeno, P.A. Dirmeyer, 2017, Moisture origin and transport processes in Colombia, northern South America: Climate Dynamics, v. 50, p. 971 – 990. https://doi.org/10.1007/s00382-017-3653-6

Huang Y., J. Evaristo and Z. Li, 2019, Multiple tracers reveal different groundwater recharge mechanisms in deep loess deposits. Geoderma, v. 353, p. 204–212, https://doi.org/10.1016/j.geoderma.2019.06.041

IAEA/WMO (2020). Global Network of Isotopes in Precipitation. The GNIP Database. Accessible at: https://nucleus.iaea.org/wiser.

Jimenez, L., A. Mora, W. Casallas, A. Silva, E. Tesón, J. Tamara, J. Namson, C. Higuera-Díaz, A. Lasso, and D. Stockli, 2013, Segmentation and growth of foothill thrustbelts adjacent to inverted grabens: The case of the Colombian Llanos foothills, in M. Nemcok, A. Mora, and J. Cosgrove, eds., Thick-skin-dominated orogens: From initial inversion to full accretion: Geological Society, London, Special Publications 2013, v. 377, n. 1, p. 189–220, https://doi.org/10.1144/SP377.11

Johnson, A. M., 1976, The climate of Peru, Bolivia and Ecuador, in Climates of Central and South America, World Survey of Climatology, v. 12, ed. W. Schwerdtfeger (Elsevier), 147–200.

Junquas, C., K. Takahashi, T. Condom, J. C. Espinoza, S. Chavez, J. E. Sicart and T. Label, 2018, Understanding the influence of orography over the precipitation diurnal cycle and the associated atmospheric processes in the central Andes. Clim Dyn, v. 50, p. 3995 – 4017, doi: 10.1007/s00382-017-3858-8

Kendall C. and E.A. Caldwell, 1998, Fundamentals of Isotope Geochemistry, in C. Kendall and J. J. McDonnell, eds., Isotope tracers in catchment hydrology: Elsevier, p. 51 – 86, https://doi.org/10.1016/B978-0-444-81546-0.50009-4

Kong Y., Z. Pang, J. Pang, Y. Wang and F. Yang, 2017, Stable isotopes of deep groundwater in the Xiongxian geothermal field: Procedia Earth and Planetary Science v. 17, p. 512 – 515, https://doi.org/10.1016/j.proeps.2016.12.129

Kumar S., Y.S. Vidal, A. S. Moya-Álvarez, and D. Martínez-Castro, 2019, Effect of the surface wind flow and topography on precipitating cloud systems over the Andes and associated Amazon basin: GPM observations: Atmospheric Research, v. 225, p. 193 – 208, https://doi.org/10.1016/j.atmosres.2019.03.027

Lerner, D.N., A.S. Issar, and I. Simmers, 1990, Groundwater recharge. A guide to understanding and estimating natural recharge. International Contributions to Hydrogeology: Verlag Heinz Heise, v. 8, p. 345, https://doi.org/10.2134/jeq1992.00472425002100030036x

Liu Y., and T. Yamanaka, 2012, Tracing groundwater recharge sources in a mountain–plain transitional area using stable isotopes and hydrochemistry: Journal of Hydrology, v. 464 – 465, p. 116 – 126, http://dx.doi.org/10.1016/j.jhydrol.2012.06.053

Lloyd, J.W., 1986, A Review of Aridity and Groundwater: Hydrological Processes, v. 1, p. 63 – 78, https://doi.org/10.1002/hyp.3360010107

Mejia, J. F., O. Mesa, G. Poveda, and J. I. Velez, C. Hoyos, R. Mantilla, J. Barco, A. Cuartas, M. Montoya, 1999, Distribución espacial y ciclos anual y semianual de la precipitación en Colombia: Dyna, v. 127, p. 7–14.

Monjerezi, M., R.D. Vogt, P. Aagaard, A.G. Gebru, J.D.K. Saka, 2011, Using 87Sr/86Sr, $\delta^{18}O$ and δ2H isotopes along with major chemical composition to assess groundwater salinization in lower Shire

valley, Malawi: Applied Geochemistry, v.26, p. 2201–2214, https://doi.org/10.1016/j.apgeochem.2011.08.003

Mora, A., R.A. Gómez, C. Diaz, V. Caballero, M. Parra, C. Villamizar, A. Lasso, R.A. Ketcham, F. González-Penagos, J. Rico, J.P. Arias-Martinez, 2019, Water flow, oil biodegradation, and hydrodynamic traps in the Llanos Basin, Colombia: AAPG Bulletin, v. 103, n. 5, p. 1225–1264, https://doi.org/10.1306/1003181611317237

Mora, A., B.K. Horton, A. Mesa, J. Rubiano, R.A. Ketcham, M. Parra, V. Blanco, D. García, and D.F. Stockli, 2010a, Migration of Cenozoic Deformation in the Eastern Cordillera of Colombia interpreted from fission-track results and structural relationships: Implications for petroleum systems: AAPG Bulletin, v. 94, n. 10, p. 1543–1580, https://doi.org/10.1306/01051009111

Mora, A., R. A. Ketcham, I. C. Higuera-Diaz, B. Bookhagen, L. Jimenez, and J. Rubiano, 2014, Formation of passive-roof duplexes in the Colombian subandes and Perú: Lithosphere, v. 6, n. 6, p. 456–472, https://doi.org/10.1130/L340.1

Mora, A., M. Parra, M.R. Strecker, E. R. Sobel, H. Hooghiemstra, V. Torres, and J. Vallejo-Jaramillo, 2008, Climatic forcing of asymmetric orogenic evolution in the Eastern Cordillera of Colombia: Geological Society of America Bulletin, v. 120, n. 7–8, p. 930–949, https://doi.org/10.1130/B26186.1

Mora, A., M. Parra, M. R. Strecker, E. R. Sobel, G. Zeilinger, C. Jaramillo, S. F. Da Silva, and M. Blanco, 2010b, The eastern foothills of the Eastern Cordillera of Colombia: An example of multiple factors

controlling structural styles and active tectonics: Geological Society of America Bulletin, v. 122, n. 11–12, p. 1846–1864, https://doi.org/10.1130/B30033.1

Mora, A., A. Reyes-Harker, G. Rodriguez, E. Tesón, J.C. Ramirez-Arias, M. Parra, V. Caballero J.P. Mora, I. Quintero, V. Valencia, M. Ibañez, B.K. Horton and D.F. Stockli, 2013, Inversion tectonics under increasing rates of shortening and sedimentation: Cenozoic example from the Eastern Cordillera of Colombia: in M. Nemcok, A. Mora, and J. W. Cosgrove, eds., Thick-skin-dominated orogens: From initial inversion to full accretion: Geological Society, London, Special Publications 2013, v. 377, p. 411–442, https://doi.org/10.1144/SP377.6, https://doi.org/10.1144/SP377.17

Moreno, N., A. Silva, A. Mora, E. Teson, I. Quintero, L. E. Rojas, C. Lopez et al., 2013, Interaction between thin- and thick-skinned tectonics in the foothill areas of an inverted graben. The Middle Magdalena Foothill belt, in M. Nemcok, A. R. Mora, and J. W. Cosgrove, eds., Thickskin - dominated orogens: From initial inversion to full accretion: Geological Society, London, Special Publications 2013, v. 377, p. 221–255, https://doi.org/10.1144/SP377.18

Moreno-López, M.C., and A. Escalona, 2015, Precambrian– Pleistocene tectono-stratigraphic evolution of the southern Llanos Basin, Colombia: AAPG Bulletin, v. 99, n. 8, p. 1473–1501, https://doi.org/10.1306/11111413138

Negrel, P., H. Pauwels, B. Dewandel, J.M. Gandolfi, and C. Mascré, 2011, Understanding groundwater systems and their functioning through the study of stable water isotopes in a hard-rock aquifer (Maheshwaram watershed, India): Journal of Hydrology, v. 397, p.55–70, https://doi.org/10.1016/j.jhydrol.2010.11.033

Negrel, P., R. Millot, C. Guerrot, , G.E. Petelet, A. Brenot, and E. Malcuit, 2012, Heterogeneities and interconnections in groundwaters: Coupled B, Li and stable-isotope variations in a large aquifer system (Eocene Sand aquifer, Southwestern France): Chemical Geology, v. 296–297, p. 83–95, https://doi.org/10.1016/j.chemgeo.2011.12.022

Parra, M., A. Mora, C. Jaramillo, M. R. Strecker, E. R. Sobel, L. I. Quiroz, M. Rueda, and V. Torres, 2009, Orogenic wedge advance in the northern Andes: Evidence from the Oligocene–Miocene sedimentary record of the Medina Basin, Eastern Cordillera, Colombia: Geological Society of America Bulletin, v. 121, n. 5–6, p. 780–800, https://doi.org/10.1130/B26257.1

Parra, M., A. Mora, C. Jaramillo, V. Torres, G. Zeilinger, and M. R. Strecker, 2010, Tectonic controls on Cenozoic foreland basin development in the north-eastern Andes, Colombia: Basin Research, v. 22, p. 874–903, https://doi.org/10.1111/j.1365-2117.2009.00459.x

Person, M., D. Butler, C.W. Gable, T. Villamil, D. Wavrek, and D. Schelling, 2012, Hydrodynamic stagnation zones: Anew play concept for the Llanos Basin, Colombia: AAPG Bulletin, v. 96, n. 1, p. 23–41, https://doi.org/10.1306/08101111019

Poveda G., 2004, La hidroclimatología de Colombia: una síntesis desde la escala inter-decadal hasta la escala diurna: Revista Academia Colombiana de Ciencias, v. 28, p. 201–222.

Poveda, G., H.A. Moreno, S.C. Vieira, P.A. Agudelo, P.A. Arias, L.F. Salazar, O.J. Mesa, F. Alvarez, V. Toro, A. Jaramillo, and O. Guzmán, 2001, Caracterización del Ciclo Diurno de la precipitación en los

Andes tropicales de Colombia. Memorias IX Congreso Latinoamericano e Ibérico de Meteorología, Buenos Aires, Argentina, 7-11 de May 2001.

Poveda, G., P. R. Waylen, and R. Pulwarty, 2006, Modern climate variability in northern South America and southern Mesoamerica: Palaeogeography, Palaeoclimatology,. Palaeoecology, v. 234, p. 3–27. doi: 10.1016/j.palaeo.2005.10.031

Poveda, G., L. Jaramillo, and L. F. Vallejo, 2014, Seasonal precipitation patterns along pathways of South American low-level jets and aerial rivers: Water Resources Research, v. 50, p. 98 – 118, doi: 10.1002/2013WR014087

Piper, A.M., 1944, A graphic procedure in the geochemical interpretation of water-analyses. Eos, Transactions American Geophysical Union, v. 25 n. 6, p. 914-928, https://doi.org/10.1029/TR025i006p00914

Rangel, T. F., N. R. Edwards, P. B. Holden, J. A. F. Diniz-Filho, W. D. Gosling, M. T. P. Coelho, F.A.S Cassemiro, C. Rahbek and R. K. Colwell, 2018, Modeling the ecology and evolution of biodiversity: Biogeographical cradles, museums, and graves: Science, v. 361:eaar5452, p. 1 – 13, doi: 10.1126/science.aar5452

Reyes-Harker, A., C. F. Ruiz-Valdivieso, A. Mora, J. C. Ramirez-Arias, G. Rodriguez, F. De la Parra, V. Caballero, M. Parra, N. Moreno, B.K. Horton, J.E. Saylor, A. Silva, V. Valencia, D. Stockli and V. Blanco, 2015, Cenozoic paleogeography of the Andean foreland and retroarc hinterland of Colombia: AAPG Bulletin, v. 99, n. 8, p. 1407–1453, https://doi.org/10.1306/06181411110

Ricaurte, L. F., J. E. Patiño, D. F. Restrepo Zambrano, J.C. Arias-G, O. Acevedo, C. Aponte, R. Medina, M. González, S. Rojas, C. Flórez, L.M. Estupinan-Suarez, et al., 2019, A classification system for Colombian wetlands: an essential step forward in open environmental policy-making: Wetlands, v. 39, p. 971–990, https://doi.org/10.1007/s13157-019-01149-8

Rodriguez C., 2004, Isotopic meteoric line for Colombia. Meteorología Colombiana v. 8, p. 43–51.

Ronchail, J., and R. Gallaire, 2006, ENSO and rainfall along the Zongo Valley (Bolivia) from the Altiplano to the Amazon Basin: International Journal of Climatology, v. 26, p. 1223 – 1236, doi: 10.1002/joc.1296

Rozanski K., L. Araguas-Araguas and R. Gonfiantini, 1993, Isotopic patterns in modem global precipitation: In Climate Change in Continental Isotopic Records, eds. P. K. Swart, K. C. Lohman, J. McKenzie and S. Savin, Geophysical Monograph, v. 78, p. 1-36 American Geophysical Union, https://doi.org/10.1029/GM078p0001

Salati. E., A. Dall'Olio, E. Matsui, and J.R. Gat, 1979, Recycling of Water in the Amazon Basin: An Isotopic Study: Water Resources Research, v. 15, n. 5, p. 1250 – 1258, https://doi.org/10.1029/WR015i005p01250

Saylor J. E., A. Mora, B. K. Horton and J. Nie, 2009, Controls on the isotopic composition of surface water and precipitation in the Northern Andes, Colombian Eastern Cordillera: Geochimica et Cosmochimica Acta, v. 73, n. 23, p. 6999 – 7018, https://doi.org/10.1016/j.gca.2009.08.030

Segura, H., J. C. Espinoza, C. Junquas, and K. Takahashi, 2016, Evidencing Decadal and Interdecadal Hydroclimatic Variability over the Central Andes: Environmental Research Letters, v. 11:094016, p. 1 – 8, doi: 10.1088/1748-9326/11/9/094016

Sharma, M.L. and M.W. Hughes, 1985, Groundwater recharge estimation using chloride, deuterium and oxygen-18 profiles in the deep coastal sands of Western Australia: Journal of Hydrology, v. 81, n. 1-2, p. 93-109, https://doi.org/10.1016/0022-1694(85)90169-6

Sierra, J. P., P. A. Arias, and S. C. Vieira, 2015, Precipitation over Northern South America and Its Seasonal Variability as Simulated by the CMIP5 Models: Advances in Meteorology, v. 2015:634720, p. 1 – 22, http://dx.doi.org/10.1155/2015/634720

Simmers, I., 1997, Groundwater recharge principles, problems and developments. In: Ian Simmers, I. Simmers, J.M.H. Hendrickx, G.P. Kruseman and K.R. Rushton, Eds. Recharge of Phreatic Aquifers in (Semi-) Arid Areas, p. 1-18, https://doi.org/10.1201/9780203741191

Springer A.E., E.M. Bold and K.M. Junghans, 2016, Regional Groundwater Flow Delineation from Stable Isotopes at Western North America Springs: Groundwater, v. 55, n. 1, p. 1-10, doi:10.1111/gwat.12442

Staal, A., O. A. Tuinenburg, J.H.C. Bosmans, M. Holmgren, E. H. van Nes, M. Scheffer, D. C. Zemp and S.C. Dekker, 2018, Forest-rainfall cascades buffer against drought across the Amazon: Nature Climate Change, v. 8, p. 539 – 543. https://doi.org/10.1038/s41558-018-0177-y

Swenson H.A., and H.L. Baldwin, 1965, A primer on water quality: Report USGS Unnumbered Series, p. 1-27, https://doi.org/10.3133/7000057

Tirumalesh K., D.A. Sharma, M.S. Rishi, D. Pant, H.V Mohokar, A.K. Jaryal & U.K. Sinha, 2017, Isotope investigation on groundwater recharge and dynamics in shallow and deep alluvial aquifers of southwest Punjab: Applied Radiation and Isotopes, v. 129, p. 163-170, https://doi.org/10.1016/j.apradiso.2017.07.022

Villegas, M. E., S. Bachu, J.C. Ramon, and J.R. Underschultz, 1994, Flow of formation waters in the Cretaceous–Miocene succession of the Llanos Basin, Colombia: AAPG Bulletin, v. 78, n. 12, p. 1843–1862, https://doi.org/10.1306/A25FF319-171B-11D7-8645000102C1865D

Xu N., J. Gong and G. Yang, 2017, Using environmental isotopes along with major hydro-geochemical compositions to assess deep groundwater formation and evolution in eastern coastal China: Journal of Contaminant Hydrology, v. 208, p. 1-9, https://doi.org/10.1016/j.jconhyd.2017.11.003

Yang Y, D.N. Lerner, M.H. Barrett and J.H. Tellam, 1999, Quantification of groundwater recharge in the city of Nottingham, UK. Environmental Geology v. 38, n.3, p. 183 – 198, https://doi.org/10.1007/s002540050414

Zabala, M.E., M. Manzano, and L. Vives, 2015, The origin of groundwater composition in the Pampeano Aquifer underlying the Del Azul Creek basin, Argentina. Science of the Total Environment, v. 518–519, p. 168–188, https://doi.org/10.1016/j.scitotenv.2015.02.065

Zemp, D. C., C. F. Schleussner, H. M. J. Barbosa, R. J. van der Ent, J. F. Donges, J. Heink, G. Sampaio and A. Rammig, 2014, On the importance of cascading moisture recycling in South America: Atmospheric Chemistry and Physics, v. 14, p. 13337 – 13359, doi: 10.5194/acp-14-13337-2014

Zemp, D. C., C. F. Schleussner, H. M. Barbosa, M. Hirota, V. Montade, G. Sampaio, A. Staal, L. Wang-Erlandsson and A. Rammig, 2017, Self-amplified Amazon forest loss due to vegetation-atmosphere feedbacks: Nature Communications, v. 8:14681, p. 1 – 10, doi: 10.1038/ncomms14681

**Table 1**. $\delta^{18}O$ and δD compositions of meteoric water samples for dry and rainy season (n = 162) and IAEA-GNIP (station average). For IAEA-GNIP is reported the mean of multiyear database for each station. For analysis were used n =1011 stable isotope compositions. (Colombia: 33 stations, Brasil: 2 stations, Ecuador: 1 station and Peru: 1 Station)

| Sample ID | Lat (N) | Long (W) | Sample Elevation (m) | $\delta^{18}O$ (‰ VSMOW) | | δD (‰ VSMOW) | | d-excess (‰ VSMOW) | | Location |
|---|---|---|---|---|---|---|---|---|---|---|
| | | | | Dry | Rainy | Dry | Rainy | Dry | Rainy | |
| IE-001 | 1.7417 | 75.6376 | 691 | - | -7.34 | - | -43.7 | - | 15.02 | Hacha River, Florencia City (Caquetá) |
| IE-002 | 1.4986 | 75.7252 | 267 | - | -6.88 | - | -39.8 | - | 15.24 | Bodoquero River, Florencia-Morelia Road (Caquetá) |
| IE-003 | 1.4270 | 75.8713 | 304 | - | -6.76 | - | -39.8 | - | 14.28 | Pescado River, Belen de los Andaquíes Town (Caquetá) |
| IE-004 | 1.3279 | 75.9745 | 380 | - | -6.99 | - | -39.9 | - | 16.02 | Fragua-Chorroso River, San José de Fragua Town (Caquetá) |
| IE-005 | 1.0726 | 75.9934 | 244 | - | -7.37 | - | -43.2 | - | 15.76 | Caquetá River, Curillo City (Caquetá) |
| IE-006 | 1.1963 | 75.6993 | 240 | - | -6.7 | - | -38.3 | - | 15.30 | Pescado River, Valparaiso City (Caquetá) |
| IE-007 | 1.5632 | 75.5293 | 261 | - | -7.16 | - | -41.1 | - | 16.18 | Orteguaza River, Florencia City (Caquetá) |
| IE-008 | 1.8269 | 75.2276 | 309 | - | -6.96 | - | -39.1 | - | 16.58 | Esmeraldas River, Paujil-Puerto Rico Road (Caquetá) |
| IE-009 | 1.9309 | 75.1572 | 283 | - | -7.08 | - | -41.8 | - | 14.84 | Guayas River, Puerto Rico City (Caquetá) |
| IE-010 | 2.5222 | 74.7544 | 563 | - | -6.88 | - | -40.1 | - | 14.94 | Perlas River, San Vicente del Caguán City (Caquetá) |
| IE-011 | 2.1825 | 74.7774 | 284 | - | -6.95 | - | -40.9 | - | 14.70 | Caguán River, San Vicente del Caguán City (Caquetá) |
| IE-012 | 2.2411 | 74.4521 | 304 | - | -6.09 | - | -35.4 | - | 13.32 | Lozada River, San Juan de Lozada Town (Caquetá) |
| IE-013 | 2.5683 | 74.1863 | 303 | - | -6.96 | - | -40.4 | - | 15.28 | Guayabero River, San Juan de Lozada-La Julia Road (Meta) |
| IE-014 | 2.6597 | 74.2304 | 365 | - | -6.62 | - | -39.5 | - | 13.46 | Cafre Creek, Tinigua National Park (Meta) |
| IE-015 | 2.9340 | 74.1746 | 380 | -6.42 | -7.18 | -38.4 | -43.0 | 12.96 | 14.44 | Santo Domingo River, San Isidro-Santo Domingo Road (Meta) |
| IE-016 | 3.3705 | 74.0291 | 514 | -6.69 | -7.91 | -38.2 | -47.3 | 15.32 | 15.98 | Lucía River, Limón Bridge, Granada-La Macarena Road (Meta) |
| IE-018 | 3.3413 | 73.9415 | 426 | -5.61 | -7.18 | -29.9 | -44.1 | 14.98 | 13.34 | Guejar River, La Recebera-San Juan de Arama (Meta) |
| IE-019 | 3.4963 | 74.0647 | 737 | -5.8 | -7.25 | -31.7 | -42.7 | 14.70 | 15.30 | Guejar River, Guejar Pools (Meta) |
| IE-020 | 3.5778 | 74.0609 | 823 | -8.07 | -9.56 | -49.4 | -60.5 | 15.16 | 15.98 | Guape River, Fallen Bridge- Lejanías (Meta) |
| IE-021 | 4.5723 | 72.9607 | 234 | -8.44 | -8.25 | -52.6 | -50.4 | 14.92 | 15.60 | Upía River, Barranca de Upia Town, (Meta) |

| Sample ID | Lat (N) | Long (W) | Sample Elevation (m) | $\delta^{18}O$ (‰ VSMOW) | | δD (‰ VSMOW) | | d-excess (‰ VSMOW) | | Location |
|---|---|---|---|---|---|---|---|---|---|---|
| | | | | Dry | Rainy | Dry | Rainy | Dry | Rainy | |
| IE-022 | 4.4917 | 73.1057 | 233 | -5.14 | -5.53 | -32.3 | -29.4 | 8.82 | 14.84 | Cabuyarito River, Barranca de Upia-Paratebueno Road (Meta) |
| IE-023 | 4.4413 | 73.1710 | 266 | -5.23 | -6.14 | -32.9 | -35.6 | 8.94 | 13.52 | Rayo Creek, Barranca de Upia-Paratebueno Road (Meta) |
| IE-024 | 4.3910 | 73.2923 | 300 | -6.44 | -7.15 | -37.2 | -41.7 | 14.32 | 15.50 | Humea River, Paratebueno-Cumaral Road (Cundinamarca) |
| IE-025 | 4.2841 | 73.4827 | 419 | -6.63 | -8 | -37.7 | -47.8 | 15.34 | 16.20 | Guacavía River, Cumaral City (Meta-Cundinamarca Boundary) |
| IE-026 | 4.2673 | 73.5459 | 471 | -6.17 | -6.9 | -35.6 | -40.7 | 13.76 | 14.50 | Caney River, Cumaral-Restrepo Road (Meta) |
| IE-027 | 4.2627 | 73.5707 | 516 | -6.02 | -7 | -34.5 | -40.8 | 13.66 | 15.20 | Upin River, Restrepo City (Meta) |
| IE-029 | 4.1769 | 73.6378 | 471 | -7.6 | -8.56 | -46.6 | -53.8 | 14.20 | 14.68 | Guatiquía River, Villavicencio City (Meta) |
| IE-030 | 4.0818 | 73.7058 | 509 | -6.36 | -6.79 | -37.2 | -38.8 | 13.68 | 15.52 | Ocoa River, Villavicencio-Acacias Road (Meta) |
| IE-031 | 4.0514 | 73.7647 | 554 | -7.37 | -9.1 | -43.7 | -56.7 | 15.26 | 16.10 | Guayuriba River, Villavicencio-Acacías Road (Brigde)-(Meta) |
| IE-032 | 4.0201 | 73.7762 | 560 | -6.25 | -7.43 | -33.9 | -43.0 | 16.10 | 16.44 | Sardinata River, Villavicencio-Acacías Road (Meta) |
| IE-033 | 3.9593 | 73.7827 | 570 | -5.87 | -6.94 | -32.2 | -39.2 | 14.76 | 16.32 | Acacías River, Acacías City (Meta) |
| IE-034 | 3.9304 | 73.7679 | 554 | -5.96 | -6.96 | -33.4 | -39.7 | 14.28 | 15.98 | Orotoy River, Acacías-Guamal Road (Meta) |
| IE-036 | 3.8139 | 73.7517 | 466 | -5.93 | -6.8 | -33.9 | -38.9 | 13.54 | 15.50 | Humadea River, Guamal-San Martín Road (Meta) |
| IE-037 | 3.7940 | 73.8987 | 663 | -6.15 | -7.35 | -33.3 | -41.9 | 15.90 | 16.90 | Aguas Claras Creek, Cubarral-Angosturas Road (Meta) |
| IE-040 | 3.7932 | 73.9237 | 683 | -7.4 | -9.07 | -42.9 | -55.9 | 16.30 | 16.66 | Ariari River, Angosturas-Cubarral Road (Meta) |
| IE-041 | 3.1054 | 73.7765 | 259 | -6.16 | -6.24 | -35.3 | -37.9 | 13.98 | 12.02 | Guejar River, Vista Hermosa Town-Macarena Range (Meta) |
| IE-042 | 3.0818 | 73.7937 | 277 | -6.18 | -6.5 | -35.8 | -37.6 | 13.64 | 14.40 | Blanco Creek, Vista Hermosa-Maracaibo Road-Macarena Range (Meta) |
| IE-043 | 3.0443 | 73.8270 | 284 | -6.22 | -6.75 | -36.2 | -39.6 | 13.56 | 14.40 | Guapaya River, Vista Hermosa-Maracaibo Road-Macarena Range (Meta) |
| IE-044 | 3.0191 | 73.8411 | 293 | -6.32 | -6.93 | -36.4 | -41.0 | 14.16 | 14.44 | Sardinata Creek, Vista Hermosa-Maracaibo Road-Macarena Range (Meta) |
| IE-045 | 3.0258 | 73.8673 | 406 | -6.52 | -6.92 | -38 | -39.8 | 14.16 | 15.56 | Borrascosas Creek, Borrascosas-Maracaibo-Macarena Range (Meta) |
| IE-046 | 2.9555 | 73.8286 | 307 | -6.01 | -6.78 | -34.5 | -39.0 | 13.58 | 15.24 | Guio Creek, Maracaibo-Santo Domingo Road-Macarena Range (Meta) |

| Sample ID | Lat (N) | Long (W) | Sample Elevation (m) | $\delta^{18}O$ (‰ VSMOW) | | δD (‰ VSMOW) | | d-excess (‰ VSMOW) | | Location |
|---|---|---|---|---|---|---|---|---|---|---|
| | | | | Dry | Rainy | Dry | Rainy | Dry | Rainy | |
| IE-047 | 2.8520 | 73.8182 | 401 | -6.34 | -6.98 | -35.1 | -40.6 | 15.62 | 15.24 | Cafre Creek, Santo Domingo Town-Macarena Range (Meta) |
| IE-048 | 2.8767 | 73.8072 | 285 | -6.31 | -6.8 | -35.3 | -39.5 | 15.18 | 14.90 | Rojo Creek, Santo Domingo Town-Macarena Range (Meta) |
| IE-049 | 2.9124 | 73.8272 | 297 | -6.4 | -6.89 | -36.2 | -39.9 | 15.00 | 15.22 | Tubo Creek, Santo Domingo Town-Macarena Range (Meta) |
| IE-050 | 2.9895 | 73.8361 | 296 | -6.53 | -7.22 | -37.6 | -42.5 | 14.64 | 15.26 | Fisto Creek, Maracaibo-Santo Domingo Road-Macarena Range (Meta) |
| IE-051 | 2.9933 | 73.8372 | 289 | -6.32 | -7.08 | -35.7 | -41.3 | 14.86 | 15.34 | Unión Creek, Maracaibo-Santo Domingo Road-Macarena Range (Meta) |
| IE-052 | 2.4537 | 72.7549 | 260 | -5.68 | -5.61 | -32 | -31.5 | 13.44 | 13.38 | Yamu Creek, Nueva Tolima-Lindosa Range-San José del Guaviare-(Guaviare) |
| IE-054 | 2.5073 | 72.6408 | 221 | -2.83 | -5.39 | -18 | -31.7 | 4.64 | 11.42 | Lindosa Creek, Lindosa Range-San José del Guaviare-(Guaviare) |
| IE-055 | 2.5355 | 72.6864 | 206 | -5.94 | -5.28 | -35.1 | -30.1 | 12.42 | 12.14 | La María Creek, San José del Guaviare City (Guaviare) |
| IE-056 | 2.5689 | 72.7506 | 198 | -5.44 | -6.58 | -29.1 | -39.1 | 14.42 | 13.54 | Guaviare River, Nowey Bridge-San José del Guaviare-Villavicencio Road (Guaviare-Meta Boundary) |
| IE-057 | 2.5797 | 72.8662 | 199 | -5.56 | -6.52 | -30.2 | -38.6 | 14.28 | 13.56 | Guayabero River-Raudal of Guayabero-Lindosa Range (Guaviare) |
| IE-058 | 2.6215 | 72.7634 | 203 | -6.41 | -6.68 | -36.8 | -41.1 | 14.48 | 12.34 | Ariari River, Puerto Concordia Town (Meta) |
| IE-059 | 3.6934 | 73.7029 | 432 | -6.16 | -5.95 | -37.2 | -36.4 | 12.08 | 11.20 | Camoa Creek, San Martín Town (Meta) |
| IE-060 | 3.6487 | 73.7048 | 403 | -5.64 | -6.19 | -34 | -37.3 | 11.12 | 12.22 | Iraca Creek, San Martín-Granada Road (Meta) |
| IE-061 | 3.5021 | 73.7303 | 321 | -7.25 | -8.4 | -41.9 | -53.2 | 16.10 | 14.00 | Ariari River, Granada City (Meta) |
| IE-062 | 3.4909 | 73.7369 | 324 | -8.19 | -8.94 | -50.9 | -57.9 | 14.62 | 13.62 | Guape River, Granada (Meta) |
| IE-063 | 3.3867 | 73.9067 | 491 | -3.2 | -6.07 | -20.4 | -37.2 | 5.20 | 11.36 | Piedras Creek, Granada- Mesetas Road (Meta) |
| IE-065 | 3.3749 | 73.9494 | 500 | -4.16 | -6.23 | -24.5 | -37.1 | 8.78 | 12.74 | Curia Creek, Granada- Mesetas Road (Meta) |
| IE-066 | 3.3603 | 73.9754 | 490 | -2.07 | -6.15 | -13.6 | -38.0 | 2.96 | 11.20 | La Lajosa Creek, Granada- Mesetas Road (Meta) |
| IE-067 | 3.3539 | 74.0440 | 529 | -6.77 | -7.48 | -38.9 | -45.5 | 15.26 | 14.34 | Cafre River, Mesetas - Uribe Road (Meta) |
| IE-069 | 3.2814 | 74.1621 | 720 | -5.94 | -6.8 | -33.7 | -40.7 | 13.82 | 13.70 | Las Peñas Creek, Jardín de las Peñas, Mesetas-Uribe Road (Meta) |

| Sample ID | Lat (N) | Long (W) | Sample Elevation (m) | $\delta^{18}O$ (‰ VSMOW) | | δD (‰ VSMOW) | | d-excess (‰ VSMOW) | | Location |
|---|---|---|---|---|---|---|---|---|---|---|
| | | | | Dry | Rainy | Dry | Rainy | Dry | Rainy | |
| IE-070 | 3.2685 | 74.2061 | 796 | -4.93 | -6.71 | -28.5 | -40.6 | 10.94 | 13.08 | Cuncia Creek, Mesetas - Uribe Road (Meta) |
| IE-071 | 3.2585 | 74.2294 | 750 | -3.98 | -6.66 | -23.2 | -39.6 | 8.64 | 13.68 | Guapo Creek, Mesetas - Uribe Road (Meta) |
| IE-072 | 3.2587 | 74.2529 | 662 | -5.78 | -6.66 | -33.5 | -40.1 | 12.74 | 13.18 | Pailas Creek, Mesetas-Uribe Road (Meta) |
| IE-073 | 3.2477 | 74.2664 | 605 | -7.55 | -7.93 | -45.9 | -49.0 | 14.50 | 14.44 | Guape River, Mesetas-Uribe Road (Meta) |
| IE-074 | 3.2270 | 74.2827 | 579 | -5.73 | -6.63 | -32.6 | -38.7 | 13.24 | 14.34 | La Dusana Creek, Mesetas - Uribe (Road) |
| IE-075 | 3.2352 | 74.3589 | 645 | -7.95 | -8.38 | -49.5 | -51.7 | 14.10 | 15.34 | Duda River, La Uribe Town (Meta) |
| IE-076 | 4.0600 | 73.0528 | 195 | -4.6 | -5.36 | -30.8 | -28.0 | 6.00 | 14.88 | Black River, Pachaquiaro - Puerto López Road (Meta) |
| IE-077 | 4.0738 | 72.9877 | 190 | -5.71 | -4.99 | -35.9 | -27.1 | 9.78 | 12.82 | La Venturosa Creek, Pachaquiaro - Puerto López Road (Meta) |
| IE-078 | 4.1007 | 72.9374 | 184 | -6.02 | -6.67 | -37.4 | -38.8 | 10.76 | 14.56 | Meta River, Puerto López City (Meta) |
| IE-079 | 4.2150 | 72.5020 | 201 | -6.06 | -5.11 | -37 | -30.0 | 11.48 | 10.88 | La Bonga Creek, Puerto López - Puerto Gaitán Road (Meta) |
| IE-080 | 4.3463 | 72.1907 | 159 | -5.56 | -5.04 | -35 | -27.5 | 9.48 | 12.82 | Palenque-1 Creek, Puerto López - Puerto Gaitán Road (Meta) |
| IE-082 | 4.3405 | 72.1563 | 149 | -5.49 | -5.6 | -34 | -31.1 | 9.92 | 13.70 | Yucao River, Puerto López - Puerto Gaitán Road (Meta) |
| IE-083 | 4.3131 | 72.0754 | 156 | -4.35 | -5.49 | -27.6 | -30.0 | 7.20 | 13.92 | Manacarías River, Puerto Gaitán City (Meta) |
| IE-084 | 4.2626 | 72.7776 | 175 | -5.92 | -6.87 | -35.2 | -40.8 | 12.16 | 14.16 | Meta River, Cabuyaro Road (Meta) |
| IE-087 | 4.0680 | 73.7114 | 496 | -6.28 | -6.24 | -36.3 | -34.5 | 13.94 | 15.42 | Aguas Claras Creek, Villavicencio - Acacías Road (Meta) |
| IE-088 | 4.0521 | 73.7297 | 513 | -6.2 | -6.53 | -35.9 | -37.0 | 13.70 | 15.24 | Coburgo Creek, Villavicencio - Acacías Road (Meta) |
| IE-089 | 4.0504 | 73.7644 | 559 | -6.67 | -6.92 | -38.5 | -39.1 | 14.86 | 16.26 | Spring, Villavicencio - Acacías Road (Meta) |
| IE-090 | 4.0647 | 73.7899 | 799 | -5.62 | - | -31.4 | - | 13.56 | - | Bavaria Creek, Panamá Path (Meta) |
| IE-091 | 4.0712 | 73.7860 | 849 | -6.05 | -6.89 | -34.6 | -38.2 | 13.80 | 16.92 | Sagu Road Creek, Panamá Path (Meta) |
| IE-092 | 4.0777 | 73.7842 | 819 | -6.34 | -7.17 | -35 | -39.9 | 15.72 | 17.46 | Sagu Creek, Panamá Path (Meta) |
| IE-093 | 4.0316 | 73.7771 | 574 | -5.09 | -6.8 | -27.4 | -39.3 | 13.32 | 15.10 | Chupado Creek, Ladrillera Road, La Pradera Path (Meta) |
| IE-094 | 2.4293 | 72.6728 | 232 | -5.81 | - | -33.2 | - | 13.28 | - | Lindosa-1 Creek, Nueva Tolima-San José del Guaviare Road (Guaviare) |
| IE-095 | 2.4408 | 72.6834 | 244 | -6.17 | - | -34.9 | - | 14.46 | - | Lindosa-2 Creek, Nueva Tolima-San José del Guaviare Road (Guaviare) |

| Sample ID | Lat (N) | Long (W) | Sample Elevation (m) | $\delta^{18}O$ (‰ VSMOW) | | δD (‰ VSMOW) | | d-excess (‰ VSMOW) | | Location |
|---|---|---|---|---|---|---|---|---|---|---|
| | | | | Dry | Rainy | Dry | Rainy | Dry | Rainy | |
| IE-096 | 2.4425 | 72.6867 | 246 | -6.04 | - | -33.8 | - | 14.52 | - | Lindosa-3 Creek, Nueva Tolima-San José del Guaviare Road (Guaviare) |
| IE-097 | 2.5449 | 72.7098 | 215 | -5.59 | - | -33.1 | - | 11.62 | - | Retiro Creek, San José del Guaviare - Granada Road (Meta) |
| IE-098 | 3.3043 | 73.3617 | 249 | -1.99 | - | -13.1 | - | 2.82 | - | Lomalinda Lake, San José del Guaviare - Granada Road (Meta) |
| IE-099 | 3.5321 | 74.0201 | 685 | -7.98 | - | -48 | - | 15.84 | - | Guape River, Bridge-Lejanías (Meta) |
| IE-100 | 3.3704 | 74.0281 | 511 | -5.3 | - | -27.6 | - | 14.80 | - | Guejar River, Limón Bridge, Granada-La Macarena Road (Meta) |
| IE-101 | 3.2404 | 74.3555 | 724 | -2.73 | - | -5.9 | - | 15.94 | - | Precipitation Sample, Uribe Town (Meta) |
| IE-102 | 2.9917 | 74.2102 | 416 | -7.45 | - | -44.9 | - | 14.70 | - | Duda River, La Julia Town (Meta) |
| IE-103 | 4.3532 | 72.1798 | 161 | -5.45 | - | -33.7 | - | 9.90 | - | Palenque-2 Creek, Puerto López - Puerto Gaitán Road (Meta) |
| IE-104 | 4.1161 | 72.0447 | 222 | -5.81 | - | -34.2 | - | 12.28 | - | Spring-1 - Manacacías High - Rubiales Road El Palmar Farm (Meta) |
| IE-105 | 4.1163 | 72.0455 | 204 | -6.23 | - | -38 | - | 11.84 | - | Spring-2 - Manacacías High - Rubiales Road El Palmar Farm (Meta) |
| IE-106 | 3.8786 | 71.9136 | 175 | -3.97 | - | -25.7 | - | 6.06 | - | Planas River, Rubiales Road (Meta) |

| Sample ID | Lat (N) | Long (W) | Sample Elevation (m) | δ18O (‰ VSMOW) | δD (‰ VSMOW) | d-excess (‰ VSMOW) | Location |
|---|---|---|---|---|---|---|---|
| IAEA-1 | 3.4405 | 76.0017 | 3000 | -10.55 | -75.27 | 9.16 | Albania IAEA GNIP Station- Tolima (2003-2004) |
| IAEA-2 | 10.8800 | 74.7800 | 14 | -4.64 | -30.26 | 6.86 | Barranquilla IAEA GNIP Station (1971 - 1990) |
| IAEA-3 | 7.1894 | 72.8717 | 3307 | -10.27 | -70.06 | 12.10 | Belin IAEA GNIP Station- Santander (2005-2007) |
| IAEA-4 | 4.7000 | 74.1300 | 2547 | -9.15 | -62.9 | 10.30 | Bogotá IAEA GNIP Station-Bogotá (1971-2016) |
| IAEA-5 | 7.1333 | 73.1833 | 1189 | -6.59 | -42.51 | 10.21 | Bucaramanga Airport IAEA GNIP Station- Santander (2004-2005) |
| IAEA-6 | 11.2194 | 72.3633 | 118 | -4.55 | -27.11 | 9.29 | Carraipía IAEA GNIP Station-Guajira (2002-2003) |
| IAEA-7 | 4.5755 | 74.1665 | 2665 | -9.49 | -64.21 | 11.71 | Casa Blanca IAEA GNIP Station-Bogotá (1998-1999) |

| Sample ID | Lat (N) | Long (W) | Sample Elevation (m) | $\delta^{18}O$ (‰ VSMOW) | | δD (‰ VSMOW) | | d-excess (‰ VSMOW) | | Location |
|---|---|---|---|---|---|---|---|---|---|---|
| | | | | Dry | Rainy | Dry | Rainy | Dry | Rainy | |
| IAEA-8 | 4.9128 | 73.8934 | 2800 | -10.56 | | -69.02 | | 15.46 | | El Angulo IAEA GNIP Station-Bogotá (1999) |
| IAEA-9 | 4.6182 | 74.1284 | 3000 | -10.15 | | -67.45 | | 13.75 | | El Delirio IAEA GNIP Station-Bogotá (1998-1999) |
| IAEA-10 | 4.5014 | 74.2909 | 3150 | -10.87 | | -74.4 | | 12.56 | | El Hato IAEA GNIP Station-Bogotá (1998-1999) |
| IAEA-11 | 7.1128 | 72.9697 | - | -11.06 | | -75.2 | | 13.28 | | El Picacho IAEA GNIP Station-Santader (2005-2007) |
| IAEA-12 | 5.1796 | 74.0052 | 3140 | -9.58 | | -63.45 | | 13.19 | | El Salitre IAEA GNIP Station- Bogotá (1999) |
| IAEA-13 | 9.3571 | 75.2892 | 198 | -4.98 | | -31.67 | | 8.17 | | El Tesoro (Formerly Corozal) IAEA GNIP Station-Sucre (2005-2016) |
| IAEA-14 | 4.6533 | 74.0989 | 3250 | -10.48 | | -68.77 | | 15.07 | | El Verjón IAEA GNIP Station-Bogotá (1998-1999) |
| IAEA-15 | 7.1447 | 73.1250 | 1025 | -6.53 | | -41.54 | | 10.7 | | IDEAM IAEA GNIP Station-Santander (2004-2005) |
| IAEA-16 | 7.2083 | 72.9381 | 2660 | -8.57 | | -57.3 | | 11.26 | | La Casita IAEA GNIP Station-Santander (2004-2006) |
| IAEA-17 | 7.1256 | 73.0600 | 1848 | -7.43 | | -47.12 | | 12.32 | | La Galvicia IAEA GNIP Station-Santander (2005-2007) |
| IAEA-18 | 3.3014 | 76.0804 | 2100 | -9.79 | | -67.81 | | 10.51 | | La María IAEA GNIP Station-Valle del Cauca (2003-2004) |
| IAEA-19 | 7.1256 | 73.0103 | - | -8.69 | | -56.76 | | 12.76 | | La Mariana IAEA GNIP Station-Santander (2005-2007) |
| IAEA-20 | 5.0053 | 74.1382 | 2703 | -7.41 | | -46.64 | | 12.64 | | La Pradera IAEA GNIP Station-Bogotá (1999) |
| IAEA-21 | 3.3060 | 76.0700 | 2605 | -10.06 | | -69.09 | | 11.39 | | La Sirena IAEA GNIP Station-Valle del Cauca (2003-2004) |
| IAEA-22 | 4.4692 | 74.3696 | 3780 | -11.98 | | -81.02 | | 14.82 | | Los Tunjos IAEA GNIP Station - Bogotá (1998-1999) |
| IAEA-23 | 11.3726 | 72.2474 | 45 | -5.1 | | -32.24 | | 8.56 | | Maicao IAEA GNIP Station-Guajira (2002-2004) |
| IAEA-24 | 9.5450 | 75.2203 | 225 | -6.27 | | -43.68 | | 6.48 | | Ovejas IAEA GNIP Station-Sucre (2002-2003) |
| IAEA-25 | 7.0000 | 73.0833 | 1000 | -7.21 | | -47.17 | | 10.51 | | Piedecuesta IAEA GNIP Station-Santander (2004-2006) |
| IAEA-26 | 3.3300 | 76.1300 | 1170 | -9.23 | | -65.95 | | 7.89 | | Planta Nima IAEA GNIP Station-Valle del Cauca (2003-2004) |
| IAEA-27 | 7.1022 | 73.0694 | 1532 | -8.21 | | -54.22 | | 11.46 | | San Antonio IAEA GNIP Station-Santander (2005-2007) |
| IAEA-28 | 4.6938 | 74.0286 | 2647 | -7.83 | | -56.62 | | 6.02 | | Santa Ana IAEA GNIP Station-Bogotá (1999) |
| IAEA-29 | 7.2042 | 72.9314 | 2869 | -9.3 | | -62.05 | | 12.35 | | Tembladal IAEA GNIP Station-Santander (2004-2005) |
| IAEA-30 | 3.3060 | 76.1000 | 1550 | -9.22 | | -64.95 | | 8.81 | | Tenjo IAEA GNIP Stationd-Valle del Cauca (2003-2004) |
| IAEA-31 | 4.9788 | 73.9656 | 2698 | -8.97 | | -61.4 | | 10.36 | | Tibitoc IAEA GNIP Station-Bogotá (1999) |
| IAEA-32 | 7.1986 | 72.9739 | 2660 | -8.21 | | -54.06 | | 11.62 | | Tona IAEA GNIP Station-Santander (2005-2007) |
| IAEA-33 | 7.7899 | 76.6508 | 30 | -5.45 | | -33.49 | | 10.11 | | Tulenapa IAEA GNIP Station-Antioquia (2013-2016) |

| Sample ID | Lat (N) | Long (W) | Sample Elevation (m) | $\delta^{18}O$ (‰ VSMOW) | | δD (‰ VSMOW) | | d-excess (‰ VSMOW) | | Location |
|---|---|---|---|---|---|---|---|---|---|---|
| | | | | Dry | Rainy | Dry | Rainy | Dry | Rainy | |
| IAEA-34 | 0.6167 | 69.2000 | 123 | -4.88 | | -26.93 | | 12.11 | | Lauarete IAEA GNIP Station-Brazil (1972-1973) |
| IAEA-35 | 4.3800 | 69.9800 | 65 | -6.49 | | -38.3 | | 13.62 | | Benjamin Constant IAEA GNIP Station-Brazil (1990) |
| IAEA-36 | 0.0833 | 76.8667 | 297 | -5.36 | | -30.62 | | 12.26 | | Lago Agrio IAEA GNIP Station-Ecuador (1992-1996) |
| IAEA-37 | 3.8240 | 73.3774 | 98 | -5.94 | | -36.89 | | 10.63 | | Puerto Almendras IAEA GNIP Station-Peru (2006-2012) |

**Table 2**. $\delta^{18}O$ and $\delta D$ compositions of groundwater samples from five (5) oil fields of the southern Llanos basin (n = 109). Prefix F1, F2, F3, F4 and F5 indicate the number of Field from map showed in **Figure-1**. Prefix EW: Exploratory Well.

| Sample ID | Lat (N) | Long (W) | Formation | Depth (TVDSS) (Km) | $\delta^{18}O$ (‰VSMOW) | $\delta D$ (‰VSMOW) | d-excess (‰VSMOW) |
|---|---|---|---|---|---|---|---|
| F1-1 | 3.5860 | 73.6647 | Barco, Mirador, Guadalupe, Une | -2.02 | -7.62 | -43.6 | 17.36 |
| F1-2 | 3.9773 | 73.6423 | Barco, Mirador | -2.01 | -7.39 | -46 | 13.12 |
| F1-3 | 3.9640 | 73.6562 | Guadalupe, Une | -2.11 | -7.58 | -46.7 | 13.94 |
| F1-4 | 3.9669 | 73.6578 | Barco, Mirador | -2.00 | -7.08 | -39.7 | 16.94 |
| F1-5 | 3.9731 | 73.6722 | Barco, Mirador | -2.06 | -7.04 | -39.8 | 16.52 |
| F1-6 | 3.9500 | 73.6724 | Guadalupe, Une | -2.04 | -7.69 | -43.8 | 17.72 |
| F1-7 | 3.9733 | 73.6678 | Barco, Mirador | -2.04 | -7.35 | -43.2 | 15.60 |
| F1-8 | 3.9774 | 73.6423 | Barco, Mirador | -2.09 | -7.48 | -43.5 | 16.34 |
| F1-9 | 3.9673 | 73.6434 | Barco, Mirador | -1.99 | -7.37 | -43.4 | 15.56 |
| F1-10 | 3.9834 | 73.6510 | Barco, Mirador | -2.11 | -7.48 | -43.8 | 16.04 |
| F1-11 | 3.9330 | 73.6844 | Guadalupe, Une | -2.03 | -7.6 | -45 | 15.80 |
| F1-12 | 3.9263 | 73.7245 | Guadalupe, Une | -2.11 | -7.37 | -43.4 | 15.56 |
| F1-13 | 3.9170 | 73.7356 | Barco, Mirador | -2.09 | -7.36 | -43.5 | 15.38 |
| F1-14 | 3.9045 | 73.7514 | Barco, Mirador | -2.18 | -7.45 | -43.3 | 16.30 |
| F1-15 | 3.9410 | 73.6789 | Guadalupe, Une | -2.06 | -7.67 | -44.7 | 16.66 |
| F1-16 | 3.9520 | 73.6690 | Barco, Mirador | -1.89 | -7.44 | -42.9 | 16.62 |
| F1-17 | 3.9674 | 73.6696 | Guadalupe, Une | -2.10 | -7.5 | -42.9 | 17.10 |
| F1-18 | 3.9665 | 73.6577 | Une | -2.21 | -8.18 | -52.9 | 12.54 |
| F1-19 | 3.9640 | 73.6562 | Guadalupe, Une | -2.11 | -8.09 | -51.3 | 13.42 |
| F1-20 | 3.9355 | 73.6825 | Barco, Mirador | -2.02 | -7.73 | -47.4 | 14.44 |
| F1-21 | 3.9500 | 73.6724 | Guadalupe, Une | -2.04 | -7.25 | -45.1 | 12.90 |
| F1-22 | 3.9376 | 73.6808 | Guadalupe | -2.02 | -7.06 | -42.4 | 14.08 |
| F1-23 | 3.9774 | 73.6423 | Barco, Mirador | -2.09 | -6.87 | -41.3 | 13.66 |
| F1-24 | 3.9170 | 73.7356 | Barco, Mirador | -2.09 | -6.64 | -40.8 | 12.32 |
| F1-25 | 3.9732 | 73.6723 | Barco, Mirador | -2.05 | -6.61 | -40.1 | 12.78 |
| F1-26 | 3.9670 | 73.6578 | Une | -2.21 | -6.59 | -40 | 12.72 |
| F1-27 | 3.9673 | 73.6697 | Barco, Mirador | -2.00 | -6.55 | -39.4 | 13.00 |
| F1-28 | 3.9326 | 73.6934 | Une | -2.21 | -6.38 | -39.2 | 11.84 |
| F1-29 | 3.9673 | 73.6434 | Barco, Mirador | -1.99 | -7.64 | -46.4 | 14.72 |
| F1-30 | 3.9045 | 73.7514 | Barco, Mirador | -2.18 | -7.68 | -46.6 | 14.84 |
| F1-31 | 3.9170 | 73.7356 | Barco, Mirador | -2.09 | -7.66 | -46.5 | 14.78 |
| F1-32 | 3.9410 | 73.6789 | Guadalupe, Une | -2.06 | -7.87 | -46.7 | 16.26 |
| F1-33 | 3.9733 | 73.6678 | Barco, Mirador | -2.04 | -7.72 | -46.9 | 14.86 |
| F1-34 | 3.9640 | 73.6562 | Guadalupe, Une | -2.11 | -7.76 | -46.8 | 15.28 |
| F1-35 | 3.9669 | 73.6578 | Barco, Mirador | -2.00 | -7.81 | -46.6 | 15.88 |
| F1-36 | 3.5860 | 73.6647 | Barco, Mirador, Guadalupe, Une | -2.02 | -7.82 | -46.6 | 15.96 |
| F1-37 | 3.9774 | 73.6423 | Barco, Mirador | -2.09 | -7.84 | -46.4 | 16.32 |

| Sample ID | Lat (N) | Long (W) | Formation | Depth (TVDSS) (Km) | $\delta^{18}O$ (‰VSMOW) | δD (‰VSMOW) | d-excess (‰VSMOW) |
|---|---|---|---|---|---|---|---|
| F1-38 | 3.9500 | 73.6724 | Guadalupe, Une | -2.04 | -7.84 | -46.5 | 16.22 |
| F1-39 | 3.9773 | 73.6423 | Barco, Mirador | -2.01 | -7.84 | -46.3 | 16.42 |
| F1-40 | 3.9263 | 73.7245 | Barco, Mirador | -2.11 | -7.77 | -46.9 | 15.26 |
| F1-41 | 3.9674 | 73.6696 | Guadalupe, Une | -2.10 | -7.78 | -46.7 | 15.54 |
| F1-42 | 3.9731 | 73.6722 | Barco, Mirador | -2.06 | -7.8 | -46.7 | 15.70 |
| F1-43 | 3.9330 | 73.6844 | Guadalupe, Une | -2.03 | -7.69 | -46.4 | 15.12 |
| F1-44 | 3.9520 | 73.6690 | Barco, Mirador | -1.89 | -7.79 | -46.3 | 16.02 |
| F1-45 | 3.9834 | 73.6510 | Barco, Mirador | -2.11 | -7.65 | -46.5 | 14.7 |
| F2-1 | 3.9521 | 73.7200 | Barco, Mirador | -2.16 | -6.15 | -38.5 | 10.70 |
| F2-2 | 3.9517 | 73.7201 | Barco, Mirador | -2.20 | -6.16 | -38.6 | 10.68 |
| F2-3 | 3.9368 | 73.7383 | Barco, Mirador | -2.20 | -6.62 | -33.8 | 19.16 |
| F2-4 | 3.9791 | 73.6808 | Barco, Mirador | -2.12 | -6.87 | -40.9 | 14.06 |
| F2-5 | 3.9793 | 73.6807 | Barco, Mirador | -2.26 | -6.06 | -37 | 11.48 |
| F3-1 | 3.8429 | 73.6541 | Guadalupe | -1.55 | -7.4 | -44.4 | 14.80 |
| F3-2 | 3.8463 | 73.6593 | Guadalupe | -1.58 | -7.5 | -46.3 | 13.70 |
| F3-3 | 3.8217 | 73.6803 | Guadalupe | -1.61 | -5.9 | -34.8 | 12.40 |
| F3-4 | 3.8228 | 73.6715 | Guadalupe | -1.63 | -7.4 | -45.6 | 13.60 |
| F3-5 | 3.8328 | 73.6495 | Guadalupe | -1.71 | -8.5 | -53.7 | 14.30 |
| F3-6 | 3.8626 | 73.6207 | Guadalupe | -1.65 | -7.2 | -44.1 | 13.50 |
| F3-7 | 3.8528 | 73.6775 | Guadalupe | -1.66 | -7.7 | -47.1 | 14.50 |
| F3-8 | 3.8681 | 73.6593 | Guadalupe | -1.70 | -7 | -45.3 | 10.70 |
| F3-9 | 3.8648 | 73.6569 | Guadalupe | -1.66 | -7.4 | -45.1 | 14.10 |
| F3-10 | 3.8646 | 73.6567 | Guadalupe | -1.72 | -7.6 | -45.1 | 15.70 |
| F3-11 | 3.8372 | 73.6762 | Guadalupe | -1.60 | -7.6 | -45 | 15.80 |
| F3-12 | 3.8216 | 73.6805 | Guadalupe | -1.59 | -7.3 | -43.9 | 14.50 |
| F3-13 | 3.8609 | 73.6540 | Guadalupe | -1.62 | -7.3 | -44.4 | 14.00 |
| F3-14 | 3.8795 | 73.6512 | Guadalupe | -1.76 | -7.5 | -45.3 | 14.70 |
| F3-15 | 3.8903 | 73.6319 | Guadalupe | -1.83 | -7.4 | -49.3 | 9.90 |
| F3-16 | 3.8730 | 73.6143 | Guadalupe | -1.95 | -7.7 | -51 | 10.60 |
| F3-17 | 3.8860 | 73.6086 | Guadalupe | -2.00 | -8.3 | -53.2 | 13.20 |
| F3-18 | 3.8829 | 73.6535 | Guadalupe | -1.79 | -7.3 | -45.2 | 13.20 |
| F3-19 | 3.8747 | 73.6387 | Guadalupe | -1.57 | -7 | -42.9 | 13.10 |
| F3-20 | 3.8886 | 73.6168 | Guadalupe | -1.79 | -7.4 | -45.5 | 13.70 |
| F3-21 | 3.9051 | 73.6251 | Guadalupe | -1.86 | -7.3 | -44.6 | 13.80 |
| F3-22 | 3.8829 | 73.6360 | Guadalupe | -1.77 | -7.3 | -45.8 | 12.60 |
| F3-23 | 3.8745 | 73.6384 | Guadalupe | -1.70 | -7.3 | -43.8 | 14.60 |
| F3-24 | 3.8907 | 73.6319 | Guadalupe | -1.78 | -7.6 | -44.6 | 16.20 |
| F4-1 | 4.0875 | 73.373 | Guadalupe | -2.99 | -8.45 | -55.6 | 12.00 |
| F4-2 | 4.0862 | 73.3741 | Guadalupe | -2.94 | -8.43 | -54.6 | 12.84 |
| F4-3 | 4.0737 | 73.3835 | Une | -2.95 | -8.33 | -54.2 | 12.44 |
| F4-4 | 4.0648 | 73.3875 | Barco, Mirador | -2.95 | -8.22 | -54.1 | 11.66 |

| Sample ID | Lat (N) | Long (W) | Formation | Depth (TVDSS) (Km) | $\delta^{18}O$ (‰VSMOW) | δD (‰VSMOW) | d-excess (‰VSMOW) |
|---|---|---|---|---|---|---|---|
| F4-5 | 4.0248 | 73.4450 | Barco, Mirador | -2.96 | -8.36 | -53.6 | 13.28 |
| F4-6 | 4.0287 | 73.4552 | Une | -2.90 | -8.06 | -51.1 | 13.38 |
| F4-7 | 4.0282 | 73.4505 | Une | -2.84 | -7.94 | -50.6 | 12.92 |
| F4-8 | 4.0425 | 73.4392 | Barco, Mirador | -2.81 | -7.74 | -48.1 | 13.82 |
| F4-9 | 4.0483 | 73.4297 | Une | -2.89 | -7.71 | -49.1 | 12.58 |
| F4-10 | 4.0396 | 73.4353 | Barco, Mirador | -2.75 | -7.55 | -48.1 | 12.30 |
| EW-1 | 3.9057 | 73.7828 | Barco, Mirador | -2.17 | -6.4 | -40.9 | 10.30 |
| EW-2 | 3.9057 | 73.7828 | Barco, Mirador | -2.17 | -7.08 | -43.6 | 13.04 |
| F5-1 | 3.7923 | 71.4285 | Carbonera C7 | -0.62 | -7.38 | -43.6 | 15.44 |
| F5-2 | 3.8058 | 71.5108 | Carbonera C7 | -0.65 | -7.24 | -42.2 | 15.72 |
| F5-3 | 3.8821 | 71.4788 | Carbonera C7 | -0.69 | -7.37 | -44.4 | 14.56 |
| F5-4 | 3.8821 | 71.4788 | Carbonera C7 | -0.69 | -7.34 | -43.9 | 14.82 |
| F5-5 | 3.7574 | 71.4478 | Carbonera C7 | -0.78 | -7.4 | -43.7 | 15.50 |
| F5-6 | 3.7882 | 71.5215 | Carbonera C7 | -0.64 | -7.36 | -43.6 | 15.28 |
| F5-7 | 3.7502 | 71.4176 | Carbonera C7 | -0.59 | -7.16 | -43.7 | 13.58 |
| F5-8 | 3.8058 | 71.5108 | Carbonera C7 | -0.65 | -7.14 | -42.4 | 14.72 |
| F5-9 | 3.8103 | 71.4816 | Carbonera C7 | -0.64 | -7.47 | -43.7 | 16.06 |
| F5-10 | 3.7828 | 71.5597 | Carbonera C7 | -0.66 | -7.57 | -44.5 | 16.06 |
| F5-11 | 3.7664 | 71.4182 | Carbonera C7 | -0.62 | -7.45 | -43.9 | 15.70 |
| F5-12 | 3.7689 | 71.4021 | Carbonera C7 | -0.59 | -7.37 | -43.7 | 15.26 |
| F5-13 | 3.7894 | 71.4423 | Carbonera C7 | -0.61 | -7.22 | -42.3 | 15.46 |
| F5-14 | 3.7664 | 71.4181 | Carbonera C7 | -0.59 | -7.34 | -43.5 | 15.22 |
| F5-15 | 3.8356 | 71.4643 | Carbonera C7 | -0.66 | -7.58 | -43.9 | 16.74 |
| F5-16 | 3.8891 | 71.5093 | Carbonera C7 | -0.70 | -7.47 | -43.5 | 16.26 |
| F5-17 | 3.8422 | 71.4584 | Carbonera C7 | -0.66 | -7.37 | -43.4 | 15.56 |
| F5-18 | 3.7727 | 71.5128 | Carbonera C7 | -0.64 | -7.54 | -44.2 | 16.12 |
| F5-19 | 3.7614 | 71.4303 | Carbonera C7 | -0.60 | -7.45 | -44 | 15.60 |
| F5-20 | 3.7665 | 71.4183 | Carbonera C7 | -0.59 | -7.32 | -44.8 | 13.76 |
| F5-21 | 3.7923 | 71.4285 | Carbonera C7 | -0.62 | -7.09 | -43.3 | 13.42 |
| F5-22 | 3.7920 | 71.3792 | Carbonera C7 | -0.59 | -7.21 | -44.1 | 13.58 |
| F5-23 | 3.8305 | 71.4847 | Carbonera C7 | -0.68 | -7.48 | -44.5 | 15.34 |

**Table 3**. Summary of anions (-) and cations (+) in ppm for surface and groundwater samples from the southern Llanos basin.

| Parameter | | Hydrochemical Composition of Water Samples (Surface and Wells from Fields) | | | | | |
|---|---|---|---|---|---|---|---|
| | | **Surface Water** | **Field 1** | **Field 2** | **Field 4** | **Field 5** | **Exploratory Wells** |
| | | **n = 67** | **n = 11** | **n = 15** | **n = 20** | **n = 23** | **n = 24** |
| | | **(Min - Max), Average** | | | | | |
| **Anion (ppm)** | **$HCO_3^-$** | (0 - 174), 22.53 | (30.5-2120), 388.9 | (732-1556), 924.8 | ( 53 - 1281), 240 | (549 - 1281), 804 | (99 - 1300), 403.6 |
| | **$CO_3^{-2}$** | 0 | 0 | 0 | (0 - 7.5), 0.8 | (0 - 34), 4.3 | (0 - 120), 6 |
| | **$SO_4^{-2}$** | (0.51 - 408), 12.85 | (0 - 17), 5 | (3.9 - 135), 38.5 | (0 - 160), 32.9 | (0 - 72), 8 | (0 - 114), 13.9 |
| | **$Cl^-$** | (0.51 - 92.1), 2.12 | (5.8 - 1267), 187 | (359 - 1080), 534.8 | (4.1 - 1278), 304.6 | (72 - 541), 223.2 | (5 -1177), 176.3 |
| **Cation (ppm)** | **$Na^+$** | (1.14, 12.58), 7.2 | (4.7 - 1589), 228.4 | (558 - 1749), 787.8 | (14.2 - 1333), 247.8 | (310 - 889), 446.2 | (35.5 - 1128), 281.8 |
| | **$K^+$** | (0.87 - 7.01), 3.9 | (4.3 - 118.8), 19.6 | (12.3 - 29.6), 23 | (3.6 - 53.8), 16.7 | (6 - 48.1), 19.1 | (2.2 - 165), 22.11 |
| | **$Ca^{+2}$** | (0.22 - 183), 59.2 | (5.9 -110.8), 28.2 | (15.6 - 75.4), 32 | (8 - 136), 36.2 | (1.2 -52.2), 13.6 | (0 - 68.8), 21.1 |
| | **$Mg^{+2}$** | (0.01 - 21.7), 4.3 | (1 - 8), 2.4 | (1.7 - 4.6), 3.5 | (0.9 - 13.1), 3.9 | (0 - 44), 7.7 | (0.1 -54), 5.8 |
| **Temperature (°C)** | | (28 - 32), 30 | (82 - 104), 93 | (99 - 105), 102 | (113 - 126), 119.5 | (58 - 61), 59.5 | (60 - 100), 80 |
| **Pressure (Psi)** | | 14.86 Psi | (900 -1400), 1150 | (2000 - 3000), 2500 | (1800 - 4500), 3150 | (600 - 1200), 900 | (600 - 3500), 2050 |
| **Depth TVDSS (Km)** | | 149 - 849 | (-1.89 to - 2.21), 2.05 | (-2.12 to - 2.26), 2.19 | (-2.75 to - 2.99), 2.87 | (-0.59 to - 0.78), 0.685 | (0.6 - 2.5), 1.55 |
| ***Field-3** | | **T (°C)**: (82 - 88), 85; **P (Psi)**: (1800 - 2400), 2100; **TVDSS (Km)**: (-1.55 to -2.00), -1. 78 | | | | | |

# 4. TRABAJOS FUTUROS

Producto de la presente la investigación se proponen algunas temáticas para dar respuesta a preguntas de interés científico que permitan contribuir al conocimiento de este tipo de sistemas hidrodinámicos en cuencas *foreland* conformados por acuíferos profundos que llegan a afectar el potencial de almacenamiento de hidrocarburos. De esta manera se identificaron tres temáticas claves encaminadas a la comprensión de la dinámica del flujo de aguas subterráneas en este tipo de sistemas reconocidos en el área.

El primer tema de investigación está relacionado con la estimación de las velocidades de flujo y tiempos de residencia de las aguas subterráneas en este tipo de acuíferos profundos, lo cual representa un desafío para la obtención de parámetros hidráulicos debido a las profundidades de este tipo de sistemas, limitando así, el entendimiento de la dinámica en la recarga hídrica de un área determinada. Aunque para este tipo de sistemas acuíferos profundos se esperan relativamente altos tiempos de residencia teniendo en cuenta los efectos de la presión confinante y las características petrofísicas propias de las unidades acuíferas (ej. cementación por diagénesis, capilaridad, bajas conductividades hidráulicas), aún existe alta incertidumbre asociada a la estimación de estos parámetros. Esta problemática puede abordarse con tecnologías de dataciones múltiples en muestras de aguas usando isótopos radioactivos (ej. $^{14}C$, $^{32}Si$, $^{35}S$, $^{36}Cl$, $^{39}Ar$, $^{81}Kr$) marcadores de eventos (ej. $^{3}H$, $^{36}Cl$, $^{85}Kr$, CFC´s and $SF_6$) y trazadores radiogénicos (ej. $^{4}He$, $^{222}Rn$), los cuales permitirían establecer rangos de edades del agua, desde el orden de unos pocos días hasta millones de años. Así, el uso de estas técnicas multi-trazadores, permitirían establecer tiempos de tránsito del agua subterránea, que a futuro contribuya con el manejo adecuado del recurso hídrico asociado a este tipo de sistemas acuíferos profundos.

El segundo tema propuesto para investigaciones futuras está asociado con el conocimiento de los límites y zonas de descarga de este tipo de sistemas acuíferos en cuencas *foreland*. Para el caso particular de la cuenca de Llanos, se desconocen los límites del sistema hidrodinámico hacia el sector oriental donde han sido reconocidos los valores más bajos de cabezas hidráulicas de todo el sistema del sector sur de la cuenca de Llanos. A su vez, hacia este mismo sector, se interpretan cambios en la dirección de flujo de las aguas subterráneas, lo cual es explicado a partir de hipótesis relacionadas tanto con procesos tectónicos (tectónica activa), límites estructurales propios de la configuración de la cuenca e incluso recarga hídrica proveniente desde el sector oriental. A su vez,

la descarga de este sistema aún es desconocida, y aunque se presume que estaría hacia el sector norte de la cuenca, aún no se cuentan con evidencias que soporten dicha hipótesis. De esta forma, uno de los temas a evaluar estaría relacionado con el control que ejerce el rasgo estructural de mayor extensión hacia el *forebulge* de la cuenca, asociado al Alto de Guyana, el cual estaría constituyendo un posible límite del sistema hidrodinámico hacia el este de la cuenca de Llanos. Así mismo, sería necesario evaluar la continuidad de la Unidad de Flujo Basal hacia el sector norte de la cuenca y los estilos estructurales que dominarían la posible zona de descarga hacia el sector norte-noreste de la cuenca de Llanos.

Como tercer tema de investigación se propone analizar los tiempos de estabilización de las interfaces agua-aceite, considerando tanto el fenómeno hidrodinámico como el efecto neto de la fuerza boyante del hidrocarburo en unidades acuíferas. El análisis de los tiempos de estabilización de las interfaces agua-aceite en el sector sur de Llanos ayudaría a descartar o confirmar hipótesis acerca de la inclinación de los contactos agua-aceite por efecto del basculamiento tectónico de la cuenca. De esta manera, considerando las características fisicoquímicas de los fluidos, propiedades petrofísicas de las rocas, y las condiciones de presión y temperatura de los yacimientos, esta temática puede ser abordada usando técnicas de modelamiento numérico para establecer las tasas de estabilización de las interfaces agua-aceite, y así contrastar con datos de tasas de levantamiento tectónico del área. Esta propuesta puede ser aplicada en campos de petróleo donde se tienen datos conocidos de los ángulos de inclinación de los contactos agua-aceite.